MATHEMATICAL MODELING AND CONTROL OF ASYNCHRONOUS MOTOR FOR MULTI-PHYSICAL MODELS

A Thesis

by

İlayda Demircioğlu

Submitted to the
Graduate School of Sciences and Engineering
In Partial Fulfillment of the Requirements for
the Degree of

Master of Science

in the
Department of Electrical and Electronics Engineering

Özyeğin University
July 2021

MATHEMATICAL MODELING AND CONTROL OF ASYNCHRONOUS MOTOR FOR MULTI-PHYSICAL MODELS

Approved by:

Asst. Prof. Göktürk Poyrazoğlu, Advisor
Department of Electrical and Electronics Engineering
Özyeğin University

Assoc. Prof. Cenk Demiroğlu
Department of Electrical and Electronics Engineering
Özyeğin University

Asst. Prof. Abdül Balıkçı
Department of Electrical and Electronics Engineering
Dokuz Eylül University

Date Approved: 5 July 2021

To My Family

ABSTRACT

Asynchronous motor is a good choice for the industry due to its low cost, high efficiency, robustness, high reliability, ability to work in bad environmental conditions, easy recycling, good dynamic performance, high maximum speed, and high range of field weakening [1, 3]. Although the scalar control method is sufficient in speed control applications by keeping the stator voltage/frequency ratio constant in asynchronous motors, in cases where the continuity of torque control is important, the scalar control method is not sufficient and therefore cannot compete with the direct current method [4]. With the scalar control method, a large range of speed control could be made at the nominal torque of the induction motor. However, the scalar control method was not sufficient in applications where continuous speed and torque control were required. Current components forming the flux and torque in the direct current motor are controlled independently from each other. The excitation flux forming the flux can be kept constant and the moment can be controlled by the armature winding current. However, there are no such two perpendicular current components in an asynchronous motor. There is only stator current with amplitude angle and phase available. Therefore, the stator current is transformed into two perpendicular current components, one forming the flux and the other the torque, using Clarke and Park transformations. The desired torque control can be achieved by controlling these two current components separately. Closed-loop volt/hertz controllers were developed to control torque and speed. In this control method, the moment can be brought to the desired values in the continuous regime, but the moment in the transient regime cannot be controlled. The speed control method, which is sufficient in many applications, is not sufficient in applications where the torque should be controlled continuously.

This study aims to perform mathematical modeling of asynchronous motor and simulation of the rotor flux-oriented vector control method on a user-friendly platform. Besides, the obtained model is created as a PhiSim library [9], a product of Sherpa Engineering [8]. This library was created using the bond-graph theory. Asynchronous motor is a good choice for electric vehicles due to its simple structure, low cost, high efficiency, robustness, high reliability, ability to work in bad environmental conditions, good dynamic performance, and wide speed range. The outputs from this study will serve the automotive industry. This simulation tool will be beneficial in investment decision-making processes and research.

ÖZETÇE

Asenkron motor, düşük maliyetli , yüksek verimli, dayanıklı , yüksek güvenilirliği , kötü çevre koşullarında çalışabilmesi, kolay geri dönüşümü , iyi dinamik performansı, yüksek maksimum hızı ve yüksek alan zayıflatma aralığı nedeniyle endüstri için iyi bir seçimdir. Asenkron motorlarda stator gerilim/frekans oranını sabit tutarak hız kontrol uygulamarında skaler kontrol yöntemleri yeterli olmaktaydı . Hız kontrolü asenkron motorun nominal torkunda geniş bir aralıkta yapılabilmekteydi. Ancak , tork ve hız kontrolünün sürekli kontrol edilmesi gereken durumlarda skaler kontrol yöntemi yeterli olmamaktadır. Bu nedenle doğru akım motoru bu uygulamalarda tercih edilmekteydi. Doğru akım motorunda akı ve torku oluşturan akım bileşenleri birbirinden bağımsız olarak kontrol edilmektedir. Akıyı oluşturan uyarma akısı sabit tutulabilir ve moment, armatür sargı akımı ile kontrol edilebilir. Ancak asenkron bir motorda böyle dik iki akım bileşeni yoktur. Sadece genlik açı ve faza sahip stator akımı mevcuttur. Bu nedenle, stator akımı, Clarke ve Park dönüşümleri kullanılarak biri akı ve diğeri torku oluşturan iki dikey akım bileşenine dönüştürülür. Bu iki akım bileşeni ayrı ayrı kontrol edilerek istenilen tork kontrolü sağlanabilir. Tork ve hızı kontrol etmek için kapalı döngü volt/hertz kontrolörleri geliştirildi. Bu kontrol yönteminde sürekli rejimde moment istenilen değerlere getirilebilirken, geçici rejimde moment kontrol edilemez. Birçok uygulamada yeterli olan hız kontrol yöntemi, torkun sürekli kontrol edilmesi gereken uygulamalarda yeterli olmamaktadır. Bu çalışma ile asenkron motorun matematiksel modellemesini ve rotor akısından oryantasyonlu vektör kontrol yönteminin simülasyonunu kullanıcı dostu bir platformda gerçekleştirmeyi amaçlamaktadır. Ayrıca elde edilen model, Sherpa Engineering [8] ürünü olan PhiSim kütüphanesinde [9] Bond- Graph teorisi

kullanılarak oluşturulmuştur. Asenkron motor, basit yapısı, düşük maliyeti, yüksek verimi, sağlam- lığı, yüksek güvenilirliği, kötü çevre koşullarında çalışabilmesi, iyi dinamik performansı ve geniş hız aralığı nedeniyle elektrikli araçlar için iyi bir seçimdir. Bu çalışmanın çıktıları otomotiv endüstrisine hizmet edecektir. Bu simülasyon aracı, yatırım karar verme süreçlerinde ve araştırmalarda faydalı olacaktır.

ACKNOWLEDGEMENTS

I would like to thank Asst. Prof. Göktürk Poyrazoğlu for his support during the thesis, for always motivating me, for his systematic guidance and great effort.

I would like to express my deepest sense of thank to Mert Mokukcu for his continuous advice and encouragement throughout the project. Thank you for his systematic guidance and the great effort he has put into training me in the technical field. In addition, I would like to thank the Sherpa Engineering R&D team for their technical support and tool sponsorship during this project.

TABLE OF CONTENTS

LIST OF TABLES

LIST OF FIGURES

CHAPTER I

INTRODUCTION

Asynchronous motor is a good choice for the industry due to its low cost, high efficiency, robustness, high reliability, ability to work in bad environmental conditions, easy recycling, good dynamic performance, high maximum speed, and high range of field weakening [1, 3]. An induction motor or asynchronous motor is an AC electric motor in which the excitation current in the rotor needed to produce torque is obtained by electromagnetic induction from the magnetic field of the stator winding. An induction motor can therefore require no physical electrical conduction to the rotor. Only an AC source is required to operate because it does not require DC excitation like a synchronous motor. Therefore, there are no sparks during the operation because of no brush in an induction motor. Asynchronous motors with a simple design require lower costs and lower maintenance costs compared to other motors [1]. The efficiency of the induction motor is varying from 85 to 95 % [2]. It is a highly efficient motor for automotive applications [3]. Moreover, its speed regulation (SR) is very high [3] so it can be used in applications where load variation is higher.

Although the scalar control method is sufficient in speed control applications by keeping the stator voltage/frequency ratio constant in asynchronous motors, in cases where the continuity of torque control is important, the scalar control method is not sufficient and therefore cannot compete with the direct current method [4].

Current components forming the flux and torque in the direct current motor are controlled independently from each other. The excitation flux forming the flux can be kept constant and the moment can be controlled by the armature winding current. However, there are no such two perpendicular current components in an asynchronous motor. There is only stator current with amplitude angle and phase available. Therefore, the stator current is transformed into two perpendicular current components, one forming the flux and the other the torque, using Clarke and Park transformations. The desired torque control can be achieved by controlling these two current components separately. Closed-loop volt/hertz controllers were developed to control torque and speed. In this control method, the moment can be brought to the desired values in the continuous regime, but the moment in the transient regime cannot be controlled. The speed control method, which is sufficient in many applications, is not sufficient in applications where the torque should be controlled continuously. In order to overcome all these limitations, Hasse and Blaschke [5] developed the flux-oriented control method in the 1970s. Later, Takahashi [6] and Depenbrock [7] developed the direct torque control method in the mid-1980s and these control methods laid the foundation for the high-performance control methods used today.

"In 1824, the French physicist François Arago formulated the existence of a rotating magnetic field [15]. In 1879, Walter Baily demonstrated the effects of the first primitive asynchronous motor" [15]. Galileo Ferrais, who independently invented the first alternating current collector-less asynchronous motor, in 1885, and Nicola Tesla in 1887, showed their motor modeling studies [15].

Asynchronous machines consist of two main parts. Cross section of induction machine and induction machine with wound rotor and slip rings are shown in Figures 2 and 3. The stator and stator windings that do not rotate are the rotor and rotor windings that rotate. Asynchronous machines are electromechanical machines that convert the electrical energy received from the stator windings as a motor to mechanical energy by making rotational movement from the rotor and convert the rotational mechanical energy received from the rotor as a generator, under some conditions, into electrical energy in the stator windings. Compared to other rotating electrical machines, they are more robust, require less maintenance, and are cheaper. In recent years, with the technological developments in semiconductor power electronics, asynchronous machines can be easily controlled. Speed and torque control can be done easily in systems where high-power IGBTs are used. With these developments, speed control, torque control, and soft-starting processes of asynchronous motors and these machines, with their other superior structural features, have begun to take their place in the industry of DC machines. The stator is the non-rotating part of the machine. There are stator sheet packages and stator windings that transmit magnetic flux in the stator. The rotor is the rotating part of the induction motor and consists of rotor sheet pack and rotor windings.

Asynchronous motors are divided into two parts according to the rotor structure. Asynchronous machines with short-circuited rotor or squirrel-cage, instead of windings in the rotor, aluminum rods are placed in corrugation and short-circuited at both ends by aluminum rings in the form of a cage structure. In Figure 1, a diagram of a squirrel cage induction motor is given. The windings in the rotor of the wound-rotor or double-fed asynchronous machines are similar to the windings in the stator, they are generally star connected and the star point is not taken out, but the other winding ends are taken out with the help of the ring-brush. Since there is no tip coming out of the rotor of the squirrel-cage induction motor, the control of this motor can only be made from the electrical terminals on the stator. However, since the rotor winding ends of the wound-rotor induction motor are taken out with the help of the ring and brush, the control of this motor can be done from both the stator winding ends and the rotor winding ends. By connecting a resistor or an independent voltage source to these terminals, the speed and torque control of the induction motor is made.

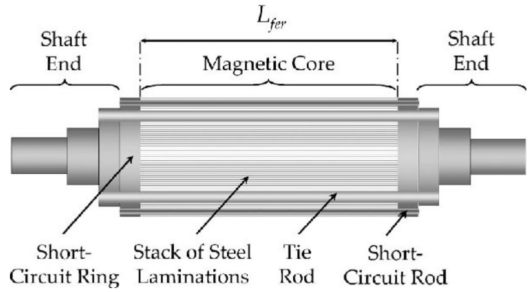

Figure 1: Diagram of a squirrel cage induction-motor [16]

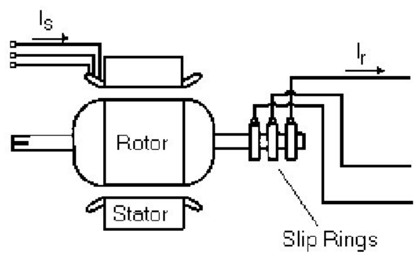

Figure 2: Induction machine with wound rotor and slip rings [17]

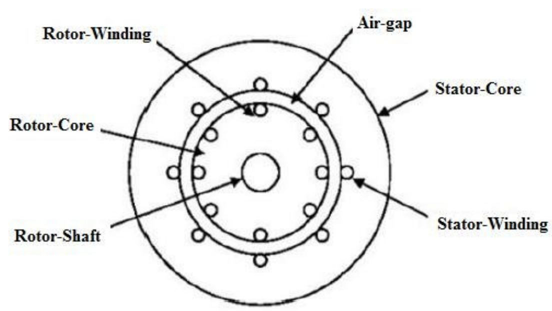

Figure 3: Cross Section of induction machine [18]

Asynchronous motor is a good choice due to its simple structure, low cost, high efficiency, robustness, high reliability, ability to work in bad environmental conditions, good dynamic performance, and wide speed range. However, there are some disadvantages of induction motor. These are expensive speed control, poor positioning control, high start control, low power factor in case of light load condition, and the motor cannot use in such applications where high starting torque is necessary like traction and lifting weight.

CHAPTER II

MULTI-PHYSICAL MODELS AND TOOLS

This project was designed in PhiSim Toolbox with the support of Sherpa Engineering, and in this section, information about the toolbox and Sherpa Engineering will be given.

2.1 About Sherpa Engineering

Sherpa Engineering is a service company founded in France in 1997, specializing in modeling and instrumentation. Its projects are part of systems engineering that combines the design, implementation, and verification processes of technical systems and their control.

It is based on Sherpa Engineering's development and systematic use of a consistent set of overall models at all stages of the design cycle. Sherpa engineering supports many industries with services that follow companies technology, supported by a model-based methodology throughout innovation processes ranging from applied basic research to industrialization.Its fields of activity are automotive, aerospace, process industry, construction, and marine. Sherpa Engineering's service delivery also relies on its ability to create tools that leverage the experience of completed projects. Modeling develops best practices in modeling and simulation of complex systems in various industries through simulation tools and business libraries. Therefore, the company's solutions and products are also suitable for systems that are transferred between industries.

2.2 PhiSUITE Toolbox

Designed by PhiSUITE Sherpa Engineering. PhiSUITE covers the following parts.

2.2.1 PhiSystem

PhiSystem is based on Papyrus which provides and integrated and user-consumable environment for editing an UML-SysML Model [9]. It provides a description of the system architecture, the definition of requirements and testing, the definition of connections, the management and creation of information for allocation and traceability. Thus, the performance of the system is verified at all design stages thanks to PhiSystem. These design stages are shown in Figure 4.

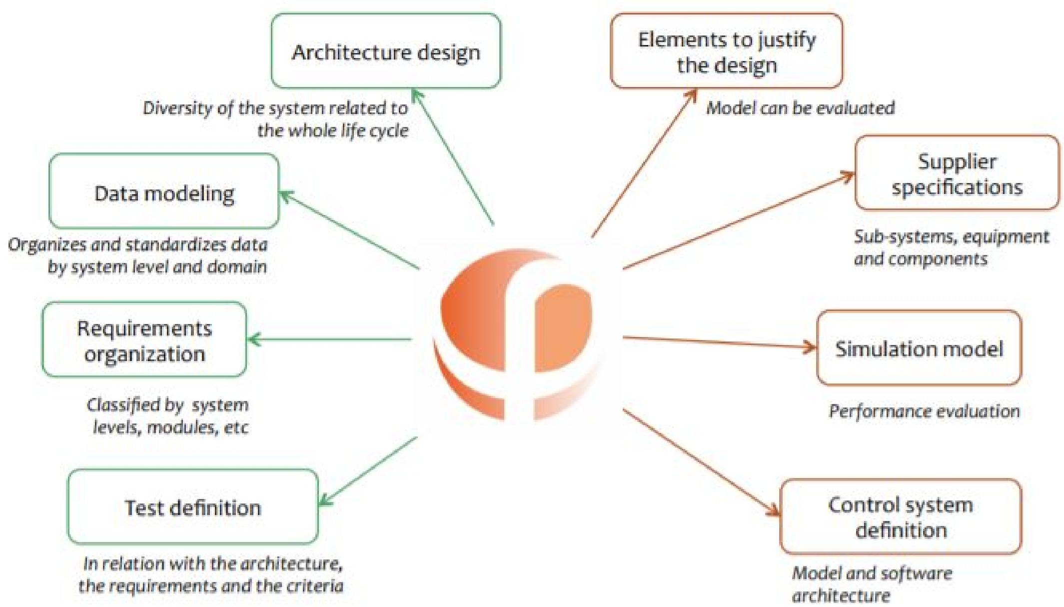

Figure 4: Diagram of the PhiSystem [9]

2.2.2 PhiEMI

The representation of the system in its sphericity (Physics and control) with a high level of abstraction is compatible with the lack of knowledge in the first steps of the development cycle. It provides quick evaluation in the simulation of different architectures before technological choices [8].

2.2.3 PhiSim

It contains different physical domains in its structure as shown in Figure 5. These are thermal-fluid, gas mixture, moist gas, thermal , hydraulics, mechanics, electrical,and control signal, faults, diagnostic.

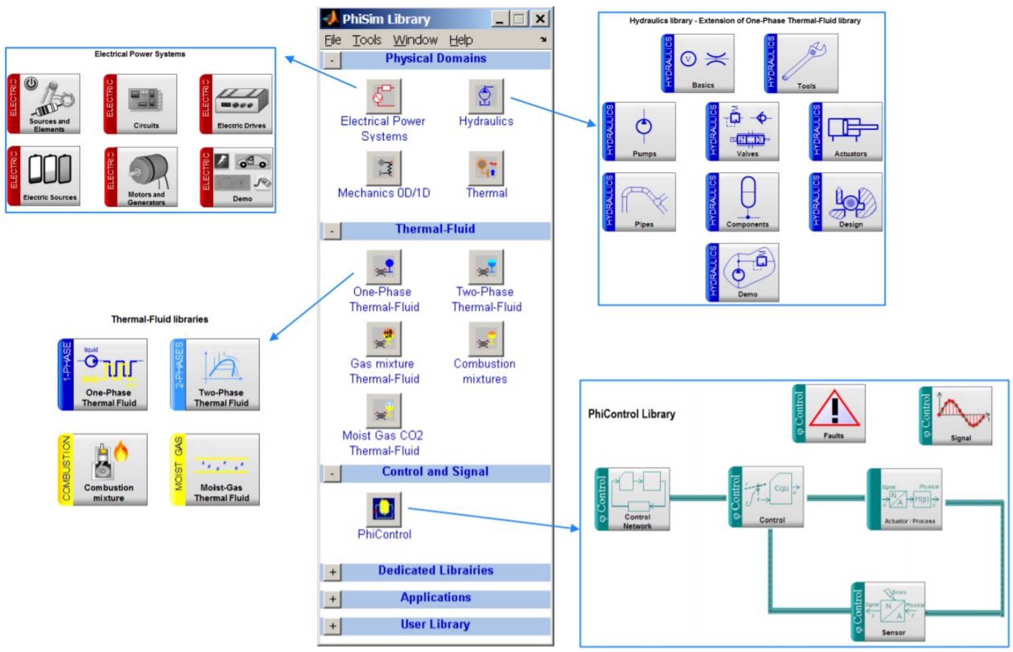

Figure 5: Interface of the PhiSim library [9]

PhiSim is a toolkit designed by Sherpa Engineering for engineers who have to model open-loop and closed-loop physical multi-domain dynamical systems.It allows physical and control systems models to be processed in a multi-port environment offering greater flexibility and less maintenance due to low polymorphic base elements [8]. PhiSim includes physical and application libraries, tools, and utilities that facilitate modeling and simulation of systems dynamically. In addition to the available libraries, the user can create their own libraries by developing their own components or by combining or customizing existing components to easily adapt them to their use case [9]. There are multi-domain system libraries for designing models by combining and customizing basic polymorphic elements. These are 0D/1D mechanics , electrical power systems, thermal fluids, thermal, hydraulics, and PhiControl [9].

PhiControl structure in model-based control design is given in Figure 6. PhiControl is a library of Simulink modules for the design, tuning, analysis and simulation of advanced control. It includes PFC predictive control modules and PID control modules to control most systems. It enables rapid design of the complete control loop, taking into account constraints, operating modes and management of faults. All control modules are suitable for C code generation [9].

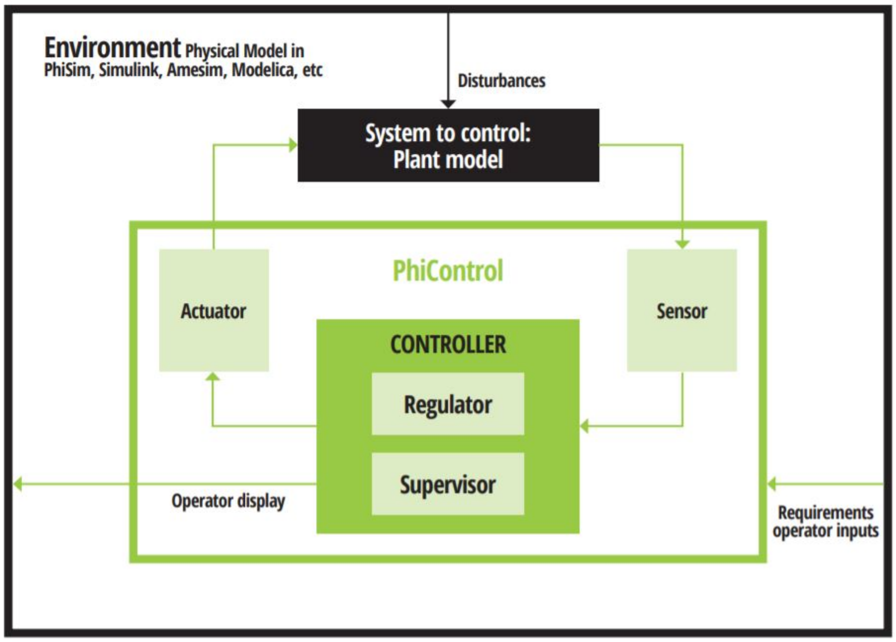

Figure 6: PhiControl in model based control design [8]

In software development, the V-cycle represents a development process. The V-cycle shows each stage in the development life-cycle and how they relate to each other. Due to the complexity of the system's software, it is an important cycle for improving quality, increasing development efficiency, and planning a development process that will eliminate systematic software errors. V-cycle is applied in automotive engineering. As seen in Figure 7 , the left side of the V-cycle consists of vehicle requirements , sub-systems design and test , components design and test in standard automotive systems engineering. The right side of the V concentrates the main verification and validation activities.

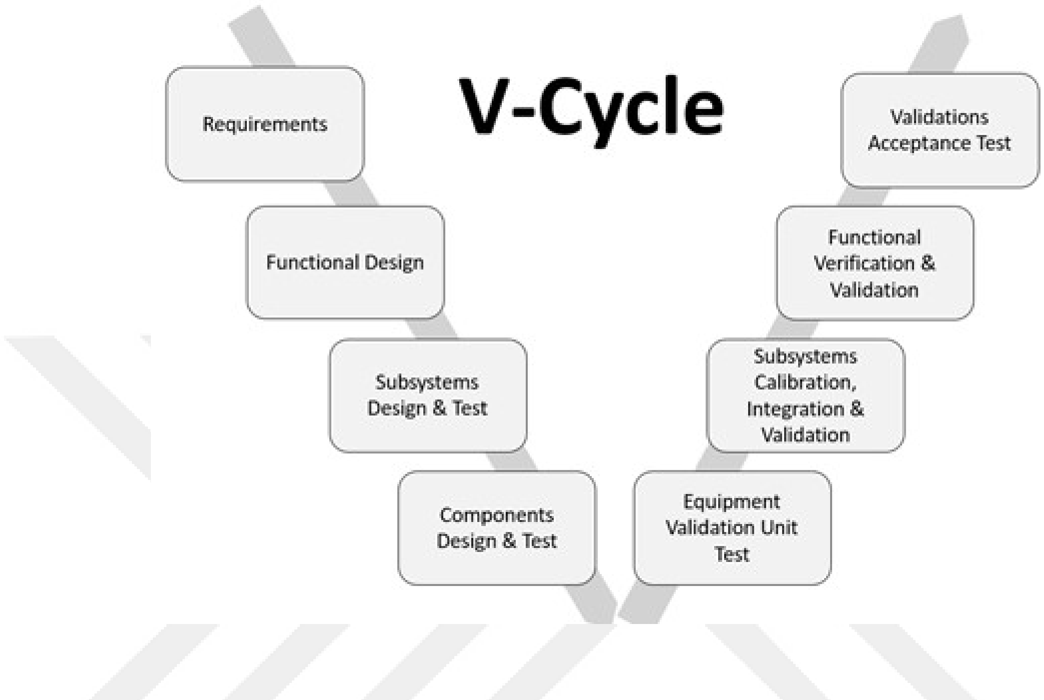

Figure 7: V-Cycle for automotive system engineering [9]

Vehicle requirements provide the service architecture and tool requirements, write use cases, and traceability of allocations. Subsystem design and testing enables building multi-physical sub-systems, choosing physical architecture, and sizing components to meet vehicle requirements. Components design and testing enables to design components and establish requirements for suppliers.

However, in the new automotive systems engineering, the functional design step is included on the left side of the V-cycle. The functional design step, especially the new tasks expected from hybrid and electric vehicles, concerns many subsystems. It allows managing the connections and complexity between vehicle requirements and physical sub-systems. Global energy management is mainly studied here. PhiSystem is used for vehicle requirements step and systemic models step . PhiSystem and PhiEMI are used for key functional architecture step and entire vehicle models. PhiSim and

PhiControl are used for multi physic models. After these steps are completed, the right side of the V-cycle starts to be applied.

CHAPTER III

CONTROL METHODS OF ASYNCHRONOUS MOTOR

Asynchronous motors were previously connected directly to the mains, in this case the speed of the motor was dependent on the mains frequency and speed control was not possible. In open loop control, the motor could not be controlled in transient mode and could draw excessive current. At constant torque, speed control was not possible.

Closed-loop volt/hertz controllers were developed to control torque and speed. In this control method, the moment can be brought to the desired values in the continuous regime, but the moment in the transient regime cannot be controlled. The speed control method, which is sufficient in many applications, is not sufficient in applications where the torque should be controlled continuously. In order to overcome all these limitations, Hasse and Blaschke [5] developed the flux-oriented control method in the 1970s. Later, Takahashi [6] and Depenbrock [7] developed the direct torque control method in the mid-1980s and these control methods laid the foundation for the high-performance control methods used today.

There are many asynchronous motor control methods. The scalar control method can be implemented without the need for axial transformations and complex algorithms in applications where speed control is sufficient. With the development of power electronics and fast signal processors, the vector control method has started to be preferred, so the asynchronous motor has come to the point of showing the same performance as the direct current motor. On the basis of the vector control method, it is aimed to express the torque expression as in the direct current motor. By separating the air gap flux into the components of the d-q axis perpendicular to each other, one of these components is accepted as zero.($\psi_q = 0$) [19], [20].

We can divide the flux oriented vector control method into two groups.

- Direct vector control method ;

  The flux amplitude and angle are measured using hall probes or special windings or calculated by the observer.

- Indirect vector control method ;

  The flux amplitude and angle are found using the measured rotor current and speed. Finding the rotor speed by calculating instead of measuring is an important issue for vector control.

3.1 Speed Control Methods

Asynchronous machines are used in industrial applications and mostly in variable speed drive systems. For this reason, the working conditions of the machine at variable speed should be examined. For this purpose, considering the torque expression obtained from the equivalent circuit in the continuous sinusoidal state, it is necessary to change the stator voltage, stator winding pole pair, stator frequency, rotor resistance for the asynchronous machine to operate at variable speed.

3.1.1 Speed Control by Changing the Stator Voltage

In this method, the speed can be changed between the synchronous speed value determined by the frequency of the voltage and the speed value corresponding to the overturning torque when the machine is loaded with a fixed nominal load.In a standard machine, this range is quite small. That is, the speed can only be changed between the synchronous speed and a lower value of about 10% of this speed. Because there is a square relationship between the stator voltage value and the torque value, a small change in the stator voltage creates a big change in the torque produced by the machine due to the square relationship. The speed control range is very small in the case of constant load torque. It is therefore not suitable for variable speed drive systems. However, it is suitable for a limited application with fan-type loads that produce load torque directly proportional to the square of the speed. If the point where the torque produced by the machine is equal to the load torque is stable, the machine can operate stably at the torque and speed value at this point.

3.1.2 Speed Control by Changing the Number of Poles

The synchronous speed (n_s) of the asynchronous machine depends on the frequency of the stator voltage and the number of poles of the stator windings of the machine. The synchronous speed (n_s) of the asynchronous machine is calculated by Eq. (1) .

$$n_s = \frac{60 f_s}{p} \tag{1}$$

Changing the number of poles directly affects the synchronous speed. As the number of poles is increased, the synchronous speed of the motor will decrease. In order to do this, the stator phase windings must be of special construction so that the number of poles can be changed. Changing the number of poles, increasing the number increases the steps involved in the changes in the speed of the motor, but it is not very suitable because of the complexity of the switches that must be used to obtain more than two different pole numbers from a winding. Therefore, it requires the use of different windings, which shows that the method is not economical.

3.1.3 Speed Control by Changing Rotor Resistance

This method can only be applied to wound-rotor asynchronous motors. The synchronous speed and overturning moment of the machine do not change with the rotor resistance. The tipping slip varies linearly with the rotor resistance. The speed control of the machine can be made by changing the rotor resistance, thus the current flowing through the rotor. With this method, there is a fairly large range of speed control. Since the rotor ends of the wound rotor induction motors are taken out, resistance can be added to the rotor from the outside. Speed control by adding resistors to the rotor is more lossy than starting by adding resistors. The reason for this is that the resistors added to the rotor are deactivated after the starting event takes place in a short time and ends. On the other hand, to reach the desired speed values in speed control, the resistance value connected to the rotor must remain constant throughout the adjusted speed value. These losses increase even more when operating with rated load, especially at low speeds, which require the connection of larger additional resistors [12].

3.1.4 Speed Control by Changing the Amplitude and Frequency of the Stator Voltage

While the frequency of the voltage applied to the motor is reduced, the fact that the amplitude remains constant causes the machine to draw more current from the source it is connected to. As can be seen from the maximum torque and current expressions, it is necessary to change the frequency together with the amplitude both to control the speed and to prevent the current and torque from increasing during this control.

The methods based on the variation of the amplitude and frequency of the stator voltage are as follows;

3.1.4.1 Scalar Control Methods

The control method performed by changing the voltage and frequency of the induction motor is known as scalar control. It is the most convenient method of speed control. It is generally used in fans of ventilation systems, heating systems where precise speed control is not required [21].

In the condition that the stator resistance is neglected, by keeping the voltage/frequency ratio constant, the speed of the motor can be controlled in a large range so that the maximum torque of the asynchronous motor remains constant in the entire speed range, except for low speed values. However, in the low speed region, where the frequency is around 10 Hz, 15 Hz, the voltage drop caused by the stator resistance becomes significant and causes the motor to not produce the required torque in the starting state. For this reason, at low-speed values, the stator voltage is chosen higher than the voltage/frequency ratio. This is also known as I.R compensation. The relationship between the magnitude of the stator voltage and the frequency is shown in Figure 8. When the speed of the asynchronous motor is desired to exceed the nominal speed, the voltage must increase to keep the voltage/frequency ratio constant. However, the voltage shouldn't exceed the nominal voltage as this situation will damage the winding insulations. Thus, it is possible to operate in the constant voltage region. Since the voltage remains constant with increasing frequency, the torque that the motor can produce will decrease due to the air gap flow. This method of operation is known as field weakening.

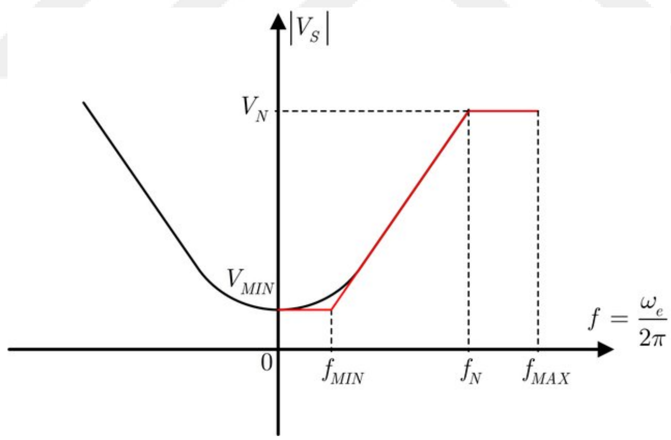

Figure 8: Relationship between the magnitude of the stator voltage and frequency [22]

The nominal torque and the maximum torque of the machine are calculated by Eqs. (2) and (3).

$$T_{e_n} = \frac{3R'_r p}{s w_n} . \frac{V_{s_n}^2}{\left[R_s + \frac{R'_r}{s}\right]^2 + \left[\chi_{s\sigma} + \chi'_{r\sigma}\right]^2} \tag{2}$$

$$T_{e,max} = \frac{3}{2}p\frac{\psi_{rd}^2}{R_r'}w_r \tag{3}$$

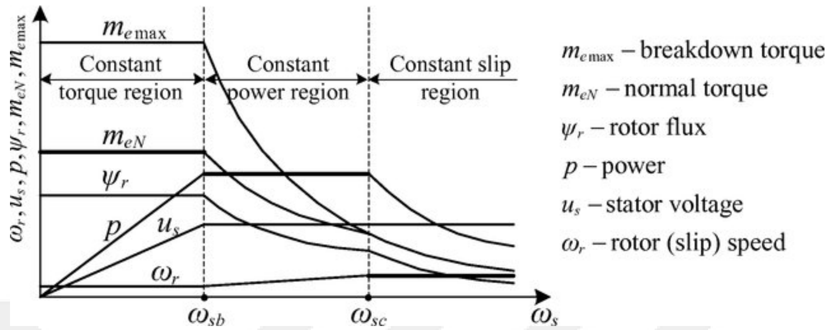

Figure 9: Control characteristics of the induction motor in constant and weakened flux regions [11]

The machine runs at its nominal torque until it reaches its nominal speed and power. After it reaches the nominal speed, it operates at its nominal power. As the speed value increases, the torque value decreases. According to the control characteristics of the induction motor in constant and weakened flux regions graph given in Figure 9, there are different rotor flux values in these two working areas, which are divided into two parts as constant torque and constant power. In the constant torque region, the rotor flux is maintained at the machine's nominal torque. In the constant power region, the rotor flux is reduced depending on the increasing speed and this is called field weakening.

3.1.4.2 Vector Control Methods

In the free-excited direct current motor, the current components that create the flux moment can be controlled separately. In this way, when the flux is kept constant, the current component that creates the moment and the excitation and armature axes are perpendicular to each other. By keeping the excitation flux constant, the torque expression can only be controlled by armature current. However, the nonlinear nature of the induction motor requires complex control and conversion algorithms. There are no two separate current components in an induction motor, only a sinusoidal stator current containing amplitude, frequency and phase information. This sinusoidal current vector can be defined in two perpendicular axes, one of which creates the flux and the other the torque, as in a direct current motor. This control method is called vector control. The process of separating the stator current into components based on the flux is called flux orientation. Although there are different flux orientations, in all these methods, the flux is kept constant with the help of the current component that creates the flux and is in the same direction as the flux, and the torque is adjusted linearly with the other current component.The rotor flux is defined on the d-axis, all other variables are defined relative to the d-axis and perpendicular to the q-axis. The stator current vector also splits into its components in both the q-axis and the d-axis. Thus, the d-axis component of the stator current will be the current component that controls the flux, and the component in the q-axis will be the current component that controls the torque [12].

In order to develop the control of this system similar to a direct current machine, both the development of non-linear control rules and the fast processing controllers (DSP: digital signal processor, etc.) are required for the implementation of these rules [12]. It should be ensured that the machine model is simple and convenient to control. Looking at the equations in the model to provide these desired properties, it is seen that the most appropriate variable to be chosen as a basis is rotor flux. Since the other magnitudes are defined according to the variable chosen as the basis, in this case, a vector control system will be in question, oriented from the rotor flux. Since the rotor flux is not a measurable quantity, it must be created with the help of measurable quantities. By obtaining the rotor flux, the component of the flux to be kept constant and the angle at which the necessary transformation vectors for the transformation of the currents will be formed should be obtained. There are two methods for obtaining rotor flux, direct and indirect. As mentioned before, the control method developed based on rotor flux is called rotor flux-oriented vector control. The basic element in obtaining a simple rotor flux-oriented model of the machine model is to keep the machine rotor flux on the d-axis. In order to achieve this, the required input to the machine is the amplitude of the stator voltage and the frequency of this voltage, and these values should be calculated and applied.

These control methods based on the d-q axes of the machine are also called vector control methods in general and are divided into two main parts:

- Direct vector control method
- Indirect vector control method

Apart from these control methods, direct torque or flux control methods are also available. The direct torque or flux control method is a method that originates from the stator flux. Direct and indirect vector control methods are generally vector control methods originating from rotor flux.The difference between direct or indirect vector control methods is based on the way the amplitude and phase of the flux are obtained.

- Direct vector control method ;

  It is the first applied vector control method. Air gap flux components are measured directly with the help of two flux sensors placed perpendicular to each other (α - β axes) in the stator with a special arrangement made on the physical structure of the machine. In order to create the amplitude and phase of the rotor flux, apart from the measured flux components, the phase currents of the machine must also be measured and the components in the α - β axes must be obtained by a conversion from a-b-c to α - β. The torque expression is written from the amplitude of the rotor flux and the component of the current in the q-axis. Since this method requires a special structure for the placement of flux sensors in the stator of the machine, its application is only possible in some machines with a special structure. Therefore, it is not a useful method.The air gap flux can be obtained from the voltages induced in special windings placed on the stator for measurement on two perpendicular axes (α - β) instead of flux sensors placed in the stator where the flux can be measured directly.

By integral the voltages induced in the windings, the air-gap fluxes are:

$$\psi_{m\alpha} = \int_0^t e_{m\alpha} dt \tag{4}$$

$$\psi_{m\beta} = \int_0^t e_{m\beta} dt \tag{5}$$

From the calculated air gap flux, the amplitude and phase of the rotor flux required for control and the machine torque will be calculated. The calculated rotor flux amplitude and torque were compared with the reference flux and torque values and the resulting flux and torque errors were applied to PI type flux and torque controllers. The control signals produced by the controllers are used as reference quantities of the d-q current components of the machine. Another magnitude produced by the flux calculator is the conversion angle. Using this conversion angle, the d-q component currents of the machine are derived from the stator phase currents of the machine to be compared with the reference currents.

Thus, current errors resulting from the comparison of the reference and real d-q current components are applied to the current controllers and the reference stator voltage components in the d-q axis set are produced. The voltage components are converted to the reference voltage magnitudes in the a-b-c axes, which are required for the PWM manufacturer, by using the conversion angle. In this method, it can only be applied in special machines such as Hall probes placed in the stator in order to measure the air gap flux. This method is also not very common because it is not general and easy to use. Due to the described problems of the methods based on the measurement of flux components, methods based on the calculation of flux components are preferred, instead of measuring which is expensive and has the result of affecting the physical structure of the machine, which is easier, cheaper and can be measured without affecting the physical structure.

- Indirect vector control method ;

  The flux amplitude and angle are found using the measured rotor current and speed. Finding the rotor speed by calculating instead of measuring is an important issue for vector control. The most common of this type of control method is the one developed by utilizing rotor flux. For this purpose, it is necessary to produce the amplitude of the rotor flux vector and the phase that will provide the transformations between a-b-c and d-q. In this method, a given ψ_{rd}^{ref} flux reference value corresponds to the $\imath_{rd}^{ref}$ d-axis reference current value. Although this method is considered quite simple in terms of application among vector control methods, it has some disadvantages. The most important of these is that the generated reference signals depend on the machine parameters, especially the rotor circuit time constant $\tau_r = L'_r/R'_r$.

  The rotor frequency is very effective on the resistance and inductance included in the rotor time constant expression. As this frequency increases, the rotor resistance increases due to the skin effect, while the rotor inductance decreases. The rotor frequency that causes this change is affected by both the stator frequency and the load connected to the spindle of the machine.

CHAPTER IV

BOND-GRAPH THEORY

Bond graphs are a domain-independent graphical description of the dynamic behavior of physical systems [14]. The Bond-Graph has an important place in the diagram of the physical systems shown in Figure 10. Bond graphs allow describing different physical systems and their interactions in a uniform algorithmizable way and transforming it into the definition of the equation of state [13]. This means that systems from different domains (cf. electrical, mechanical, hydraulic, acoustical, thermodynamic, material) are described in the same way. Bond graph is a powerful tool for modeling engineering systems when modeling different physical domains [14].

Bond-graph simplifies the construction of multi-disciplinary models, clearly shows power transfers, ensures energy balance, clearly shows cause and effect relationships. It allows the systematic writing of mathematical models associated with bond graphs. There is no black box model in the Bond graph, the unknown parameters of known physical phenomena are determined and the physical sense of the obtained mathematical model is observed. Only a couple of tools in the world are using this approach to design multi-physics models [8].

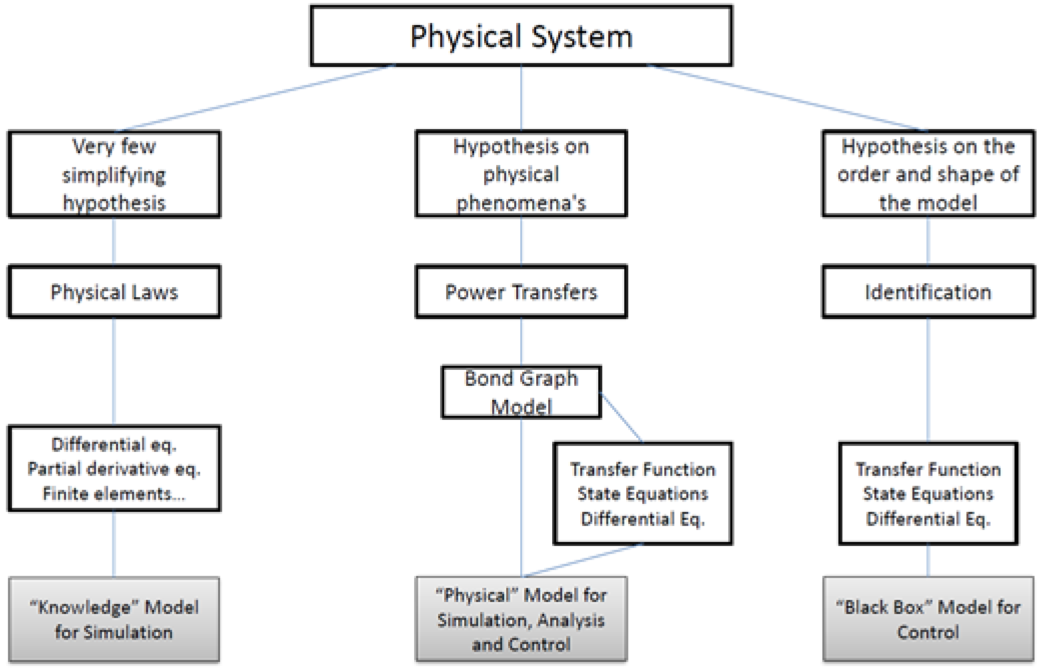

Figure 10: Diagram of the physical system [8]

A system is a functional whole in which different physical elements interact interactively to fulfill a specific purpose. System simulation, on the other hand, is the time-dependent imitation of real-life physical processes.

System simulation has an important place in the creation of digital twin models today. A digital twin is defined as a virtual model of the behavior and consequences of a physical product or service in the real world. In simpler terms, the digital twin; is a virtual model of a process, product, or service. Thanks to the studies carried out on these models, it is possible to greatly reduce the time spent on physical changes and tests. There is a common power balance and transfer according to certain principles between the elements that make up the multi-physics system. Simulating the energy exchanges between these different physical systems allows combining the modeling approach as well as the analyzes made for different physics in a common language. With the bond graphic approach, which is a practical method, the dynamic behavior of the system can be defined by the principles of energy flow, storage, and energy conversion between various subsystems. . Therefore, a dynamic system is represented by energy storage, distribution, transforming and resource elements. Energy exchange between subsystems is associated with the exchange of physical quantities such as momentum, mass, electrical charge, entropy. Each element has power outputs through which one or more energies can flow. Bond graph terminology is given in Table 1. In the bond graph method, information exchange between the elements that make up the system is realized with state variables. These state variables are expressed by external variable/effort (e) and internal variables/flow (f).

- Power variables

$$P(t) = e(t).f(t) \tag{6}$$

  e(t) : effort

  f(t) : flow

- Energy variables

$$p(t) = \int e(\tau)d\tau \tag{7}$$

$$q(t) = \int f(\tau)d\tau \tag{8}$$

  p(t) : momentum

  q(t) : displacement

- 4 generalized variables e, f, p, q

- 3 passive elements (power recivers)

  R: energy dispersal

Table 1: Bond Graph Terminology

	Effort (e)	**Flow (f)**	**Momentum (p)**	**Displacement (q)**
Mechanical Translation	Force	Speed	Impulse	Displacement
Mechanical Rotation	Torque	Angular Speed	Angular Impulse	Angle
Hydraulics	Pression	Volume Flow Rate	Pression Impulse	Volume
Electric	Voltage	Current	Magnetic Flux	Charge
Magnetic	Magneto motor Force	Derivative Magnetic Flux		Magnetic Flux
Chemical	Chemical Potential	Molar Flow		Molar Mass
Thermodynamics	Temperature	Entropy Flow		Entropy

Element R is used to model any direct algebraic constitutive relation between effort and flow. R is a dissipative element of energy. For example, Electric resistor , viscous mechanical damping , static torque velocity relationships , diode, hydraulic head loss, any friction phenomenon [8].

C, I : energy stroing

Element C is used to model any physical phenomenon linking effort and displacement.C is a potential energy storing element. For example, capacitor, spring, fluid compressibility [8].

Element I is used to model any physical phenomenon linking momentum and flow. I is a kinetic energy storing element. For example , mass, moment of inertia, fluid inertia [8].

- 2 active elements (power providers)

  Se, Sf: effort and flow sources

  The Se element is used to model any physical phenomenon where effort is imposed independently of the flow. Se is an energy source element. For example, gravity force, voltage generator [8].

The Sf element is used to model any physical phenomenon where flow is imposed independently of the effort. Sf is an energy source element. For example, applied speed, current generator [8].

- 4 junction elements (power conservers)

  0 (zero) : parallel connection (The junction 0 is used to couple the elements subjected to the same effort.)

  1 (one) : series connection (The junction 1 is used to couple the elements subjected to the same flow.)

  TF, GY : domain interconnection (The TF junction is used to link variables of the same type in different domains.For example , electrical transformer, pulley systems , gear systems , lever. The GY junction is used to couple opposite type variables (effort flow) in different domains.For example , electric motor, gyroscope, hall effect sensor.)

  They are used to interconnect active elements (Se, Sf) with passive elements (R, C, I). They describe the architecture (topology) of the studied system.

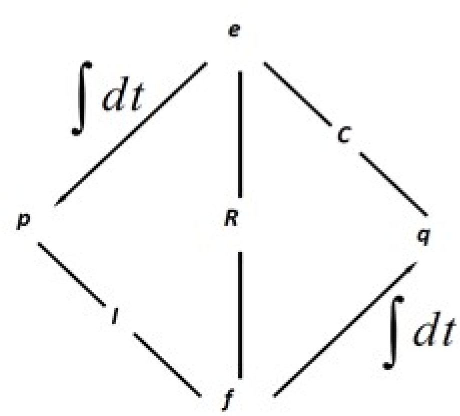

Figure 11: Representation of energy/power balance with Paynter's Tetrahedron [23]

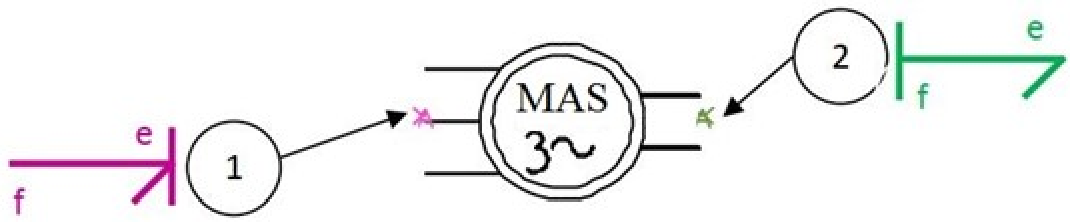

Figure 12: Bond -graph diagram of induction motor [9]

Shown in Figure 12 is the bond graph diagram of the asynchronous machine. In bond-graph representation, the asynchronous electric machine is gyrator element. The input of port 1 in the diagram represents voltage applied to the first element (three phase), and the input of port 2 represents angular speed applied to the second element and angular position to the second element.The output of port 1 in the diagram represents current fixed by second element, and the output of port 2 represents torque fixed by second element.

CHAPTER V

MODELING AND SIMULATION OF ASYNCHRONOUS MOTOR

Modeling of physical systems is possible only under certain assumptions. It will prevent the model to be obtained from these assumptions from becoming complicated and the system behavior will be determined based on this model, and the development of system and control algorithms will be facilitated. If the model does not fully reflect the system behavior, the assumptions made need to be reconsidered. The assumptions made in obtaining the model of the asynchronous machine are that the stator windings are spread evenly around the stator and it will be assumed that the flux change in the air gap changes sinusoidally. Three-phase stator windings shall be assumed to be uniformly radiated with an electric angle of 120° to the environment. The effects of saturation, tooth and groove will be neglected. Hysteresis and fuco losses will be neglected. The permeability of the magnetic parts will be considered infinite. The skin effect will be neglected. It will be assumed that the rotor bars are spread symmetrically around the circumference. The variation of resistors and inductances with temperature and frequency will be neglected. Each rod of the rotor will be assumed as a rotor phase winding.

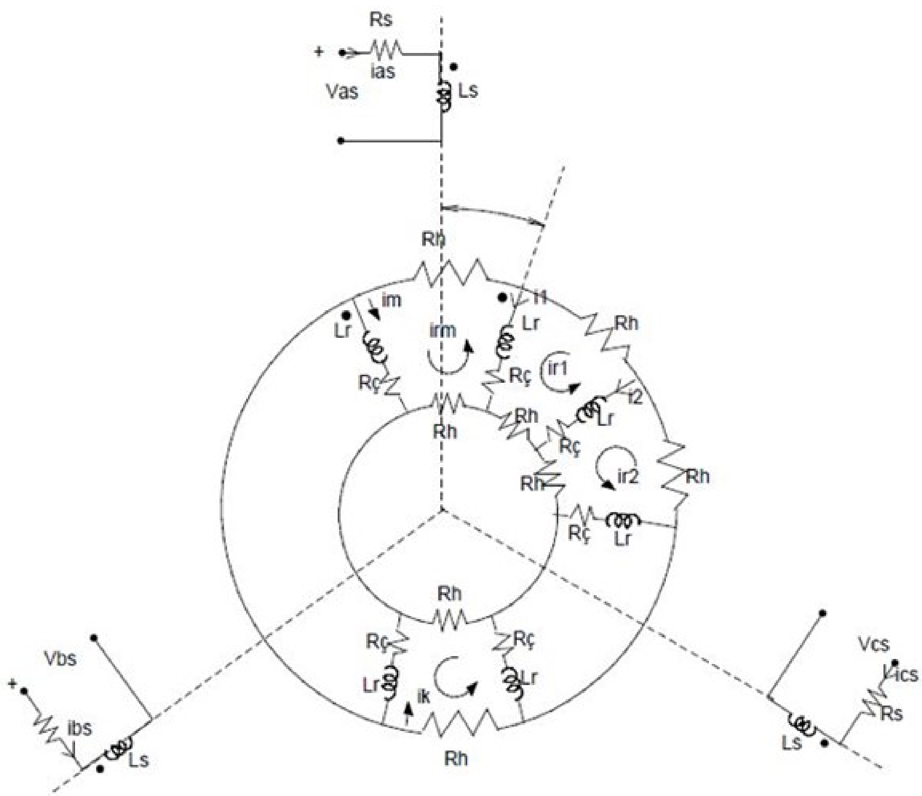

Figure 13: Equivalent circuit of asynchronous motor with stator three-phase short-circuit rotor [12]

- L_s = Stator winding inductance
- L_r = Rotor winding inductance
- M_m = The maximum value of the opposing inductance between rotor and stator
- R_s = Stator resistance
- R_h = Ring resistance between two bars
- R_c = Bar resistance
- M_{ss} = Mutual inductance between stator phase windings

- M_{rr} = Mutual inductance between stator phase windings
- g = Air gap
- A = Air gap cross section
- N_r = Number of rotor bars
- N_s = Number of stator windings
- m = Rotor phase number

The representations of these parameters are expressed as the following Equations (9-12), taking the stator three-phase and the rotor m-phase.

$$[R_s] = \begin{bmatrix} R_s & 0 & 0 \\ 0 & R_s & 0 \\ 0 & 0 & R_s \end{bmatrix}_{3x3} \tag{9}$$

$$[L_s] = \begin{bmatrix} L_s & M_{ss} & M_{ss} \\ M_{ss} & L_s & M_{ss} \\ M_{ss} & M_{ss} & L_s \end{bmatrix}_{3x3} \tag{10}$$

$$[R_r] = \begin{bmatrix} 2(R_h + R_c) & -R_c & 0... & 0... & -R_c \\ -R_c & 2(R_h + R_c) & -R_c & 0... & 0 \\ \vdots & \vdots & \vdots & \vdots & \vdots \\ \vdots & \vdots & \vdots & \vdots & \vdots \\ -R_c & 0 & 0... & -R_c & 2(R_h + R_c) \end{bmatrix}_{m*m} \tag{11}$$

$$[L_r] = \begin{bmatrix} L_r & M_{rr} & . & . & M_{rr} \\ M_{rr} & L_r & . & . & M_{rr} \\ . & . & . & . & \vdots \\ . & . & . & . & \vdots \\ M_{rr} & . & . & . & L_r \end{bmatrix}_{m*m} \tag{12}$$

The mutual inductance matrix between the stator phase windings and the rotor bars is given in Eq. (13) , depending on the angular position of the machine [12].

$$[M_{s,r}(\theta)] = M_m \begin{bmatrix} \cos(p\theta) & \cos(p\theta + \frac{2\pi}{3}) & ... & \cos(p\theta + \frac{(2m-1)\pi}{m}) \\ \cos(p\theta - \frac{2\pi}{3}) & \cos(p\theta - \frac{2\pi}{3} + \frac{2\pi}{m}) & ... & \cos(p\theta - \frac{2\pi}{3} + \frac{2(m-1))\pi}{m}) \\ \cos(p\theta + \frac{2\pi}{3}) & \cos(p\theta + \frac{2\pi}{3} + \frac{2\pi}{m}) & ... & \cos(p\theta + \frac{2\pi}{3} + \frac{2(m-1))\pi}{m}) \end{bmatrix}_{3*m} \tag{13}$$

In contrast, the mutual inductance between the rotor bars and the stator phase windings is given in Eq. (14).

$$[M_{r,s}(\theta)] = [M_{s,r}(\theta)]^T \tag{14}$$

By combining the rotor and stator inductances, the total inductance matrix is given in Eq. (15) ;

$$[L_{r,s}(\theta)] = \begin{bmatrix} [L_s] & [M_{s,r}(\theta)] \\ [M_{r,s}(\theta)] & [L_r] \end{bmatrix} \tag{15}$$

Current and voltage expressions are expressed as vectors as in Equations (16-19).

$$[I_s] = \begin{bmatrix} i_{as} \\ i_{bs} \\ i_{cs} \end{bmatrix} \tag{16}$$

$$[V_s] = \begin{bmatrix} V_{as} \\ V_{bs} \\ V_{cs} \end{bmatrix} \tag{17}$$

$$[V_r] = \begin{bmatrix} 0 \\ 0 \\ \vdots \\ 0 \end{bmatrix} \tag{18}$$

$$[I_r] = \begin{bmatrix} i_{r1} \\ i_{r2} \\ \vdots \\ i_{rm} \end{bmatrix} \tag{19}$$

The stator and rotor phase fluxes are expressed in vector form as in Eqs. (20) and (21) ;

$$[\psi_s] = \begin{bmatrix} \psi_{as} \\ \psi_{bs} \\ \psi_{cs} \end{bmatrix} \tag{20}$$

$$[\psi_r] = \begin{bmatrix} \psi_{r1} \\ \psi_{r2} \\ \vdots \\ \psi_{rm} \end{bmatrix} \tag{21}$$

Stator and rotor flux-current relations are given in Eqs. (22) and (23).

$$[\psi_s] = [L_s][I_s] + [M_{s,r}(\theta)][I_r] \tag{22}$$

$$[\psi_r] = [L_r]\,[I_r] + [M_{r,s}(\theta)]\,[I_s] \tag{23}$$

Using the expressions defined above for the stator and rotor equivalent circuit equations, Eqs. (24) and (25) are obtained in matrix form [30].

$$[V_s] = [R_s]\,[I_s] + \frac{d}{dt}\,[\psi_s] = [R_s]\,[I_s] + \frac{d}{dt}\left\{[L_s]\,[I_s] + [M_{s,r}(\theta)]\,[I_r]\right\} \tag{24}$$

$$[0] = [R_r]\,[I_r] + \frac{d}{dt}\,[\psi_r] = [R_r]\,[I_r] + \frac{d}{dt}\left\{[L_r]\,[I_r] + [M_{r,s}(\theta)]\,[I_s]\right\} \tag{25}$$

The torque equation of the machine is given in Eq. (26).

$$T_e = \frac{1}{2}\left[[I_s]^T\,[I_r]^T\right]\frac{\partial}{\partial\theta}\left[L_{s,r}\left(\theta\right)\right]\begin{bmatrix}[I_s]\\ [I_r]\end{bmatrix} = J\frac{d^2\theta}{dt^2} + B\frac{d\theta}{dt} \tag{26}$$

- p = Number of poles
- θ = The motor shaft rotation angle
- J = Rotor Inertia
- B = Total Coefficient of Friction

According to all these assumptions, since the model of the asynchronous machine in this structure is non-linear and depends on θ , it is not suitable for analysis, simulation and application of control algorithms. The machine model equations will be reduced by using the symmetrical components method. Transformation matrices will be in orthogonal structure and will be arranged according to the power invariance principle [12].

$$[\Gamma]^{-1} = [\Gamma]^{T*} \tag{27}$$

The transformation matrix given in Eq. (27) is called the matrix of symmetric components. Since the rotor and stator phase numbers are different from each other, the following transformation matrices will be used in the transformation of rotor and stator expressions is given in Eq. (28).

$$[\Gamma_S] = \frac{1}{\sqrt{3}} \begin{bmatrix} 1 & 1 & 1 \\ 1 & a & a^2 \\ 1 & a^2 & a \end{bmatrix} ; [\Gamma_R] = \frac{1}{\sqrt{m}} \begin{bmatrix} 1 & 1 & \cdots & 1 \\ 1 & b & \cdots & b^{m-1} \\ \vdots & \vdots & \vdots & \vdots \\ \vdots & \vdots & \vdots & \vdots \\ 1 & b^{m-1} & \cdots & b^{(m-1)^2} \end{bmatrix} \tag{28}$$

When the transformation matrices are applied to the current and voltage vectors, the transformed stator voltage and current expressions and rotor current expressions are given in Eq. (29).

$$[V_s]_{0,+,-} = [\Gamma_S]\,[V_s] \;\; ; [I_s]_{0,+,-} = [\Gamma_S]\,[I_s] \;\; ; [I_r]_{0,+,-} = [\Gamma_R]\,[I_r] \tag{29}$$

The components of these vectors are given in Eq. (30).

$$[V_s]_{0,+,-} = \begin{bmatrix} V_{s0} \\ V_{s+} \\ V_{s-} \end{bmatrix} \;\; ; [I_s]_{0,+,-} = \begin{bmatrix} i_{s0} \\ i_{s+} \\ i_{s-} \end{bmatrix} \;\; ; [I_r]_{0,+,-} = \begin{bmatrix} i_{r0} \\ i_{r1} \\ \vdots \\ i_{rm-1} \end{bmatrix} \tag{30}$$

The expressions and matrices described above have been applied to Eqs. (24) , (25) and (26). Then, Eqs. (31), (32) and (33) equations have been obtained [31].

$$[V_s]_{0,+,-} = [\Gamma_s]\,[R_s]\,[\Gamma_s]^{-1}\,[I_s]_{0,+,-} + [\Gamma_s]\,\frac{d}{dt}\left\{[L_s]\,[\Gamma_s]^{-1}\,[I_s]_{0,+,-} + \left[M_{s,r(\theta)}\,[\Gamma_R]^{-1}\,[I_r]_{0,+,-}\right]\right\} \tag{31}$$

$$[0] = [\Gamma_R]\,[R_r]\,[\Gamma_R]^{-1}\,[I_r]_{0,+,-} + [\Gamma_R]\,\frac{d}{dt}\left\{[L_r]\,[\Gamma_R]^{-1}\,[I_r]_{0,+,-} + \left[M_{r,s(\theta)}\,[\Gamma_s]^{-1}\,[I_s]_{0,+,-}\right]\right\} \tag{32}$$

$$T_e = \frac{1}{2}\left[[I_s]_{0,+,-}^{*T}\,[\Gamma_s]^{-1*} : [I_r]_{0,+,-}^{*T}\,[\Gamma_r]^{-1*}\right]\frac{\partial}{\partial\theta}\left\{[M_{s,r}(\theta)]\right\}\begin{bmatrix}[\Gamma_s]^{-1} & [I_s]_{0,+,-}\\ [\Gamma_r]^{-1} & [I_r]_{0,+,-}\end{bmatrix} = J\frac{d^2\theta}{dt^2}+B\frac{d\theta}{dt} \tag{33}$$

Eqs. (31), (32) and (33) have been rearranged. The new forms of these equations are given in Eqs. (34-37).

$$\begin{aligned}[V_s]_{0,+,-} = [\Gamma_s]\,[R_s]\,[\Gamma_s]^{-1}\,[I_s]_{0,+,-} + [\Gamma_s]\,[L_s]\,[\Gamma_s]\,\frac{d\,[I_s]_{0,+,-}}{dt} + ...\\ [\Gamma_s]\,\frac{\partial\,[M_{s,r}(\theta)]}{\partial\theta}\,[\Gamma_R]^{-1}\,\frac{d\theta}{dt} + [\Gamma_s]\,[M_{s,r}(\theta)]\,[\Gamma_R]^{-1}\,\frac{d\,[I_r]_{0,+,-}}{dt}\end{aligned} \tag{34}$$

$$\begin{aligned}[0] = [\Gamma_R]\,[R_r]\,[\Gamma_R]^{-1}\,[I_r]_{0,+,-} + [\Gamma_R]\,[L_r]\,[\Gamma_R]\,\frac{d\,[I_r]_{0,+,-}}{dt} + ...\\ [\Gamma_R]\,\frac{\partial\,[M_{r,s}(\theta)]}{\partial\theta}\,[\Gamma_s]^{-1}\,\frac{d\theta}{dt} + [\Gamma_R]\,[M_{r,s}(\theta)]\,[\Gamma_s]^{-1}\,\frac{d\,[I_s]_{0,+,-}}{dt}\end{aligned} \tag{35}$$

$$[L_s]_{0,+,-} = [\Gamma_s]\,[L_s]\,[\Gamma_s]^{-1} = \begin{bmatrix} L_{s0} & 0 & 0\\ 0 & L_{s+} & 0\\ 0 & 0 & L_{s-}\end{bmatrix} \tag{36}$$

$$[L_r] = [\Gamma_R]\,[L_r]\,[\Gamma_R]^{-1} = \begin{bmatrix} L_{r0} & 0 & 0 & \cdots & 0\\ 0 & L_{r1} & 0 & \cdots & 0\\ 0 & 0 & L_{r2} & \cdots & 0\\ \vdots & \vdots & \vdots & \ddots & \vdots\\ 0 & 0 & 0 & \cdots & L_{r(m-1)}\end{bmatrix} \tag{37}$$

Here ;

$$L_{s0} = L_s + 2M_{ss};\ L_{s+} = L_{s-} = L_s + M_{ss} \tag{38}$$

$$L_{r0} = L_r + mM_{rr};\ L_{rk} = L_{r(m-k)} = L_r + M_{rr};\ k = 1, 2, \cdots, m-1 \tag{39}$$

$$L_{r+} = L_{r-} = L_r + M_{rr} \tag{40}$$

When the equations are rearranged according to Eqs. (38), (39) and (40);

$$[L_{sr}]_{0,+,-} = [\Gamma_s]\,[M_{s,r}(\theta)]\,[\Gamma_R]^{-1} = \frac{\sqrt{3m}}{2} M_m \begin{bmatrix} 0 & 0 & 0 & \cdots & 0 \\ 0 & e^{jp\theta} & 0 & \ddots & 0 \\ 0 & 0 & 0 & \cdots & e^{-jp\theta} \end{bmatrix} \tag{41}$$

$$[L_{r,s}]_{0,+,-} = [L_s]^T_{0,+,-} = [\Gamma_R]\,[M_{r,s}(\theta)]\,[\Gamma_s] = \frac{\sqrt{3m}}{2} M_m \begin{bmatrix} 0 & 0 & 0 \\ 0 & e^{-jp\theta} & 0 \\ 0 & 0 & 0 \\ \vdots & \vdots & \vdots \\ 0 & 0 & e^{jp\theta} \end{bmatrix} \tag{42}$$

$$\frac{\partial\,[L_{s,r}]_{0,+,-}}{\partial\theta} = [\Gamma_s]\,\frac{\partial\,[M_{r,s}(\theta)]}{\partial\theta}\,[\Gamma_R]^{-1} = jp\frac{\sqrt{3m}}{2} M_m \begin{bmatrix} 0 & 0 & 0 & \cdots & 0 \\ 0 & e^{jp\theta} & 0 & \cdots & 0 \\ 0 & 0 & 0 & \cdots & e^{-jp\theta} \end{bmatrix} \tag{43}$$

$$\frac{\partial\,[M_{r,s}]_{0,+,-}}{\partial\theta} = \frac{\partial\,[M_{s,r}]^T_{0,+,-}}{\partial\theta} = [\Gamma_R]\,\frac{\partial\,[M_{r,s}(\theta)]}{\partial\theta}\,[\Gamma_s]^{-1} = jp\frac{\sqrt{3m}}{2} M_m \begin{bmatrix} 0 & 0 & 0 \\ 0 & e^{-jp\theta} & 0 \\ 0 & 0 & 0 \\ \vdots & \vdots & \vdots \\ 0 & 0 & e^{jp\theta} \end{bmatrix} \tag{44}$$

$$T_e = \frac{1}{2}\left[[I_s]^{*T}_{0,+,-}\,[\Gamma_s]^{-1*T}\,\frac{\partial\,[M_{r,s}]}{\partial\theta} + [\Gamma_R]^{-1}\,[I_r]_{0,+,-} + [I_r]^{*T}_{0,+,-}\,[\Gamma_R]^{-1*T}\,\frac{\partial\,[M_{r,s}]}{\partial\theta}\,[\Gamma_s]^{-1}\,[I_s]_{0,+,-} \right] = J\frac{d^2\theta}{dt^2} + B\frac{d\theta}{dt} \tag{45}$$

Here;

$$[\Gamma_s]^{-1*T}\frac{\partial\left[M_{s,r}\left(\theta\right)\right]}{\partial\theta}[\Gamma_R]^{-1}=[\Gamma_s]\frac{\partial\left[M_{s,r}\left(\theta\right)\right]}{\partial\theta}[\Gamma_R]^{-1} \tag{46}$$

$$[\Gamma_R]^{-1*T}\frac{\partial\left[M_{r,s}\left(\theta\right)\right]}{\partial\theta}[\Gamma_s]^{-1}=[\Gamma_R]\frac{\partial\left[M_{r,s}\left(\theta\right)\right]}{\partial\theta}[\Gamma_s]^{-1} \tag{47}$$

The torque expression is expressed as in Eqs. (48) and (49).

$$\begin{aligned} T_e = \begin{bmatrix} i_{s0}^* & i_{s1}^* & i_{s2}^* \end{bmatrix} = j\frac{\sqrt{3m}}{2}M_m \begin{bmatrix} 0 & 0 & 0 & \cdots & 0 \\ 0 & e^{jp\theta} & 0 & \ddots & 0 \\ 0 & 0 & 0 & \cdots & e^{-jp\theta} \end{bmatrix} \begin{bmatrix} i_{r0} \\ i_{r1} \\ i_{r2} \\ \vdots \\ i_{rm-1} \end{bmatrix} + ... \\ \begin{bmatrix} i_{r0}^* & i_{r1}^* & i_{r2}^* & \cdots & i_{rm-1}^* \end{bmatrix} jp\frac{\sqrt{3m}}{2}M_m \begin{bmatrix} 0 & 0 & 0 \\ 0 & e^{-jp\theta} & 0 \\ 0 & 0 & 0 \\ \vdots & \vdots & \vdots \\ 0 & 0 & e^{jp\theta} \end{bmatrix} \begin{bmatrix} i_{s0} \\ i_{s1} \\ i_{s2} \end{bmatrix} \end{aligned} \tag{48}$$

$$T_e = \frac{\sqrt{3m}}{4}jpM_m[i_{s1}^* i_{r1} + i_{rm-1}^* i_{s1}]e^{jp\theta} - [i_{s2}^* i_{rm-1} + i_{r1}^* i_{s1}]e^{-jp\theta}] = J\frac{\mathrm{d}^2\theta}{\mathrm{d}^2 t} + B\frac{\mathrm{d}\theta}{\mathrm{d}t} \tag{49}$$

In a balanced voltage and current system, there is no zero component. The remaining term from the rotor components forms a linearly independent system of equations. This system of equations is given in Eq. (50).

$$0 = R_r i_{rk} + L_{rk}\frac{\mathrm{d}i_{rk}}{\mathrm{d}t} \tag{50}$$

If the terms that do not affect the torque generation are not taken into account, the system can be modeled with five equations [32] . The matrix form of these five equations in which the system is modeled is given in Eq. (51). The torque equation of the machine is expressed as in Eq. (52).

$$\begin{bmatrix} V_{s+} \\ V_{s-} \\ 0 \\ 0 \end{bmatrix} = \begin{bmatrix} R_s & 0 & 0 & 0 \\ 0 & R_s & 0 & 0 \\ 0 & 0 & R_{rr} & 0 \\ 0 & 0 & 0 & R_{rr} \end{bmatrix} \begin{bmatrix} i_{s+} \\ i_{s-} \\ i_{r+} \\ i_{r-} \end{bmatrix} + ...$$

$$\begin{bmatrix} L_{s+} & 0 & \frac{\sqrt{3m}}{2} M_m e^{jp\theta} & 0 \\ 0 & L_{s-} & 0 & \frac{\sqrt{3m}}{2} M_m e^{-jp\theta} \\ \frac{\sqrt{3m}}{2} M_m e^{jp\theta} & 0 & L_{r+} & 0 \\ 0 & \frac{\sqrt{3m}}{2} M_m e^{-jp\theta} & 0 & L_{r-} \end{bmatrix} \frac{\mathrm{d}}{\mathrm{d}t} \begin{bmatrix} i_{s+} \\ i_{s-} \\ i_{r+} \\ i_{r-} \end{bmatrix} + ... \tag{51}$$

$$\frac{\mathrm{d}\theta}{\mathrm{d}t} M_m \begin{bmatrix} 0 & 0 & \frac{jp\sqrt{3m}}{2} e^{jp\theta} & 0 \\ 0 & 0 & 0 & \frac{jp\sqrt{3m}}{2} e^{jp\theta} \\ \frac{jp\sqrt{3m}}{2} e^{-jp\theta} & 0 & 0 & 0 \\ 0 & \frac{jp\sqrt{3m}}{2} e^{jp\theta} & 0 & 0 \end{bmatrix} \begin{bmatrix} i_{s+} \\ i_{s-} \\ i_{r+} \\ i_{r-} \end{bmatrix}$$

$$T_e = jp\frac{\sqrt{3m}}{4} M_m [i_{s+} i_{r+} + i_{r-} i_{s-}] e^{jp\theta} - [i_{s-} i_{r-} + i_{r+} i_{s+}] e^{-jp\theta}] \tag{52}$$

There are two important transformations used in an induction motor. These are Clarke and Park transformations. The Clarke transform converts the time-domain components of a three-phase system in an abc reference frame to components in a stationary α β 0 reference frame [10]. The Clarke-Park conversion; however, divides the stator current into two components as in a direct current motor [10].

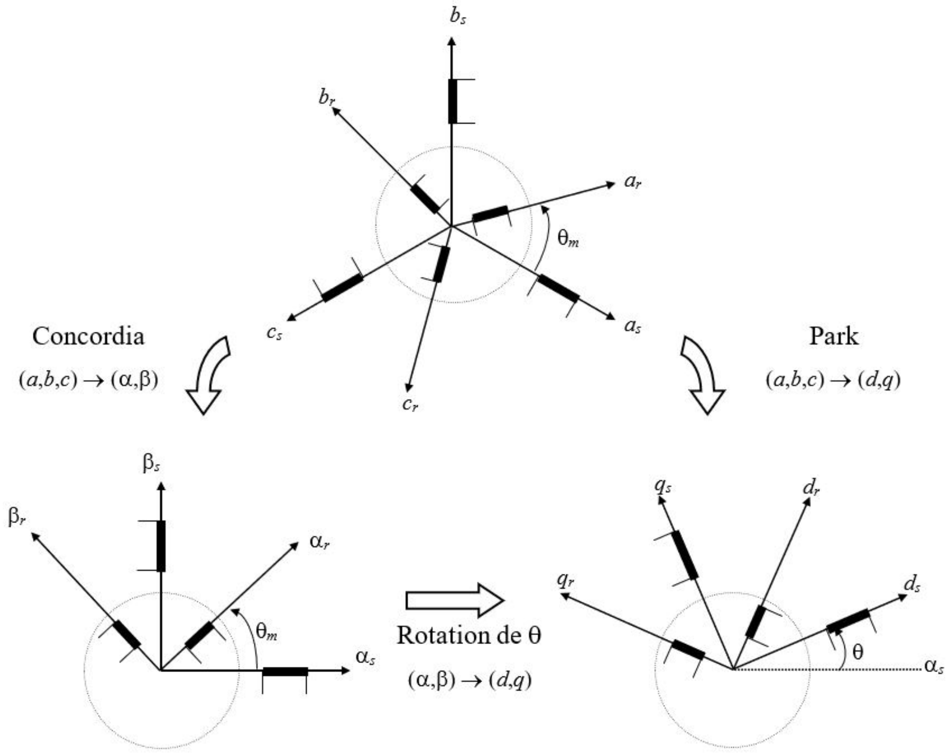

Figure 14: Park-Clarke transformation diagram [9]

5.1 *Transformation in α - β axes set*

Rotor variables are expressed in axes fixed on the rotor, and stator variables are expressed in axes fixed on the stator. The same orthogonal transform matrices can be used for the stator and rotor. The transformation matrix from the α - β -axis set to symmetrical components is expressed as in Eq. (53).

$$[\tau]_{(\alpha,\beta),(+,-)} = \frac{1}{\sqrt{2}} \begin{bmatrix} 1 & 1 \\ -j & j \end{bmatrix} \tag{53}$$

The matrix providing the inverse transform is expressed as in Eq. (54) ;

$$[\tau]_{(+,-)),(\alpha,\beta)} = [\tau]^{T*}_{(\alpha,\beta),(+,-)} \tag{54}$$

The relationship between the expressions of the current and voltage magnitudes related to the stator and rotor in the +,- axes and the axes standing on the stator and rotor are as in Equations (55-57) .

$$[V_s^S]_{\alpha,\beta} = [\tau]_{\alpha\beta,+-}[V_s]_{+,-} \tag{55}$$

$$[I_s^S]_{\alpha,\beta} = [\tau]_{\alpha\beta,+-}[I_s]_{+,-} \tag{56}$$

$$[I_r^R]_{\alpha,\beta} = [\tau]_{\alpha\beta,+-}[I_r]_{+,-} \tag{57}$$

The model of the machine in α - β axis sets in the stator and rotor is obtained as in Eqs. (58) and (59).

$$\begin{bmatrix} V_{s\alpha}^S \\ V_{s\beta}^S \\ 0 \\ 0 \end{bmatrix} = \begin{bmatrix} R_s & 0 & 0 & 0 \\ 0 & R_s & 0 & 0 \\ 0 & 0 & R_{rr} & 0 \\ 0 & 0 & 0 & R_{rr} \end{bmatrix} \begin{bmatrix} i_{s\alpha}^S \\ i_{s\beta}^S \\ i_{r\alpha}^R \\ i_{r\beta}^R \end{bmatrix} + ...$$

$$\begin{bmatrix} L_{s\alpha} & 0 & \frac{\sqrt{3m}}{2}M_{sr}\cos p\theta & -\frac{\sqrt{3m}}{2}M_{sr}\sin p\theta \\ 0 & L_{s\beta} & \frac{\sqrt{3m}}{2}M_{sr}\sin p\theta & \frac{\sqrt{3m}}{2}M_{sr}\cos p\theta \\ \frac{\sqrt{3m}}{2}M_{sr}\cos p\theta & \frac{\sqrt{3m}}{2}M_{sr}\sin p\theta & L_{r\alpha} & 0 \\ -\frac{\sqrt{3m}}{2}M_{sr}\sin p\theta & \frac{\sqrt{3m}}{2}M_{sr}\cos p\theta & 0 & L_{r\beta} \end{bmatrix} ... \tag{58}$$

$$\frac{\mathrm{d}}{\mathrm{d}t} \begin{bmatrix} i_{s\alpha}^S \\ i_{s\beta}^S \\ i_{r\alpha}^R \\ i_{r\beta}^R \end{bmatrix} + \frac{\mathrm{d}\theta}{\mathrm{d}t}\frac{p\sqrt{3m}}{2}M_{sr} \begin{bmatrix} 0 & 0 & -\sin p\theta & -\cos p\theta \\ 0 & 0 & \cos p\theta & -\sin p\theta \\ -\sin p\theta & \cos p\theta & 0 & 0 \\ -\cos p\theta & -\sin p\theta & 0 & 0 \end{bmatrix} \begin{bmatrix} i_{s\alpha}^S \\ i_{s\beta}^S \\ i_{r\alpha}^R \\ i_{r\beta}^R \end{bmatrix}$$

$$T_e = p\frac{\sqrt{3m}}{4}M_{sr}\left[\left(i_{r\alpha}^R i_{s\beta}^S - i_{r\beta}^R i_{s\alpha}^S\right)\cos p\theta - \left(i_{r\alpha}^R i_{s\alpha}^S + i_{r\beta}^R i_{s\beta}^S\right)\sin p\theta\right] \tag{59}$$

The mutual inductances in the model change sinusoidally depending on θ . Instead of this model, the rotor and stator will be reduced to a fixed α - β axis set in the stator. Rotor expressions defined in rotor standing axes must be transformed to stator axes set. For this purpose, the transformation matrix expressed in Eq. (60) was used.

$$[\Gamma]_{R,S} = \begin{bmatrix} \cos p\theta & -\sin p\theta \\ \sin p\theta & \cos p\theta \end{bmatrix} \tag{60}$$

The currents defined in the rotor axes are expressed as in Eq. (61) in the axes fixed in the stator by using the transformation matrix in Eq. (60) .

$$\begin{bmatrix} i_{r\alpha}^{S} \\ i_{r\beta}^{S} \end{bmatrix} = \begin{bmatrix} \cos p\theta & -\sin p\theta \\ \sin p\theta & \cos p\theta \end{bmatrix} \begin{bmatrix} i_{r\alpha}^{R} \\ i_{r\beta}^{R} \end{bmatrix} \tag{61}$$

The model of the machine in the α - β axis set standing still on the stator is in Eqs. (62) and (63).

$$\begin{aligned} \begin{bmatrix} V_{s\alpha} \\ V_{s\beta} \\ 0 \\ 0 \end{bmatrix} &= \begin{bmatrix} R_s & 0 & 0 & 0 \\ 0 & R_s & 0 & 0 \\ 0 & 0 & R_r^{'} & 0 \\ 0 & 0 & 0 & R_r^{'} \end{bmatrix} \begin{bmatrix} i_{s\alpha} \\ i_{s\beta} \\ i_{r\alpha} \\ i_{r\beta} \end{bmatrix} + \begin{bmatrix} L_s & 0 & L_m & 0 \\ 0 & L_s & 0 & L_m \\ L_m & 0 & L_r^{'} & 0 \\ 0 & L_m & 0 & L_r^{'} \end{bmatrix} \cdots \\ &\frac{\mathrm{d}}{\mathrm{d}t} \begin{bmatrix} i_{s\alpha} \\ i_{s\beta} \\ i_{r\alpha} \\ i_{r\beta} \end{bmatrix} + \begin{bmatrix} 0 & -L_s & L_m & 0 \\ L_s & 0 & 0 & L_m \\ L_m & 0 & 0 & -L_r^{'} \\ 0 & L_m & L_r^{'} & 0 \end{bmatrix} \begin{bmatrix} i_{s\alpha} \\ i_{s\beta} \\ i_{r\alpha} \\ i_{r\beta} \end{bmatrix} p\omega \end{aligned} \tag{62}$$

$$T_e = L_m \left(i_{s\beta} i_{r\alpha} - i_{s\alpha} i_{r\beta} \right) \tag{63}$$

As in transformers, the reduction must be done between the stator and the rotor. The reduction coefficient is expressed as in Eq. (64).

$$u = \frac{K_s N_s}{K_r N_r} \tag{64}$$

- N_s = Number of turns of stator phase windings
- N_r = Number of turns of rotor phase windings
- K_s = Stator winding factor
- K_r = Rtator winding factor

The reduction operation was applied to all rotor expressions. These expressions are given in Eqs. (65) and (66) .

$$i_{r\alpha}^S = \frac{i_{r\alpha}^R}{u} = i_{r\alpha};\ i_{r\beta}^S = \frac{i_{r\beta}^R}{u} = i_{r\beta} \tag{65}$$

$$R_r' = u^2 R_r;\ L_r' = u^2 L_r;\ L_m = u^2 \sqrt{\frac{3m}{2}} M_{sr} \tag{66}$$

The flux and current expressions in the model in the still standing axis set are as in Eqs. (67) and (68) .

$$\psi_{s\alpha} = L_s i_{s\alpha} + L_m i_{r\alpha};\ \psi_{r\alpha} = L_r^{'} i_{r\alpha} + L_m i_{s\alpha} \tag{67}$$

$$\psi_{s\beta} = L_s i_{s\beta} + L_m i_{r\beta};\ \psi_{r\beta} = L_r^{'} i_{r\beta} + L_m i_{s\beta} \tag{68}$$

The stator and rotor inductances given in Eq. (69) can be expressed in terms of the mutual inductance and leakage inductances that create the air gap flux.

$$L_s = L_{s\sigma} + L_m;\ L_r^{'} = L_{r\sigma}^{'} + L_m \tag{69}$$

- $L_{s\sigma}$ = Leakage inductance of the stator

- $L_{r\sigma}$ = Leakage inductance of the rotor

The air flux expressions are as in Equations (70-72).

$$\psi_{s\alpha} = L_{s\sigma} i_{s\sigma} + L_m (i_{r\alpha} + i_{s\alpha});\ \psi_{m\alpha} = L_m (i_{r\alpha} + i_{s\alpha}) \tag{70}$$

$$\psi_{r\alpha} = L_{r\sigma}^{'} i_{r\alpha} + L_m (i_{r\alpha} + i_{s\alpha});\ \psi_{s\beta} = L_{s\sigma} i_{s\beta} + L_m (i_{r\beta} + i_{s\beta}) \tag{71}$$

$$\psi_{m\beta} = L_m (i_{r\beta} + i_{s\beta});\ \psi_{r\beta} = L_{r\sigma}^{'} i_{r\beta} + L_m (i_{r\beta} + i_{s\beta}) \tag{72}$$

The torque expression in terms of stator and rotor fluxes is as in Eq. (73).

$$T_e = p \frac{L_m}{\sigma L_s L_r'} \left(\psi_{s\beta} \psi_{r\alpha} - \psi_{s\alpha} \psi_{r\beta} \right) \tag{73}$$

The torque expression in terms of stator current and air gap flux is as in Eq. (74).

$$T_e = p \left(i_{s\beta} \psi_{m\alpha} - i_{s\alpha} \psi_{m\beta} \right) \tag{74}$$

The definition of the leakage factor is given in Eq. (75).

$$\sigma = 1 - \frac{L_m^2}{L_s L_r'} \tag{75}$$

The stator phase voltages are defined in the a-b-c axis set with 120° phase differences from each other in the stator. Clarke transform is applied between these axes and the 0-α-β axes. This transformation is given in Eq. (76).

$$\begin{bmatrix} V_o \\ V_a \\ V_\beta \end{bmatrix} = \sqrt{\frac{2}{3}} \begin{bmatrix} \frac{\sqrt{2}}{2} & \frac{\sqrt{2}}{2} & \frac{\sqrt{2}}{2} \\ 1 & -\frac{1}{2} & -\frac{1}{2} \\ 0 & \frac{\sqrt{3}}{2} & -\frac{\sqrt{3}}{2} \end{bmatrix} \begin{bmatrix} V_{sa} \\ V_{sb} \\ V_{sc} \end{bmatrix} \tag{76}$$

Motor phase voltages are defined as in equations (77-79).

$$V_{sa} = V_m.sin(\theta_s) \tag{77}$$

$$V_{sb} = V_m.sin(\theta_s + \frac{2\pi}{3}) \tag{78}$$

$$V_{sc} = V_m.sin(\theta_s - \frac{2\pi}{3}) \tag{79}$$

Here $\theta_s = \int_0^t \omega_s dt = 2\pi \int_0^t f_s dt$. f_s is the frequency of the stator voltage. V_α and V_β terms are given in Eqs. (80) and (81).

$$V_\alpha = \sqrt{\frac{3}{2}} V_m \sin\theta_s \tag{80}$$

$$V_\beta = \sqrt{\frac{3}{2}} V_m \cos\theta_s \tag{81}$$

V_α and V_β are sinusoidal components. The model of the machine in the α and β axis is defined as in Equations (82-86).

$$\frac{\mathrm{d}i_{s\alpha}}{\mathrm{d}t} = \tfrac{1}{\sigma L_s}(\tfrac{L_m}{L_r'}(\tfrac{R_r'}{L_r'}\psi_{r\alpha} + pw\psi_{r\beta}) - R_e i_{sa} + V_{sa}) \tag{82}$$

$$\frac{\mathrm{d}i_{s\beta}}{\mathrm{d}t} = \tfrac{1}{\sigma L_s}(\tfrac{L_m}{L_r'}(\tfrac{R_r'}{L_r'}\psi_{r\beta} + pw\psi_{r\alpha}) - R_e i_{s\beta} + V_{s\beta}) \tag{83}$$

$$\frac{\mathrm{d}\psi_{r\alpha}}{\mathrm{d}t} = -(\tfrac{R_r'}{L_r'})\psi_{r\alpha} - pw\psi_{r\beta} + \tfrac{R_r'+L_m}{L_r'} i_{s\alpha} \tag{84}$$

$$\frac{\mathrm{d}\psi_{r\beta}}{\mathrm{d}t} = -(\tfrac{R_r'}{L_r'})\psi_{r\beta} + pw\psi_{r\alpha} + \tfrac{R_r'+L_m}{L_r'} i_{s\beta} \tag{85}$$

$$\frac{\mathrm{d}\omega}{\mathrm{d}t} = \tfrac{p}{J}\tfrac{L_m}{L_r'}(\psi_{r\alpha} i_{s\beta} - \psi_{r\beta} i_{s\alpha}) - \tfrac{B}{J}\omega + \frac{1}{J}T_L \tag{86}$$

The equivalent resistance is defined as in Eq. (87).

$$R_E = R_s + \frac{R_r^{'} L_m^2}{L_r^{'2}} \tag{87}$$

5.2 Transformation in d-q axes set

To simplify the model equations, we use the park representation which is a two dimensions representation of a three-phased system. The Park theory provides a fine static and dynamic representation of three-phase systems. The rotor flux-oriented vector control method defines all other variables that define the rotor flux on the d axis with respect to the d axis and the q axis perpendicular to it. Thus, the rotor flux and torque can be controlled as in a direct current motor.

Using the α-β to d-q transformation matrix, the equation models in the d-q axis set are obtained. The matrix form obtained in the d-q axes set is given in Eq. (88). The torque expression at the d-q axes set of the machine is defined in Eq. (89).

$$\begin{bmatrix} V_{sd} \\ V_{sq} \\ 0 \\ 0 \end{bmatrix} = \begin{bmatrix} R_s & 0 & 0 & 0 \\ 0 & R_s & 0 & 0 \\ 0 & 0 & R_r^{'} & 0 \\ 0 & 0 & 0 & R_r^{'} \end{bmatrix} \begin{bmatrix} i_{sd} \\ i_{sq} \\ i_{rd} \\ i_{rq} \end{bmatrix} + ...$$
$$\begin{bmatrix} L_s & 0 & L_m & 0 \\ 0 & L_s & 0 & L_m \\ L_m & 0 & L_r^{'} & 0 \\ 0 & L_m & 0 & L_r^{'} \end{bmatrix} \frac{\mathrm{d}}{\mathrm{d}t} \begin{bmatrix} i_{sd} \\ i_{sq} \\ i_{rd} \\ i_{rq} \end{bmatrix} + ... \tag{88}$$
$$\begin{bmatrix} 0 & -\omega_s L_s & \omega_s L_m & 0 \\ \omega_s L_s & 0 & 0 & \omega_s L_m \\ \omega_s L_m & 0 & 0 & -\omega_s L_r \\ 0 & \omega_s L_m & \omega_s L_r & 0 \end{bmatrix} \begin{bmatrix} i_{sd} \\ i_{sq} \\ i_{rd} \\ i_{rq} \end{bmatrix}$$

$$T_e = pL_m\left(i_{sq}i_{rd} - i_{sd}i_{rq}\right) = J\frac{d^2\theta}{dt^2} + B\frac{d\theta}{dt} \tag{89}$$

Flux and current relations are defined similarly in the d-q axis set as in the α-β axis set. This relationship is given in Eqs. (90) and (91).

$$\psi_{sd} = L_s i_{sd} + L_m i_{rd};\ \psi_{rd} = L_r' i_{rd} + L_m i_{sd} \tag{90}$$

$$\psi_{sq} = L_s i_{sq} + L_m i_{rq};\ \psi_{rq} = L_r' i_{rq} + L_m i_{sq} \tag{91}$$

The equivalents of the stator d-q current and voltages in the obtained model in a-b-c are obtained by transformation. Γ_{0dq} is used for this. Conversion expressions for voltages and currents are given in Equations (92- 95).

$$\begin{bmatrix} V_{s0} \\ V_{sd} \\ V_{sq} \end{bmatrix} = \sqrt{\frac{2}{3}} \begin{bmatrix} \frac{1}{\sqrt{2}} & \frac{1}{\sqrt{2}} & \frac{1}{\sqrt{2}} \\ \cos\theta_s & \cos\left(\theta_s - \frac{2\pi}{3}\right) & \cos\left(\theta_s + \frac{2\pi}{3}\right) \\ -\sin\theta_s & -\sin\left(\theta_s - \frac{2\pi}{3}\right) & -\sin\left(\theta_s + \frac{2\pi}{3}\right) \end{bmatrix} \begin{bmatrix} V_{as} \\ V_{bs} \\ V_{cs} \end{bmatrix} \tag{92}$$

$$\begin{bmatrix} \frac{1}{\sqrt{2}} & \frac{1}{\sqrt{2}} & \frac{1}{\sqrt{2}} \\ \cos\theta_s & \cos\left(\theta_s - \frac{2\pi}{3}\right) & \cos\left(\theta_s + \frac{2\pi}{3}\right) \\ -\sin\theta_s & -\sin\left(\theta_s - \frac{2\pi}{3}\right) & -\sin\left(\theta_s + \frac{2\pi}{3}\right) \end{bmatrix} = [\Gamma]_{0,d,q} \tag{93}$$

$$[\Gamma]_{0,d,q}^{-1} = [\Gamma]_{0,d,q}^{T} \tag{94}$$

$$\begin{bmatrix} i_a \\ i_b \\ i_c \end{bmatrix} = \sqrt{\frac{2}{3}} \begin{bmatrix} \frac{1}{\sqrt{2}} & \cos\theta_s & -sin\theta_s \\ \frac{1}{\sqrt{2}} & \cos\left(\theta_s - \frac{2\pi}{3}\right) & -\sin\left(\theta_s - \frac{2\pi}{3}\right) \\ \frac{1}{\sqrt{2}} & \cos\left(\theta_s + \frac{2\pi}{3}\right) & -\sin\left(\theta_s + \frac{2\pi}{3}\right) \end{bmatrix} \begin{bmatrix} i_{s0} \\ i_{sd} \\ i_{sq} \end{bmatrix} \tag{95}$$

In balanced systems, i_{s0} and V_{s0} values are zero. When flux and current relations are arranged, expressions in terms of rotor fluxes can be obtained instead of rotor currents. These obtained expressions are given in Equations (96-99).

$$\psi_{sd} = L_s i_{sd} + L_m i_{rd} = \left(L_s - \frac{L_m^2}{L_r'} \right) i_{sd} + \frac{L_m}{L_r'} \psi_{rd} \tag{96}$$

$$\psi_{sq} = L_s i_{sq} + L_m i_{rq} = \left(L_s - \frac{L_m^2}{L_r'} \right) i_{sq} + \frac{L_m}{L_r'} \psi_{rq} \tag{97}$$

$$\psi_{rd} = L_r' i_{rd} + L_m i_{sd};\ i_{rd} = \frac{1}{L_r'} \psi_{rd} - \frac{L_m}{L_r'} i_{sd} \tag{98}$$

$$\psi_{rq}' = L_r' i_{rq}' + M_m i_{sq};\ i_{rq}' = \frac{1}{L_r'} \psi_{rq}' - \frac{M_m}{L_r'} i_{sq} \tag{99}$$

According to equations (96-99), the expressions obtained when the machine model is rearranged according to stator currents and rotor fluxes are given in equations (100-104).

$$V_{sd} = R_s i_{sd} - \omega_s \left[\sigma L_s i_{sq} + \frac{L_m}{L_r'} \psi_{rq} \right] + \frac{d}{dt} \left[\sigma L_s i_{sd} + \frac{L_m}{L_r'} \psi_{rd} \right] \tag{100}$$

$$V_{sq} = R_s i_{sq} + \omega_s \left[\sigma L_s i_{sd} + \frac{L_m}{L_r'} \psi_{rd} \right] + \frac{d}{dt} \left[\sigma L_s i_{sq} + \frac{L_m}{L_r'} \psi_{rq} \right] \tag{101}$$

$$0 = R_r' \left[\frac{1}{L_r'} \psi_{rd} - \frac{L_m}{L_r'} i_{sd} \right] - \omega_r \psi_{rq} + \frac{d\psi_{rd}}{dt} \tag{102}$$

$$0 = R_r' \left[\frac{1}{L_r'} \psi_{rq} - \frac{L_m}{L_r'} i_{sq} \right] + \omega_r \psi_{rd} + \frac{d\psi_{rq}}{dt} \tag{103}$$

$$T_e = p \frac{L_m}{L_r'} \left(i_{sq} \psi_{rd} - i_{sq} \psi_{rq} \right) = J \frac{d\omega}{dt} + B\omega \tag{104}$$

The calculated rotor flux amplitude and torque are compared with the reference flux and torque values and the flux and torque errors are applied to the PI type controller. The control signals produced by the controllers are used as reference quantities of the d-q current components of the asynchronous motor. Using the calculated flux angle, the currents in the a-b-c axis of the asynchronous motor are converted to the d-q axis set and compared with the reference d-q current components. The current errors produced are passed through the PI type controller and reference d-q stator voltages are produced. Finally, using the flux angle, the reference voltages in the d-q axes are converted to a-b-c axes for use in the PWM generator. Rotor flux-oriented vector control method diagram is shown in Figure 15.

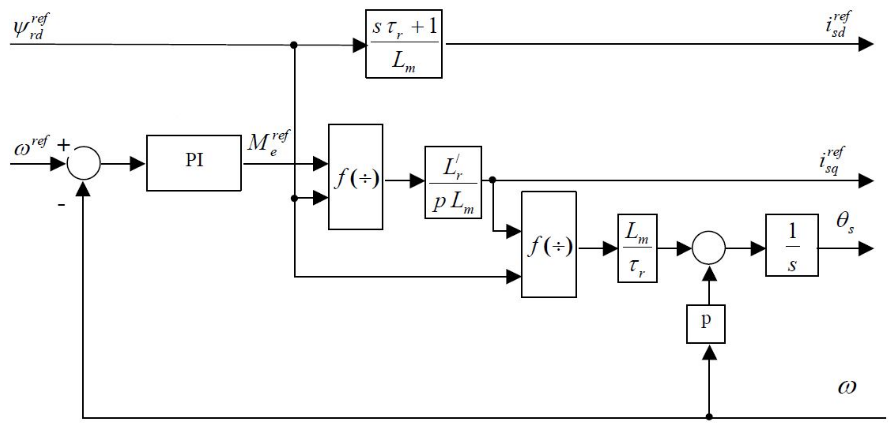

Figure 15: Diagram of vector control for induction machine [12]

For this thesis, calculations were made using the machine parameters given in Table 2.

Table 2: Machine Parameter Assumptions

R_s	Stator Resistance	2.283 ohm
R_r	Rotor Resistance	2.133 ohm
$L_{s\sigma}$	Stator Leakage Inductance	10 mH
$L_{r\sigma}$	Rotor Leakage Inductance	10 mH
J_L	Rotor Inertia	0.005kgm^2
$B_{friction}$	Total Coefficient of Friction	0.01Nms /rad
L_m	Mutual Inductance Coupling Stator and Rotor	220 mH
f_{sN}	Nominal Frequency	50 Hz
n_N	Nominal Speed	1430 rpm
p	Pole Pair Number	1430 rpm

To simplify the model equations, we use the park representation which is a two dimensions representation of a three-phased system. The Park theory provides a fine static and dynamic representation of three-phase systems. The rotor flux-oriented vector control method defines all other variables that define the rotor flux on the d axis with respect to the d axis and the q axis perpendicular to it. Thus, the rotor flux and torque can be controlled as in a direct current motor. The magnitudes converted into the d-q axis set are expressed in terms of rotor flux and stator currents. These expressions are given in Equations (105-110).

$$\frac{\mathrm{d}i_{sd}}{\mathrm{d}t} = \frac{1}{\sigma L_s}\left[-R_E i_{sd} + \sigma L_s w_s i_{sd} + \frac{L_m}{L_r'}\frac{R_r'}{L_r'}\psi_{rd} + pw\frac{L_m}{L_r'}\psi_{rq} + V_{sd}\right] \tag{105}$$

$$\frac{\mathrm{d}i_{sq}}{\mathrm{d}t} = \frac{1}{\sigma L_s}\left[-R_E i_{sd} - \sigma L_s w_s i_{sd} + \frac{L_m}{L_r'}\frac{R_r'}{L_r'}\psi_{rq} - pw\frac{L_m}{L_r'}\psi_{rd} + V_{sq}\right] \tag{106}$$

$$\frac{\mathrm{d}\psi_{rd}}{\mathrm{d}t} = \frac{R_r' L_m}{L_r'} i_{sd} - \frac{R_r'}{L_r'}\psi_{rd} + w_r\psi_{rq} \tag{107}$$

$$\frac{\mathrm{d}\psi_{rq}}{\mathrm{d}t} = \frac{R_r' L_m}{L_r'} i_{sq} - \frac{R_r'}{L_r'}\psi_{rq} - w_r\psi_{rd} \tag{108}$$

$$\frac{\mathrm{d}w}{\mathrm{d}t} = \frac{1}{J}\left(T_e - B_w - T_L\right) \tag{109}$$

$$T_e = p\frac{L_m}{L_r'}\left(i_{sq}\psi_{rd} - \psi_{rq} i_{sd}\right) \tag{110}$$

$$w_s = (p * w) + w_r \tag{111}$$

Using the parameters in Table 3, the constants to be used in the d-q model of the machine are calculated as follows.

Table 3: Machine Parameter Assumptions for Design

L_s	$L_m + L_{s\sigma}$	Stator Winding Inductance	230 mH
L'_r	$L_m + L_{r\sigma}$	Rotor Winding Inductance	230 mH
σ	$1\text{-}L_m^2/L_s L'_r$	Leakage Factor	0.0851
R_E	$R_s + (R'_r L_m^2)/L_r'^2$	Equivalent Resistance	4.2346 ohm

When the equations in the machine model are arranged to be modeled in Simulink and Laplace transform is applied to the equations, the following equations are obtained. Firstly, if we apply Laplace transform to Eqs. (105) and (107) and arrange the equations, we obtain the current and flux equations for the d axis as given in Eqs. (112) and (113), respectively.

$$i_{sd}(s) = \frac{1}{\sigma L_s s + R_E}\left[\sigma L_s w_s i_{sq}(s) + \frac{L_m}{L'_r}\frac{R'_r}{L'_r}\psi_{rd}(s) + pw\frac{L_m}{L'_r}\psi_{rq}(s) + V_{sd}\right] \tag{112}$$

$$\psi_{rd}(s) = \frac{1}{s + \frac{R'_r}{L'_r}}\left(\frac{R'_r L_m}{L'_r} i_{sd} + w_r \psi_{rq}\right) \tag{113}$$

The obtained flux and current Eqs. (112) and (113) of the d axis are modeled in PhiSim environment as in Figure 16;

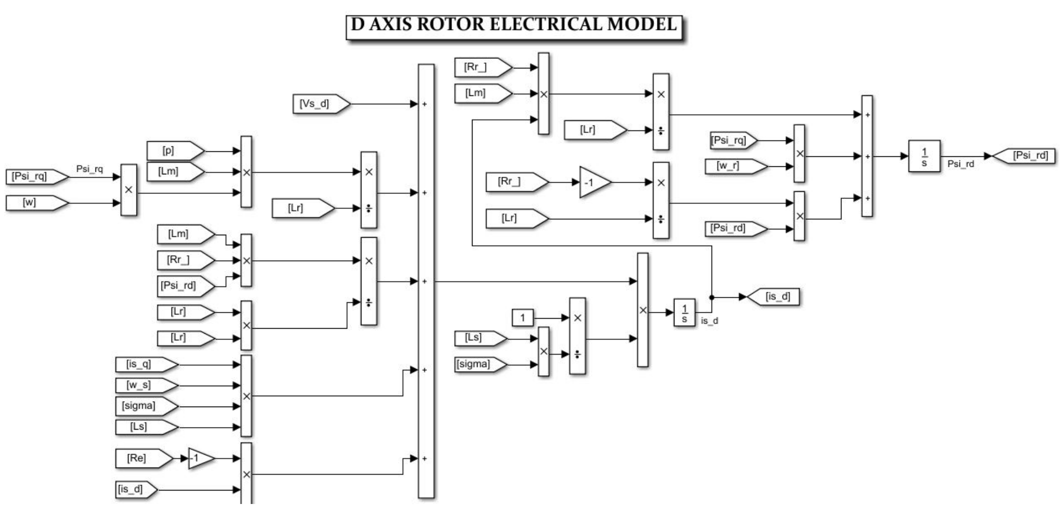

Figure 16: D-axis rotor electrical model

If we apply the same operation to the Eqs. (106) and (108) , we obtain the flux and current equations for the q axis as in Eqs. (114) and (115).

$$i_{sq}\left(s\right)=\frac{1}{\sigma L_s s+R_E}\left[\sigma L_s w_s i_{sd}\left(s\right)+\frac{L_m}{L_r'}\frac{R_r'}{L_r'}\psi_{rq}\left(s\right)+pw\frac{L_m}{L_r'}\psi_{rd}\left(s\right)+V_{sq}\right] \tag{114}$$

$$\psi_{rq}\left(s\right)=\frac{1}{s+\frac{R_r'}{L_r'}}\left(\frac{R_r' L_m}{L_r'}i_{sq}+w_r\psi_{rd}\right) \tag{115}$$

The obtained flux and current Equation (114) and (115) of the q axis are modeled in PhiSim environment as in Figure 17;

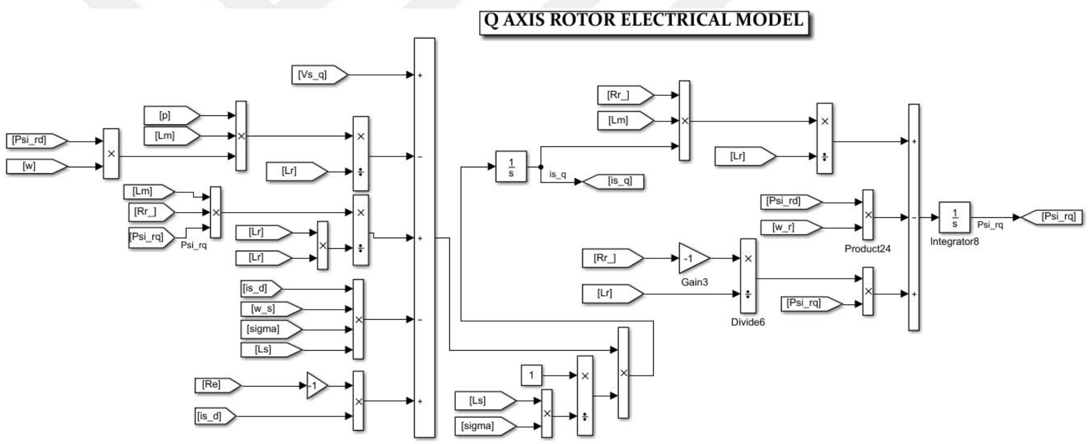

Figure 17: Q-axis rotor electrical model

Finally, if we apply the same operation to the Eqs. (109) , (110) and (111) , the torque and speed components of the machine are modeled in PhiSim environment as in Figure 18.

$$w\left(s\right)=\frac{1}{Js+B}\left(T_e-T_L\right) \tag{116}$$

$$T_e\left(s\right)=p\frac{L_m}{L_r'}\left(i_{sq}\left(s\right)\psi_{rd}\left(s\right)-\psi_{rq}\left(s\right)i_{sd}\left(s\right)\right) \tag{117}$$

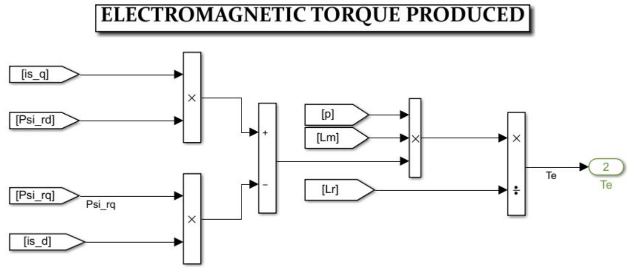

Figure 18: Electromagnetic torque produced model

5.3 Stator Currents and Rotor D-axis Flux Reference Values

5.3.1 Stator Currents Reference Values

Rotor flux is kept on the d axis and the q-axis component of rotor flux is eliminated. All other components are re-arranged according to the d-axis flux of the rotor. In this arrangement, the stator currents are also divided into d and q axes components. Accordingly, the d-axis component of the stator currents becomes the variable that controls the flux, and the q-axis component is the variable that controls the torque. Substituting zero for ψ_{rq} in Eq. (107), the rotor flux equation is obtained as in Eq. (115).

$$\frac{L'_r}{R'_r}\frac{\mathrm{d}\psi_{rd}}{\mathrm{d}t} = L_m i_{sd} \tag{118}$$

where $\tau_r = L'_r/R'_r$ is the time constant of the rotor circuit. If the Laplace transform is applied to Eq. (118), the transfer function between d-axis flux and current is obtained as given in Eq. (119).

$$\frac{\psi_{rd}\,(s)}{i_{sd}\,(s)} = \frac{L_m}{\tau_r s + 1} \tag{119}$$

Since the q-axis current is the variable that controls the torque, the q-axis current reference value is calculated from the torque reference value. The torque reference value will be calculated from the control of the speed reference value. The relation between the torque reference value and q-axis current reference value is given in Eq. (120).

$$i_{sq}^{ref} = \frac{3}{2}\frac{L'_r}{pL_m}\frac{T_e^{ref}}{\psi_{rd}^{ref}} \tag{120}$$

Stator current angular frequency is the control signal used indirectly in the d-q axis model of the machine. This value is obtained by the tenth equation. But here the angular velocity of the rotor currents is needed, and this value is obtained by using the d-axis flux reference value and the torque reference value as given in Eq. (121).

$${T_e}^{ref} = \frac{3}{2}p\frac{\left(\psi_{rd}^{ref}\right)^2}{R'_r}w_r \tag{121}$$

Stator d-q current reference values and rotor current frequency model are designed as in Figure 19 according to the above Eqs. (118), (119) and (120).

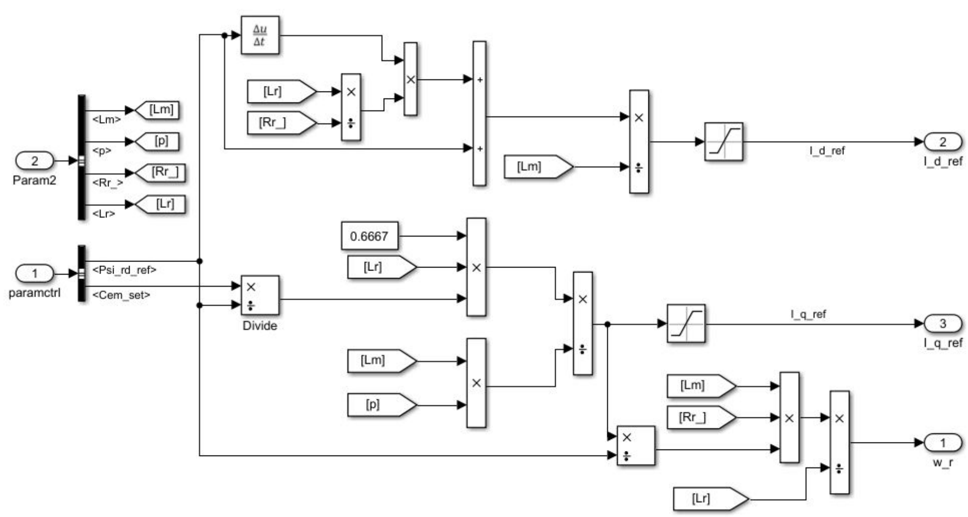

Figure 19: Stator d-q current reference values and rotor current frequency model

5.3.2 Rotor D-axis Flux Reference Value

The machine runs at its nominal torque until it reaches its nominal speed and power. After it reaches the nominal speed, it operates at its nominal power. As the speed value increases, the torque value decreases. According to the control characteristics of the induction motor in constant and weakened flux regions graph given in Figure 20, there are different rotor flux values in these two working areas, which are divided into two parts as constant torque and constant power. In the constant torque region, the rotor flux is maintained at the machine's nominal torque. In the constant power region, the rotor flux is reduced depending on the increasing speed and this is called field weakening.

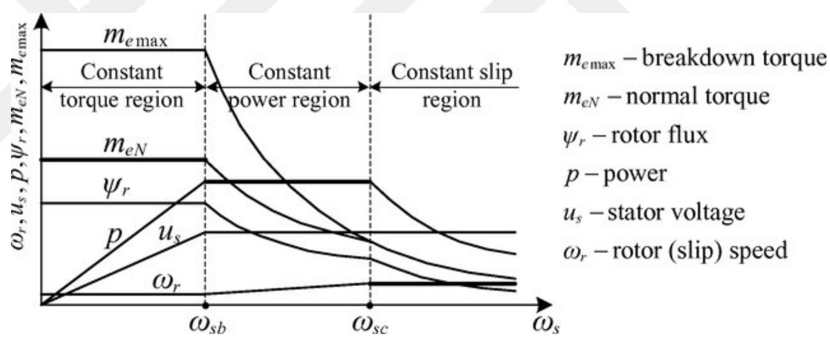

Figure 20: Control characteristics of the induction motor in constant and weakened flux regions [11]

In order to find the rotor flux value in the constant torque region, the nominal torque of the machine must be calculated. This value is equal to Eq. (123) to find the direct-axis rotor flux value required for the nominal torque.

$$T_{e_n} = \frac{3R_r'p}{sw_{s_n}} \cdot \frac{V_{s_n}^2}{\left[R_s + \frac{R_r'}{s}\right]^2 + \left[\chi_{s\sigma} + \chi_{r\sigma}'\right]^2} \tag{122}$$

$$T_e = \frac{3}{2}p\frac{\psi_{rd}^2}{R_r'}w_r \tag{123}$$

The τ_{e_n} and ψ_{rd}^{ref} values are calculated from Eqs. (122) and (123). Here, the nominal speed of the machine, 1430 rpm, is used for the slip value. For the stator current angular speed, the frequency of the machine in the nominal operating state of the machine is 50 Hz and nominal torque is obtained.

- ω_{s_n} *: nominal synchronous speed*
- ω_{m_n} *: nominal motor speed*
- s_n *: slip at nominal speed*
- ω_s *: angular velocity of stator currents*
- ω_r *: angular velocity of rotor currents*
- ω *: rotor angular velocity*

The following equations were calculated according to the values in Table 2.

$$\omega_{s_n} = 2\pi f_{s_n} = 2\pi 50 = 314,159 \ rad/s \tag{124}$$

$$\omega_{m_n} = \frac{1430 * 2\pi}{60} = 149,749 \ rad/s \tag{125}$$

$$s_n = \frac{\omega_{s_n} - p\omega_{m_n}}{\omega_{s_n}} = 0.047 \tag{126}$$

$$\chi_{s\sigma} = \chi'_{r\sigma} = \omega_{s_n} * L_{s\sigma} = 2\pi 50 * 0.001 = 3.142 \tag{127}$$

$$\omega_r = 314,159 - (2 * (149,749)) = 14,661 \ rad/s \tag{128}$$

Nominal torque value is calculated by Eq. (122) with parameters value given in Table 2.

$$T_{e_n} = \frac{3*2,133*2}{0.047*314,159}.\frac{220^2}{\left[2,283+\frac{2,133}{0,047}\right]^2+[3,142+3,142]^2} = 18,148\ Nm \tag{129}$$

ψ_{rd}^{ref} value is calculated by Eq. (123) with parameters value given in Table 2.

$$\psi_{rd}^{ref} = \sqrt{\frac{T_e R'_r}{p\omega_r}} = \sqrt{\frac{18,148*2,133}{2*14,661}} = 1,149 \tag{130}$$

This reference flux value is the value of the motor up to the nominal speed. For the values after this speed, the code written the value of the flux by keeping the slip value constant. This code is given in Appendix B. The reference flux value matrix is stored in the model as a look-up table. A switch block has been added to give a constant value up to the nominal speed as shown in Figure 21.

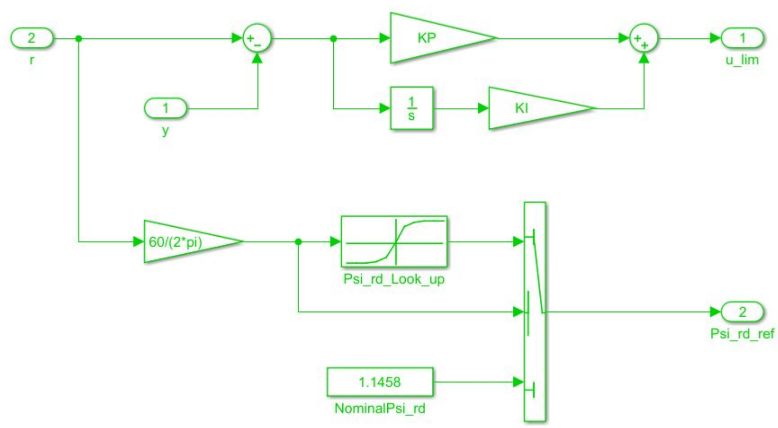

Figure 21: The block in which the reference value ψ_{rd}^{ref} is calculated

5.4 Non-Linear Compensation

The d and q axis voltages of the machine can be defined as a summation of linear and non-linear terms as given in Eq. (131) and (132), respectively since the q axis flux is zero.

$$V_{sd} = V_{sd}^{lin} + V_{sd\ comp} \tag{131}$$

$$V_{sq} = V_{sq}^{lin} + V_{sq\ comp} \tag{132}$$

where $V_{sd}^{lin} = \sigma L_s \frac{di_{sd}}{dt} + R_E i_{sd}$, $V_{sq}^{lin} = \sigma L_s \frac{di_{sq}}{dt} + R_E i_{sq}$, $V_{sd\ comp} = -\sigma L_s \omega_s i_{sq} - \frac{L_m}{L'_r}\frac{R'_r}{L'_r}\psi_{rd}$, $V_{sd\ comp} = \sigma L_s \omega_s i_{sd} + p\omega \frac{L_m}{L'_r}\psi_{rd}$

$V_{sq\ comp}$ and $V_{sd\ comp}$ distort the linearity of the equations, and these terms can be externally calculated and added later. If the Laplace transform is applied to V_{sd}^{lin} and V_{sq}^{lin} , the transfer function between current and voltage is obtained as given in Eqs. (131) and (132), respectively.

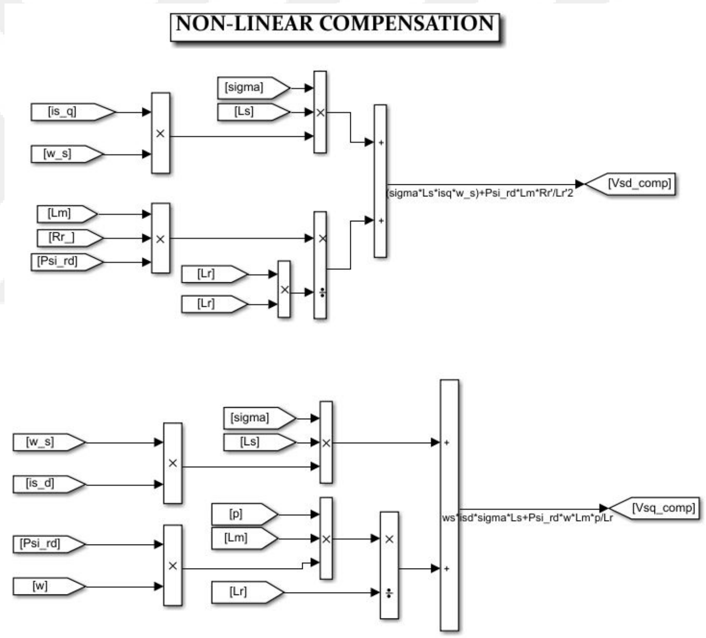

Figure 22: Non-Linear compensation model

5.5 Power Calculation Model

In this block, slip, power, torque, efficiency values are calculated. While making these calculations, the required current values are calculated by using the equivalent circuit of the asynchronous machine. The equivalent circuit of the asynchronous machine in the fixed reference frame is defined in Figure 23.

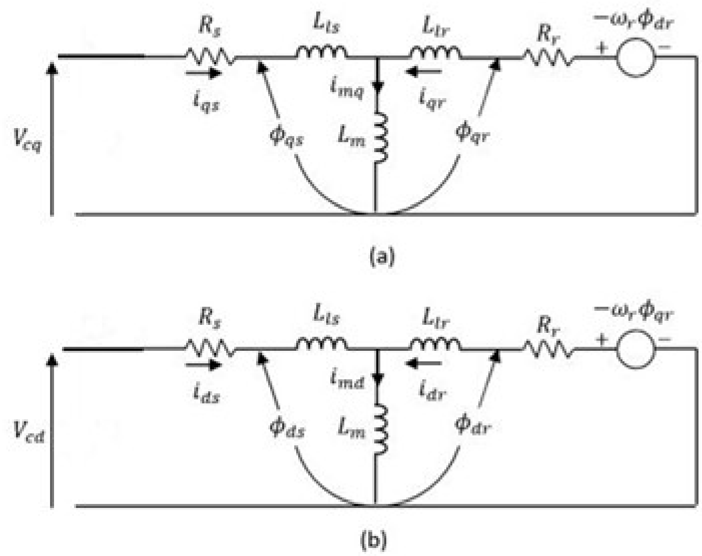

Figure 23: Equivalent circuit of an induction machine in stationary reference frame [24]

The power flow diagram of the asynchronous machine is given in Figure 24. These are electrical input power, air gap power, mechanical power, stator copper loss , rotor copper loss and rotational losses. Some assumptions have been accepted for this thesis. These saturation, gear and groove losses are neglected. Hysteresis and fuco losses are neglected. The permeability of the magnetic parts is considered infinite. The skin effect is neglected.

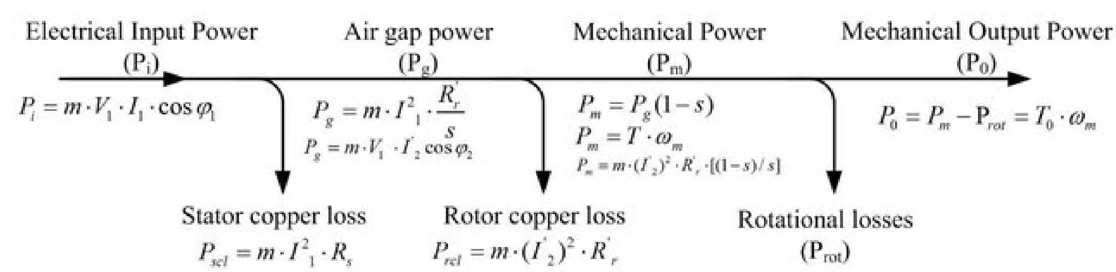

Figure 24: Power flow diagram of an induction motor [25]

Slip value in a nominal state is calculated by Eq. (133) with parameters value given in Table 2.

$$s_n = \frac{\omega_{s_n} - p\omega_{m_n}}{\omega_{s_n}} = 0.047 \tag{133}$$

Equivalent impedance of the machine is calculated by Eq. (134) with parameters value given in Table 2;

$$Z_m = \left[\left(\frac{R'_r}{s} + \chi'_{r\sigma}\right) // \chi_m\right] + (R_s + \chi_{s\sigma}) = 32.141 + 25.021i \tag{134}$$

Current in the stator a nominal state is calculated by Eq. (135) with the value from Eq. (134) parameters value given in Table 2 ;

$$|I_s| = \frac{V_s}{|Z_m|} = 5.4011\angle - 37.899 \ [A] \tag{135}$$

Magnetizing current is calculated by Eq. (136) with parameters value given in Table 2;

$$I_m = \frac{V'_r}{\chi_m} = 2.89\angle - 91.67 \ [A] \tag{136}$$

Using Eqs. (135) and (136), reduction rotor current to the stator side value was calculated as in Eq. (137).

$$I'_r = I_s - I_m = 4.367\angle - 5.60 \ [A] \tag{137}$$

Nominal output power was calculated using the parameter values given in Table 2 and Eqs. (133) and (137). This calculation is given in Eq. (138).

$$P_o = 3\,(I'_r)^2\,\frac{R'_r\,(1-s)}{s} = 2491.04 \ [W] \tag{138}$$

Nominal torque was calculated using the parameter values given in Table 2 and Eq. (133). This calculation is given in Eq. (139).

$$T_{e_n} = \frac{3R_r'p}{sw_{s_n}} \cdot \frac{V_{s_n}^2}{\left[R_s + \frac{R_r'}{s}\right]^2 + \left[\chi_{s\sigma} + \chi_{r\sigma}'\right]^2} = 18,148\ [Nm] \tag{139}$$

Input power is calculated by Eq. (140) with parameters value given in Table 2 ;

$$P_{in} = m.V_1.I_1.\cos\phi = 2812.88\ [W] \tag{140}$$

The efficiency value is calculated according to Eq. (141) based on the values obtained in Eqs. (138) and (140).

$$\eta = \frac{P_{out}}{P_{in}} = \frac{Mechanical\ output\ power}{Electrical\ input\ power} * 100 = 88.56\% \tag{141}$$

The slip torque characteristics of an induction machine are given in Figure 25. If the slip value is between 0 and 1, it will be in motor mode, if the slip value is less than 0, it will be in generator mode.

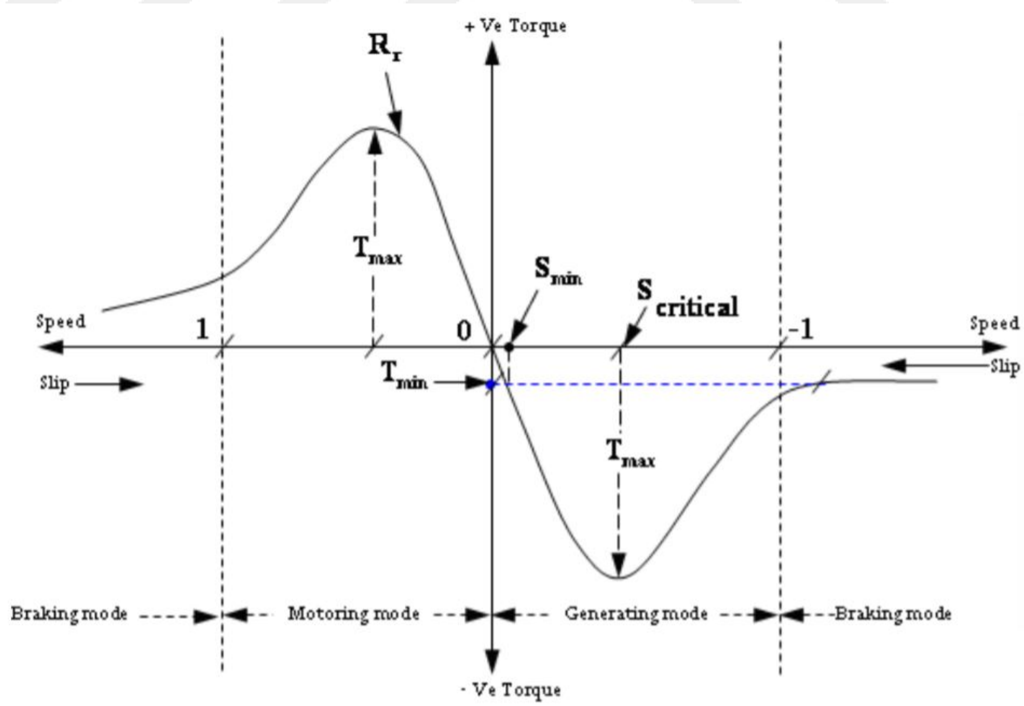

Figure 25: Slip torque characteristics of an induction machine [26]

Efficiency for motor operation mode ($0 < s < 1$) is given Eq. (142).

$$\eta = \frac{P_{out}}{P_{out} + P_{rot} + P_{stray} + P_{cr} + P_{cs} + P_c} \tag{142}$$

Efficiency for generator operation mode ($s < 0$) is given Eq. (143).

$$\eta = \frac{Mechanical\ output\ power}{Electrical\ input\ power} = \frac{P_{in}}{P_{in} + P_{rot} + P_{stray} + P_{cr} + P_{cs} + P_c} \tag{143}$$

In Figure 26, these equations are implemented on model-based design.

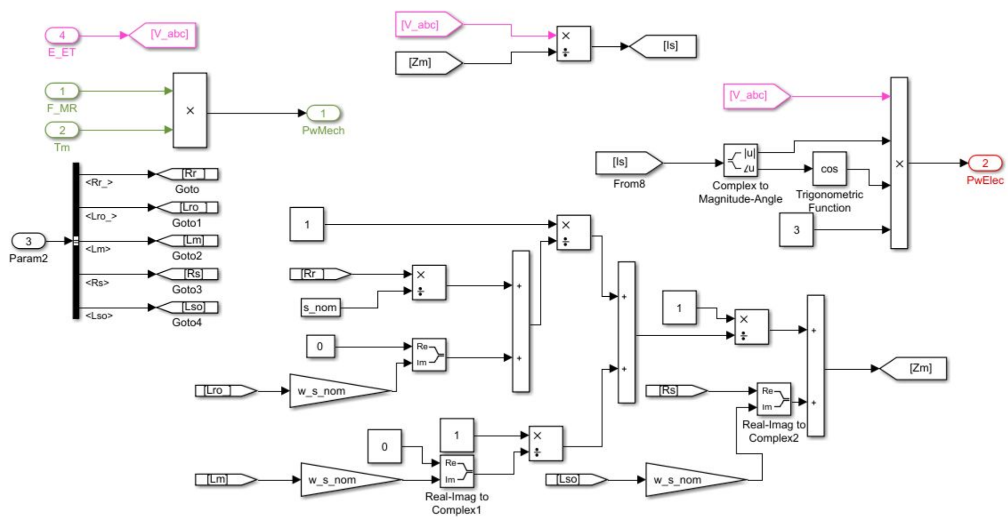

Figure 26: Power calculation block

5.6 Design of Current and Speed Controllers

The rotor flux-oriented vector control method, which was developed from the model of the machine in the d-q axis set, therefore does not include flux and torque control loops. There are current and speed loops as control loops. Figure 27 represents the control diagram of the asynchronous machine. Two current controllers and one speed controller are used.

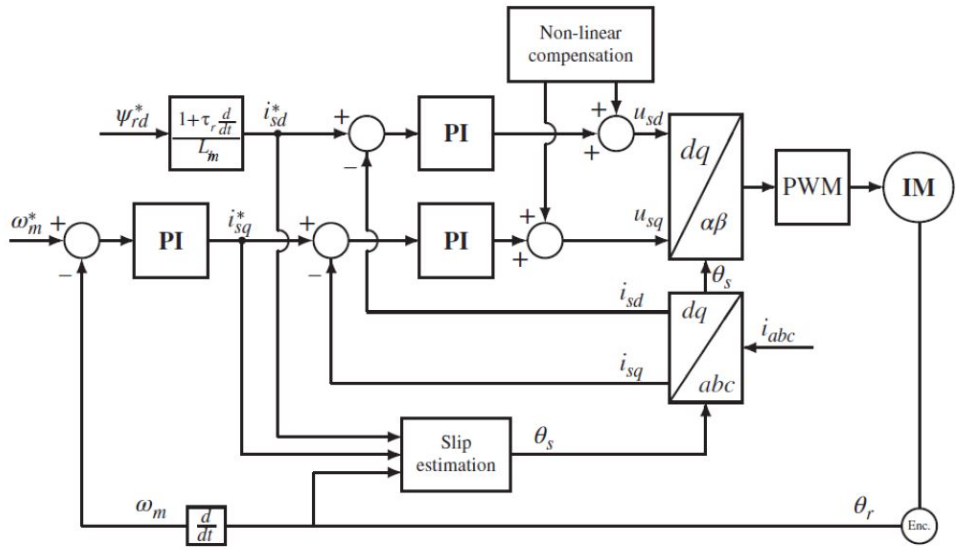

Figure 27: Asynchronous motor speed and current control diagram [12]

Most electric drive systems use PID controllers. Controller parameters should be adjusted according to performance. Parameter determination using the pole insertion method It is one of the simplest methods used. In the application of this method, the transfer function of the controlled system must be found. According to the transfer function of the system, PI is used in a first-order system and PID is used in a second-order system.

PI controller ;

If the transfer function of the system is first-order, PI controls are used. The diagram in Figure 28 represents a closed loop control system.

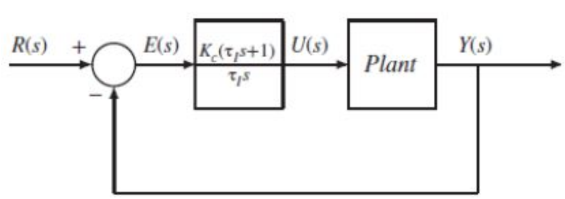

Figure 28: Closed loop diagram [12]

G(s) represents the transfer function to be used. C(s) represents the PI controller.

$$C(s) = K_c \left(1 + \frac{1}{\tau_I s}\right) \tag{144}$$

Since PI controls are used for first order equations, the expression G(s) is defined as in Eq. (145).

$$G(s) = \frac{b}{s+a};\ C(s) = \frac{c_1 s + c_0}{s} \tag{145}$$

According to Figure 28, the closed loop transfer function is obtained as in Eq. (146) by using the expressions in Eq. (145).

$$\frac{Y(s)}{R(s)} = \frac{G(s)\,C(s)}{1 + G(s)\,C(s)} = \frac{\frac{b}{s+a}\frac{c_I s + c_0}{s}}{1 + \frac{b}{s+a}\frac{c_I s + c_0}{s}} = \frac{b\,(c_I s + c_0)}{s\,(s+a) + b\,(c_I s + c_0)} \tag{146}$$

In the expression in Eq. (146), the poles are calculated as in Eqs. (147), (148), and (149).

$$s\,(s+a) + b\,(c_I s + c_0) = s^2 + 2\zeta\omega_n s + \omega_n^2 \tag{147}$$

$$a + bc_I = 2\zeta;\ bc_0 = \omega_n^2 \tag{148}$$

$$c_I = \frac{2\zeta\omega_n - a}{b};\ c_0 = \frac{\omega_n^2}{b} \tag{149}$$

Coefficients for PI controls are calculated as in Eq. (150).

$$K_c = c_I = \frac{2\zeta\omega_n - a}{b};\ \tau_I = \frac{c_1}{c_0} = \frac{2\zeta\omega_n - a}{\omega_n^2} \tag{150}$$

Response for step reference input is shown in Figure 29. ζ is usually chosen at a value between 0.707 and 1.

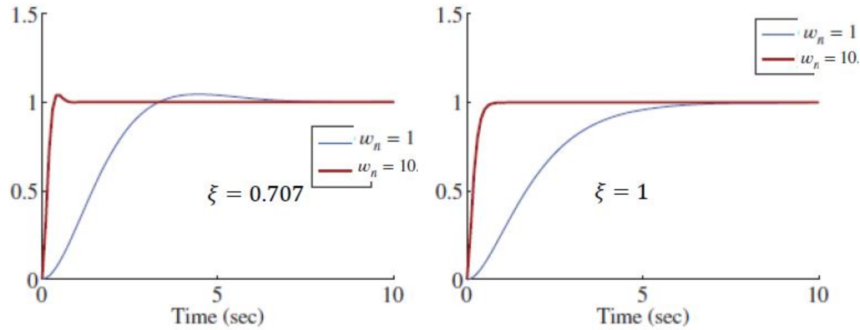

Figure 29: Response for step reference input [12]

PID controller ;

PID controls are generally used more in position control systems. Since PID controls are used for second order equations, transfer function is defined as in Eq. (151).

$$\frac{Y(s)}{R(s)} = \frac{b}{s(s+a)} \tag{151}$$

C(s) represents the PID controller as in Eq. (152).

$$C(s) = K_c\left(1 + \frac{1}{\tau_I s} + \tau_D s\right) \tag{152}$$

Coefficients for PID controls are calculated as in Eq. (153).

$$K_c = c_I;\ \tau_I = \frac{c_1}{c_0};\ \tau_D = \frac{c_2}{c_1} \tag{153}$$

According to Figure 28, the closed loop transfer function is obtained as in Eq. (154) by using the expressions in Eqs. (151), (152) and (153).

$$\frac{Y(s)}{R(s)} = \frac{G(s)C(s)}{1+G(s)C(s)} = \frac{\frac{b\left(c_2 s^2 + c_1 s + c_0\right)}{s^2(s+a)}}{1 + \frac{b(c_2 s^2 + c_1 s + c_0)}{s^2(s+a)}} = \frac{b\left(c_2 s^2 + c_1 s + c_0\right)}{s^2(s+a) + b\left(c_2 s^2 + c_1 s + c_0\right)} \tag{154}$$

In the expression in Eq. (154), the poles are calculated as in Eqs. (155), (156), (157), (158) and (159).

$$s_1 = -\zeta\omega_n + j\omega_n\sqrt{1-\zeta^2};\ s_2 = -\zeta\omega_n - j\omega_n\sqrt{1-\zeta^2};\ s_3 = -n*\omega_n(n>>1) \quad (155)$$

$$\left(s^2 + 2\zeta\omega_n s + \omega_n^2\right)(s + n*\omega_n) = s^3 + t_2 s^2 + t_1 s + t_0 \quad (156)$$

$$t_2 = (2\zeta + n)\,\omega_n;\ t_1 = (2\zeta n + 1)\,\omega_n^2;\ t0 = n\omega_n^3 \quad (157)$$

$$s^2\,(s+a) + b\left(c_2 s^2 + c_1 s + c_0\right) = s^3 + t_2 s^2 + t_1 s + t_0 \quad (158)$$

$$c_2 = \frac{t_2 - a}{b};\ c_1 = \frac{t_1}{b};\ c_0 = \frac{t_0}{b} \quad (159)$$

Coefficients for PID controls are calculated as in Eq. (160).

$$K_c = c_I = \frac{(2\zeta n + 1)\,\omega_n^2}{b};\ \tau_I = \frac{c_I}{c0} = \frac{(2\zeta n + 1)\,\omega_n^2}{n\omega_n^3};\ \tau_D = \frac{c_2}{c_1} = \frac{(2\zeta + n)\,\omega_n - a}{(2\zeta n + 1)\omega_n^2} \quad (160)$$

When the inverse laplace transform is applied, the system response is defined as in Eq. (161).

$$u(t) = -K_c y(t) + \frac{K_c}{\tau_I}\int_0^t \left(r(\tau) - y(\tau)\right) d\tau - K_c\tau_D\frac{dy(t)}{dt} \quad (161)$$

Cascade Control Structure ;

In cascade control structures, the main control element in motor control systems is position or speed control. Flow control is the second important element. In most industrial motor control systems, PI controllers with very different time constants are used as controllers. The time constant of the current controller is much smaller than the time constant of the speed controller. In order to simplify the design of the control system, different time control systems are separated from each other. Thus, the controllers can be designed independently of each other. The cascade feedback control structure structure is shown in Figure 30.

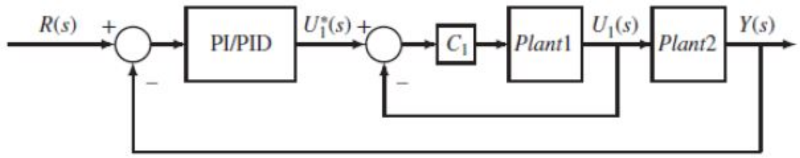

Figure 30: Cascade feedback control structure

In general, the current control loop contains non-linear expressions. Due to the non-linear elements in question, the forward path gain of the controller in the current loop, which is the inner loop, is chosen very large. In this way, the control system is not affected by both disturbances and parameter changes. Limitations against the occurrence of excessive currents in the control loop must be observed. It is one of the important performance criteria of the control system. It was mentioned that the bandwidth of the inner current loop is much higher than that of the outer velocity loop. P-type or PI-type controller structures can be used in the internal current loop.

5.6.1 Current Controller

After the compensation terms are added, the relations between current and voltage in Eqs. (162) and (163) are obtained.

$$V_{sd}^{lin} = \sigma L_s \frac{di_{sd}}{dt} + R_E i_{sd} \tag{162}$$

$$V_{sq}^{lin} = \sigma L_s \frac{di_{sq}}{dt} + R_E i_{sq} \tag{163}$$

Other terms are expressed as coupling terms. These terms are given in Eqs. (164) and (165).

$$V_{sd\ comp} = -\sigma L_s \omega_s i_{sq} - \frac{L_m}{L_r'} \frac{R_r'}{L_r'} \psi_{rd} \tag{164}$$

$$V_{sd\ comp} = \sigma L_s \omega_s i_{sd} + p\omega \frac{L_m}{L_r'} \psi_{rd} \tag{165}$$

If the Laplace transform is applied to the Eqs. (162) and (163) equations, the transfer function between current and voltage in Eqs. (166) and (167) are obtained.

$$\frac{i_{sd}}{V_{sd}^{lin}} = \frac{1}{\sigma L_s s + R_E} \tag{166}$$

$$\frac{i_{sq}}{V_{sq}^{lin}} = \frac{1}{\sigma L_s s + R_E} \tag{167}$$

Two controllers are designed as current and speed. The settling time of electrical events is much faster than mechanical events. Accordingly, when designing current and speed controllers, the bandwidth of the current loop is chosen much larger than the speed controller and so the two loops can run independently of each other. Substituting the parameters in Eqs. (166) and (167), the transfer function in Eq. (168) is obtained.

$$G_{d,q} = \frac{1}{\sigma L_s s + R_E} = \frac{51,0204}{s + 216,051} = \frac{b}{s + a} \tag{168}$$

A PI controller structure has been chosen as it is a first-order system. The proportional and integral coefficients are found with the help of Eqs. (169) and (170).

$$K_p = \frac{2\zeta\omega_n - a}{b} \tag{169}$$

$$K_i = \frac{\omega_n^2}{b} \tag{170}$$

Where ζ is the damping ratio of the system and ω_n is the natural frequency (bandwidth) of the system. $\zeta = 1$, $\omega_n = 350$. From Eqs. (169) and (170), the K_p and K_i values are calculated. $K_p = 9.485$, $K_i = 2401$

Current controller closed-loop model diagram are shown in Figure 31.

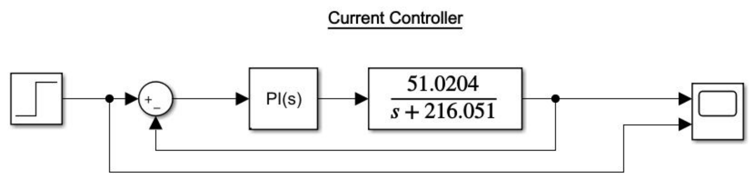

Figure 31: Current controller model

The current controller response of the system shown in Figure 31 is shown in Figure 32.

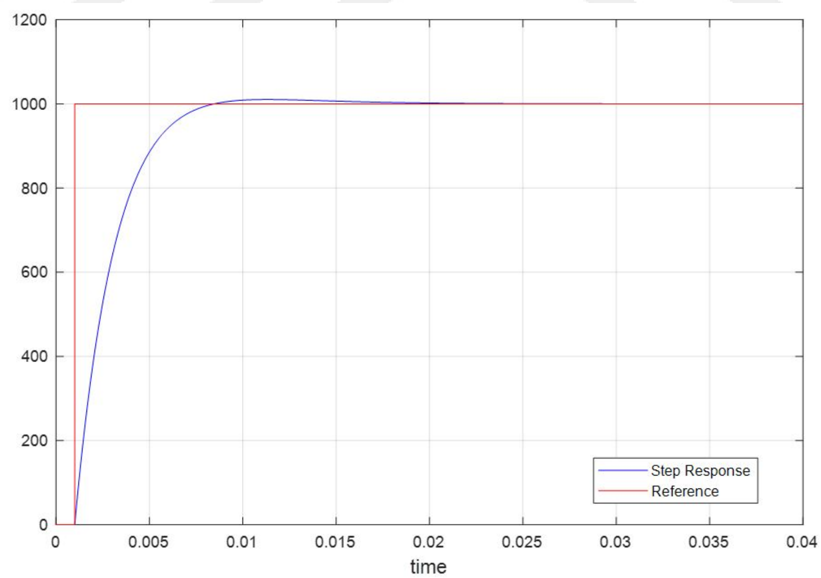

Figure 32: Current controller response

The implementation of current controller in PhiSim is shown in Figure 33.

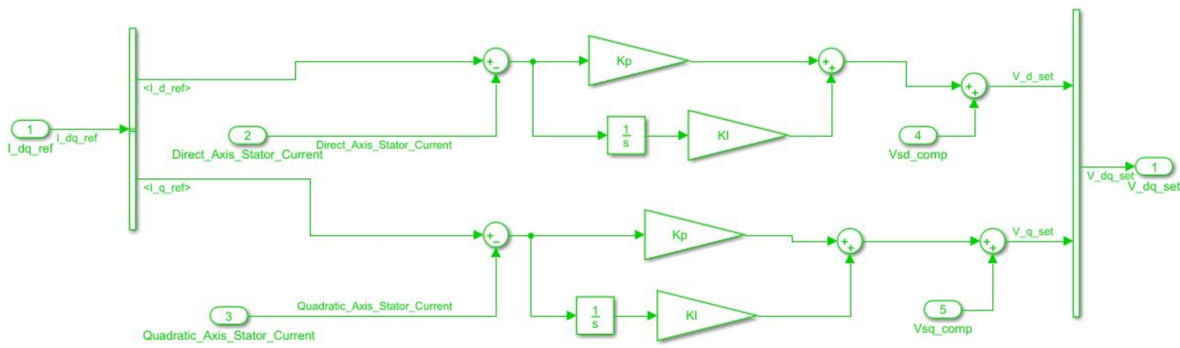

Figure 33: Current controller block

5.6.2 Speed Controller

The relationship between speed and moment in the model is as in Eq. (171).

$$G(s) = \frac{1}{Js + B} = \frac{1}{0.005s + 0.001} = \frac{200}{s + 0.2} = \frac{b}{s + a} \tag{171}$$

The settling time of electrical events is much faster than mechanical events. Accordingly, when designing current and speed controllers, the bandwidth of the current loop is chosen much larger than the speed controller and so the two loops can run independently of each other.The bandwidth of the speed controller is chosen much smaller than the bandwidth of the current controller. If one-20th of bandwidth current loop is selected for the speed loop. $\omega_n = \frac{350}{20} = 17.5$ and $\zeta = 1$.

The proportional and integral coefficients are found with the help of Eqs. (172) and (173).

$$K_p = \frac{2\zeta\omega_n - a}{b} = 0.174 \tag{172}$$

$$K_i = \frac{\omega_n^2}{b} = 1.5313 \tag{173}$$

Speed controller closed-loop model diagram are shown in Figure 34.

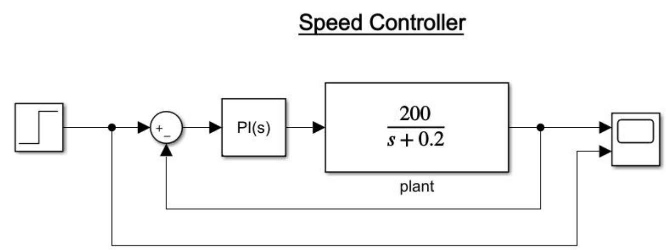

Figure 34: Speed controller model

The speed controller response of the system shown in Figure 34 is shown in Figure 35.

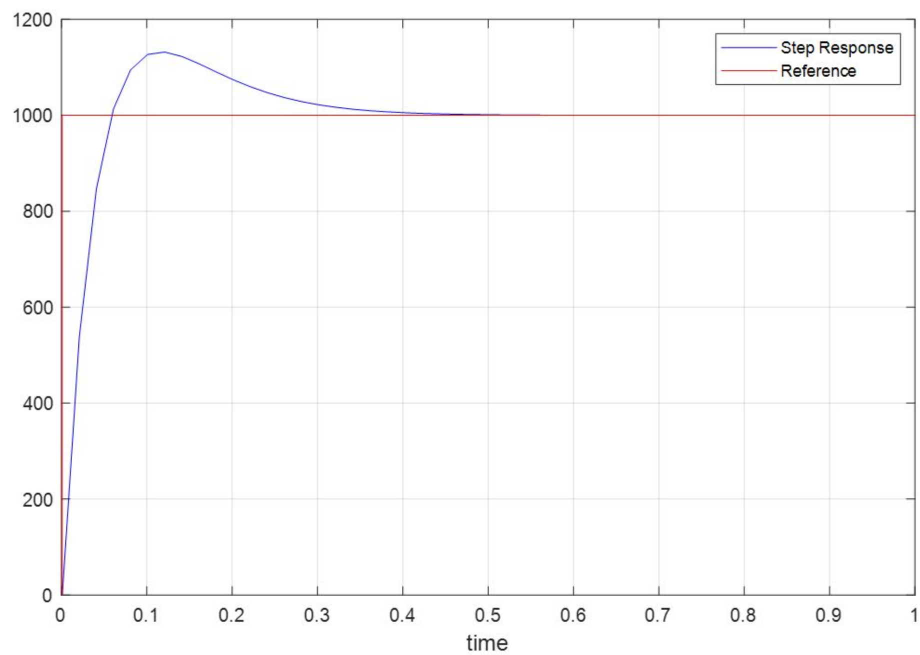

Figure 35: Speed controller response

The implementation of speed controller in PhiSim is shown in Figure 36.

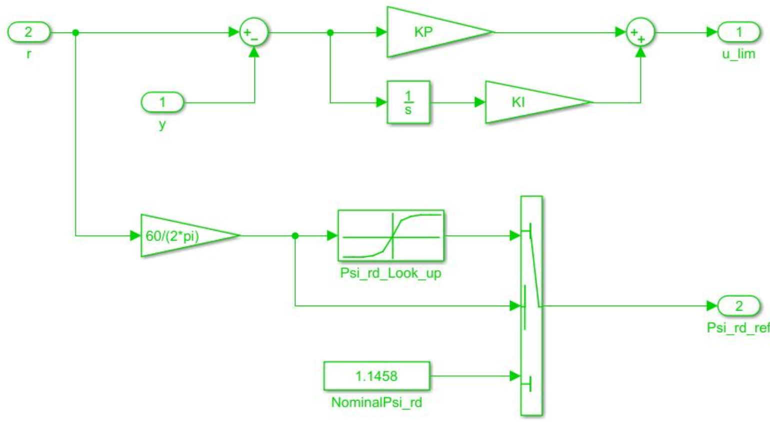

Figure 36: Speed controller block

CHAPTER VI

IMPLEMENTATION TO PHISIM

PhiSim is a set of tools designed for engineers dealing with Matlab- Simulink and physics modelling. It extends the software capabilities to handle models of physical systems in a Bloc-Diagram environment with more flexibility ,quicker and cheaper model development and simulation,easier model maintenance [9] . The basis is that bond graphs are based on energy and energy exchange [14]. A physical system can always be modeled with a nodal representation in space. “Nodes” are able to calculate the state variables of a system from a balance equation, while the neighbors “Elements” calculate the terms of this balance equation. In mechanics for example, an inertia is a node since you can write a balance equation for the forces that are applied to this inertia. In the field of dynamic systems modeling, the relations between physical variables involve time derivatives, and thus there is a choice between derivative and integration causalities. In the present libraries, we always use integration causality because it is more natural for ODE solvers like Simulink. The respect of this causality is always satisfied thanks to the node/element distinction and the rules for connecting blocs together [9].

One of the most constraining things when modelling physical systems in a bloc diagram environment is the causality of links between blocs. Indeed, in a modeller like Simulink connections between blocs are arrows showing the direction of the calculation flow. But considering a physical connection between two systems (e.g. mechanical), one cannot presume about the direction of the calculation flow and moreover information must transit in both directions (e.g. force and velocity). According to the Bond-Graph theory, physical systems are interconnected with links that carry a certain amount of energy per unit of time which is defined by the product of two variables: force and flow. To guarantee the conservation of mass and energy on a closed system, a system cannot impose both force and flow: if the flow is an output the force must be an input [9].

The Phi-Link concepts rely on the separation of basic physical phenomena into nodes and elements. This approach is based on a network representation of the system. Usually, nodes are different spatial locations on the system and calculate the state variables. Elements represent the different branches between the nodes, calculating mass and energy transfers [9]. Basically, intensive variables are calculated in nodes and extensive variables in elements. Intensive variables have the property of being uniform on the spatial location of the node. Extensive variables are proportional to the matter quantity in the system [9]. Physical connections on nodes look like Output ports and physical connections on elements look like Input ports . Nodes cannot be connected with nodes. Elements cannot be connected with elements. Any number of elements can be connected to a node port. Only one node can be connected to an element port. Each element has power outputs through which one or more energies can flow. In the bond graph method, information exchange between the elements that make up the system is realized with state variables. These state variables are expressed by external variable/effort (e) and internal variables/flow (f).

A system is a functional whole in which different physical elements interact interactively to fulfill a specific purpose. System simulation, on the other hand, is the time-dependent imitation of real-life physical processes. System simulation has an important place in the creation of digital twin models today. A digital twin is defined as a virtual model of the behavior and consequences of a physical product or service in the real world. In simpler terms, the digital twin; is a virtual model of a process, product, or service. Thanks to the studies carried out on these models, it is possible to greatly reduce the time spent on physical changes and tests.

6.1 DC Voltage Source

Figure 37 represents a single phase DC voltage source. It generates the voltage applied to the connected element. In bond-graph representation, the voltage source is an effort source element (Se).

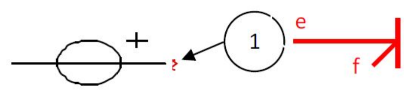

Figure 37: Bond-Graph representation for DC voltage source [9]

Table 4: Input and output definitions for DC voltage source [9]

Inputs				
Port	*Label*		*Unit*	*Description*
1	F_ES	I	A	Current applied to the voltage source
Outputs				
Port	*Label*		Unit	Description
1	E_ES	U	V	Voltage fixed by the voltage source
Parameters				
Name	*Default Value*		*Units*	*Description*
V	-		V	Amplitude Voltage
Results				
Name		*Units*		*Description*
RES		-		All results
U_DC		V		Voltage of the voltage source
I_DC		A		Current in the voltage source

6.2 Pulse-Width Modulation (PWM)

This model represents a technique for controlling electrical devices using electronic power switch, which is known as Pulse-Width Modulation (PWM). The PWM signal produces trains of pulses, whose duty cycle varies depending upon a reference signal. The on/off states of modulation are used to control switches, in order to control voltage across or current through the power device. The PWM signal is generated by intersective method : the switching points are determined by the intersection of the high frequency carrier wave and the target reference signal. The pulse width is determined by natural sampling PWM signal [9].

This model used with a sinusoidal reference wave for input (three phase). The PWM switching frequency has to be much higher than the Nyquist rate of the modulating waveform : $Fe = 3 * F_{ref}$, where Te = 1/Fe represent the PWM sampling time and Fref the three phases voltage reference frequency. Obviously, solver sample time $Fe = 3 * Ts$ should be smaller than the PWM sampling time $Te = (Ts \leq 10 * Te)$. The Modulation index should be lower or equal than 1.

If CarrierWave is greater or equeal to $Va_{ref-sampled}$ then $b1 = 1$ and switch commands T1 to turn on. Also,If CarrierWave is less than $Va_{ref-sampled}$ then $b1 = 0$ and switch commands T1 to turn off. This reasoning applies to the others sampled reference signals $Vb_{ref-sampled}$, $Vc_{ref-sampled}$, according to b2 and b3. Ratio frequency between the switching carrier (Fc) and fundamental frequency (Fref) is defined as modulation index, by $Mf = \frac{Fc}{Fref}$. Ratio amplitude between the control wave form (Vref) and the switching carrier wave $Vc = 1$ is defined as modulation level, by $Ma = \frac{Vref-max}{Vc-max}$

Three types of PWM are possible. Centered pulse modulation (triangle waveform) was used for this project.

Table 5: Input and output definitions for PWM [9]

Inputs					
Port	*Label*			*Units*	*Description*
1	SET	V_ref	V_a_ref	V	Control voltage (three phases)
			V_b_ref		
			V_c_ref		
Outputs					
Port	*Label*			*Units*	*Description*
1	CTRL	PWM	b1	-	T1 gate current pulse
			b2	-	T2 gate current pulse
			b3	-	T3 gate current pulse
Parameters					
Name	*Default value*			*Units*	*Description*
Fc	-			Hz	Carrier wave frequency
Vc_max	-			V	Carrier wave amplitude
Te	-			s	PWM sampling time
Ts	-			s	Solversampling time (should be Ts<k.Ts)
Results					
Name				*Units*	*Description*
RES				-	All results
PWM	b1			-	T1 gate current pulse
	b2			-	T2 gate current pulse
	b3			-	T3 gate current pulse
CarrierWave				-	Carrier wave
V_ref_sampled	Va_ref_sampled			-	Reference signal V_a (sampled)
	Vb_ref_sampled			-	Reference signal V_b (sampled)
	Vc_ref_sampled			-	Reference signal V_c (sampled)

6.3 DC/AC Three Phase Controlled Bridge Inverter (1P-3P)

Figure 38 represents an electrical device that converts direct current (DC) to alternative current (AC), which is known as an inverter. This converter is an arrangement of six IGBT and six diodes in a bridge circuit configuration. It is controlled by a PWM (Pulse-width modulation) signal [9]. In bond-graph representation, the DC/AC converter is a transformer element (TF).

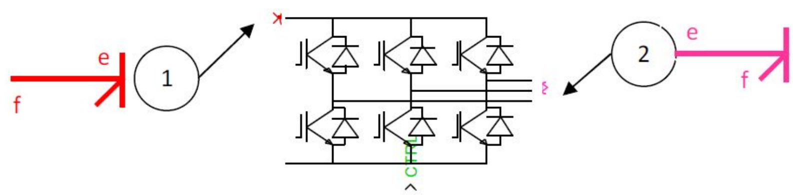

Figure 38: Bond-Graph representation for the DC/AC converter [9]

This model should be used with single phase signal for input and three phase signal for output. The diodes and semi-conductors (IGBT in that case) are supposed ideal peak loss have been neglected. The built-in voltage drop across diodes and semi-conductors is not considered.

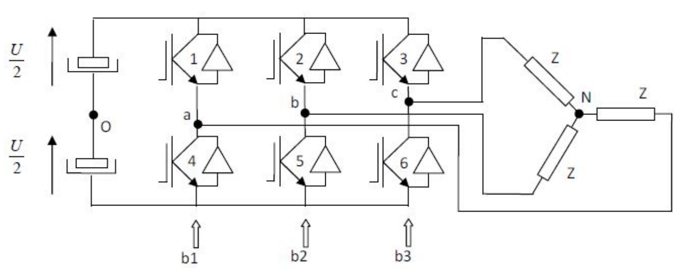

Figure 39: Structure of the DC/AC converter [9]

Table 6: Input and output definitions for DC/AC Three Phase Controlled Bridge Inverter [9]

Inputs				
Port	*Label*		*Units*	*Description*
1	E_ES	U_1	V	Voltage applied to the first element (single phase)
2	F_ET	I_2	A	Current applied to the second element(three phase)
3	CTRL	b1	-	Bit control for IGBT1 & IGBT4
		b2	-	Bit control for IGBT2 & IGBT5
		b3	-	Bit control for IGBT3 & IGBT6
Outputs				
Port	*Label*		*Units*	*Description*
1	F_ES	I_1	A	Current fixedby the first element (singlephase)
2	E_ET	U_2	V	Voltage fixed bythe second element (three phase)
Parameters				
Name	*Default value*		*Units*	*Description*
td	-		s	Forced semi-conductor device turn on delay
Results				
Name	*Units*			*Description*
RES	-			All results
U_1	V			Voltage at port 1
I_1	A			Current at port 1
V_2	V			Phase voltage at port 2 (V_an, V_bn, V_cn)
U_2	V			Line voltage at port 2 (U_ab, U_bc, U_ca)
J_2	A			Phase current at port 2 (J_ab, J_bc, J_ca)
I_2	A			Linecurrent at port 2 (I_a, I_b, I_c)
V_0	V			Midpoint voltage (V_a0, V_b0, V_c0)
IGBT_cmd	-			Semi-conductor command (IGBT_1, IGBT_2, ..., IGBT_6)

In order to present the model and its equations, we introduce the midpoint voltage source O and the three pole voltages V_{a0}, V_{b0}, V_{c0}. Bits b1, b2, b3 control respectively IGBT 14, IGBT 25, IGBT 36 and are calculated by a PWM module. The switches of any leg of the inverter couldn't be switched on simultaneously (it would result in a short circuit across the DC link) : a pairs of IGBTs shouldn't be in the same state. That's why one bit is sufficient to control two IGBTs:

- *when b1 = 1, IGBT 1 is on and IGBT 4 is off*
- *when b1 = 0, IGBT 1 is off and IGBT 4 is on*
- *when b2 = 1, IGBT 2 is on and IGBT 5 is off*
- *when b2 = 0, IGBT 2 is off and IGBT 5 is on*
- *when b3 = 1, IGBT 3 is on and IGBT 6 is off*
- *when b3 = 0, IGBT 3 is off and IGBT 6 is on*

The following table shows the link between the midvoltages VaO, VbO and VcO and the command bits:

Table 7: Midvoltages VaO, VbO and VcO and the command bits [9]

b3	**b2**	**b1**	**VaO**	**VbO**	**VcO**	**Van**	**Vbn**	**Vcn**
0	0	0	-U/2	-U/2	-U/2	0	0	0
0	0	1	U/2	-U/2	-U/2	2U/3	-U/3	-U/3
0	1	0	-U/2	U/2	-U/2	-U/3	2U/3	-U/3
0	1	1	U/2	U/2	-U/2	U/3	U/3	-2U/3
1	0	0	-U/2	-U/2	U/2	-U/3	-U/3	2U/3
1	0	1	U/2	-U/2	U/2	U/3	-2U/3	U/3
1	1	0	-U/2	U/2	U/2	-2U/3	U/3	U/3
1	1	1	U/2	U/2	U/2	0	0	0

The relation between midvoltages and command bits is done by Eq. (174) :

$$V_{a0} = \frac{U}{2}\left(2b_1 - 1\right);\ V_{b0} = \frac{U}{2}\left(2b_2 - 1\right);\ V_{c0} = \frac{U}{2}\left(2b_3 - 1\right) \tag{174}$$

The relation between midvoltages and phase voltage is done by Eq. (175):

$$V_{an} = V_{a0} - V_{n0};\ V_{bn} = V_{b0} - V_{n0};\ V_{cn} = V_{c0} - V_{n0} \tag{175}$$

As the system shall be balanced as shown in Eq. (176).

$$V_{an} + V_{bn} + V_{cn} = 0 \tag{176}$$

$$V_{an} = \frac{2V_{a0} - V_{b0} - V_{c0}}{3};\ V_{bn} = \frac{2V_{a0} - V_{b0} - V_{c0}}{3};\ V_{cn} = \frac{2V_{a0} - V_{b0} - V_{c0}}{3} \tag{177}$$

Finally, the relationship between the phase voltages and the command bits is expressed as in Eq. (178).

$$\begin{bmatrix} V_{an} \\ V_{bn} \\ V_{cn} \end{bmatrix} = \frac{U}{3}\begin{bmatrix} 2 & -1 & -1 \\ -1 & 2 & -1 \\ -1 & -1 & 2 \end{bmatrix} = \begin{bmatrix} b_1 \\ b_2 \\ b_3 \end{bmatrix} \tag{178}$$

V_{an}, V_{bn}, V_{cn} can take 5 different values : $\frac{-2U}{3}, \frac{-U}{3}, 0, \frac{U}{3}, \frac{2U}{3}$. Those values don't depend on the amplitude of the reference voltages, only but bus voltage.In reality, 2 IGBT of a same pair are not controlled at the same time. It exists a small delay to turn on a semi conductor, which does not exist when a semi conductor is turned off.

- *b1, which control the IGBT 1*
- *b2, which control the IGBT 2*
- *b3, which control the IGBT 3*

- *b4, which control the IGBT 4*

- *b5, which control the IGBT 5*

- *b6, which control the IGBT 6*

The relation between midvoltages and command bits is done by Eq. (179) :

$$V_{a0} = \frac{U}{2}(b_1 - b_4);\ V_{b0} = \frac{U}{2}(b_2 - b_5);\ V_{c0} = \frac{U}{2}(b_3 - b_6) \tag{179}$$

As the relation between midvoltages and phase voltage is still valid;

$$\begin{bmatrix} V_{an} \\ V_{bn} \\ V_{cn} \end{bmatrix} = \frac{U}{6} \begin{bmatrix} 2 & -1 & -1 \\ -1 & 2 & -1 \\ -1 & -1 & 2 \end{bmatrix} \begin{bmatrix} 1 & 0 & 0 & -1 & 0 & 0 \\ 0 & 1 & 0 & 0 & -1 & 0 \\ 0 & 0 & 1 & 0 & 0 & -1 \end{bmatrix} = \begin{bmatrix} b_1 \\ b_2 \\ b_3 \\ b_4 \\ b_5 \\ b_6 \end{bmatrix} \tag{180}$$

V_{an}, V_{bn}, V_{cn} can take 9 different values : $\frac{-4U}{6}, \frac{-3U}{6}, \frac{-2U}{6}, \frac{-U}{6}, 0, \frac{U}{6}, \frac{2U}{6}, \frac{3U}{6}, \frac{4U}{6}$.

6.4 Model Based Design of Induction Motor

PhiSim is a modeling and simulation environment for physical systems using Matlab-Simulink and dealing with physical system modeling [8]. The induction motor of direct vector control for the rotor flux model was designed in PhiSim, a multi-domain and multi-physics library developed by Sherpa Engineering. Simulation tests were carried out to validate the model. The main features of the PhiSim product are modeling of the system as a whole, integration of requirements, structures, tests, and behaviors, models that can be exported to simulation products, a level-based configuration of structures, objects, and connections from the metasystem to equipment, and is compatible with major systems engineering solutions on the market. Multi-physics modeling is often used to represent a technological equipment structure. To represent a complex system as a whole, multi-domain 0D-1D modeling is necessary and sufficient to simulate, analyze and predict its multidisciplinary performances. The components of the model are defined using analytical models that represent real electrical, mechanical, hydraulic, thermodynamic behavior.

In an asynchronous machine model, the voltage from the DC source is converted into three phases using PWM (Pulse Width Modulation) and DC/ AC three phase-controlled bridge inverter. The PWM signal produces trains of pulses, whose duty cycle varies depending upon a reference signal. The on/off states of modulation is used to control switches, in order to control voltage across or current through the power device. The PWM signal is generated by the intersective method, the switching points are determined by the intersection of the high-frequency carrier wave and the target reference signal. The pulse width is determined by a natural sampling PWM signal.

DC/AC three-phase-controlled bridge inverter represents an electrical device that converts direct current (DC) to alternative current (AC), which is known as an inverter. This converter is an arrangement of six IGBT and six diodes in a bridge circuit configuration. It is controlled by a PWM (Pulse-width modulation) signal. This should be used with a single phase signal for input and three-phase signals for output. The diodes and semi-conductors (IGBT in that case) are supposed ideal peak loss have been neglected. The built-in voltage drop across diodes and semi-conductors is not considered.

Inertia calculates the angular velocity and angular position of inertia from the torque effect. This element is an inertial element for the bond-graph representation [8]. The damper is a resistant torque between two elements. The resultant torque depends on the relative angular speed of both elements. This element is the dissipative element for the bond-graph representation.

Bond graphs are a domain-independent graphical description of the dynamic behavior of physical systems [14]. Bond graphs allow describing different physical systems and their interactions in a uniform algorithmizable way and transforming it into the definition of the equation of state [13]. This means that systems from different domains (cf. electrical, mechanical, hydraulic, acoustical, thermodynamic, material) are described in the same way. Bond graph is a powerful tool for modeling engineering systems when modeling different physical domains [14].

Bond-graph simplifies the construction of multi-disciplinary models, clearly shows power transfers, ensures energy balance, clearly shows cause and effect relationships. It allows the systematic writing of mathematical models associated with bond graphs. There is no black box model in the Bond graph, the unknown parameters of known physical phenomena are determined and the physical sense of the obtained mathematical model is observed. Only a couple of tools in the world are using this approach to design multi-physics models [8].

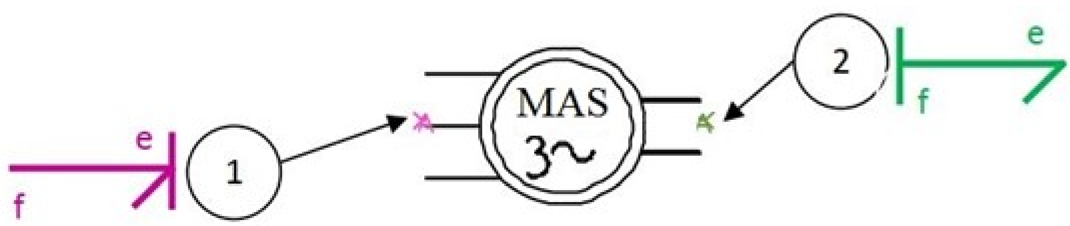

Figure 40: Bond -graph diagram of induction motor

Shown in Figure 40 is the bond graph diagram of the asynchronous machine. In bond-graph representation, the asynchronous electric machine is gyrator element.

Figure 41 shows the PhiSim implementation of the induction motor. In this model-based design, there are DC/AC bridge inverter (1P-3P), PWM, damper, DC source, mathematical model of asynchronous machine and control of asynchronous machine subsystems.

Table 8: Input and output definitions for Induction Machine [9]

Inputs				
Port	*Label*		*Units*	*Description*
1	E_ET	U	V	Voltage applied to the first element (threephase)
2	F_MR	ω	rad/s	Angular speed applied to the second element
		θ	rad	Angular position to the second element
Outputs				
Port	*Label*		*Units*	*Description*
1	F_ET	I	A	Current fixed by second element
2	E_MR	Tm	Nm	Torquefixed by second element

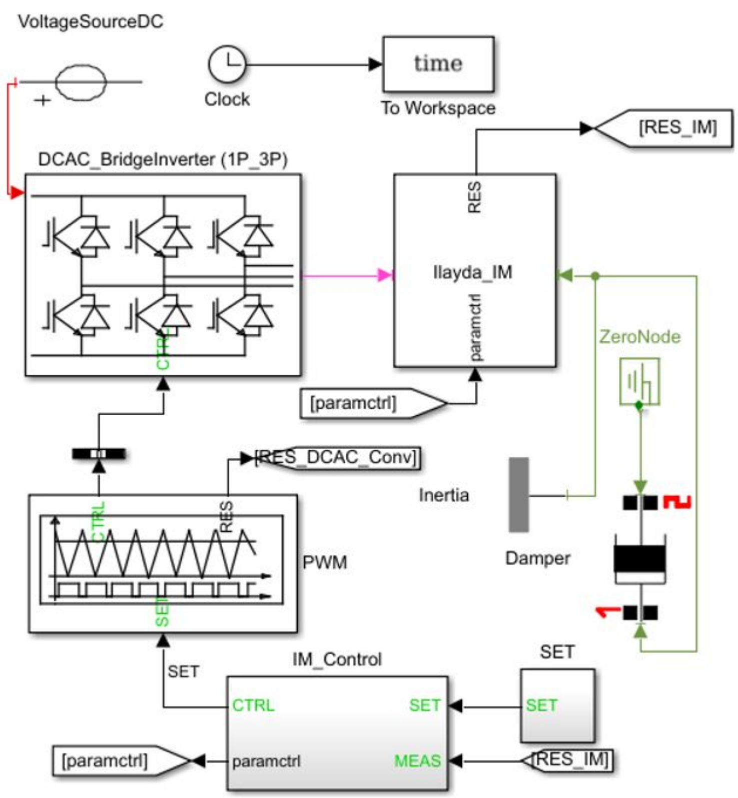

Figure 41: Induction motor PhiSim implementation of the rotor flux oriented vector control method

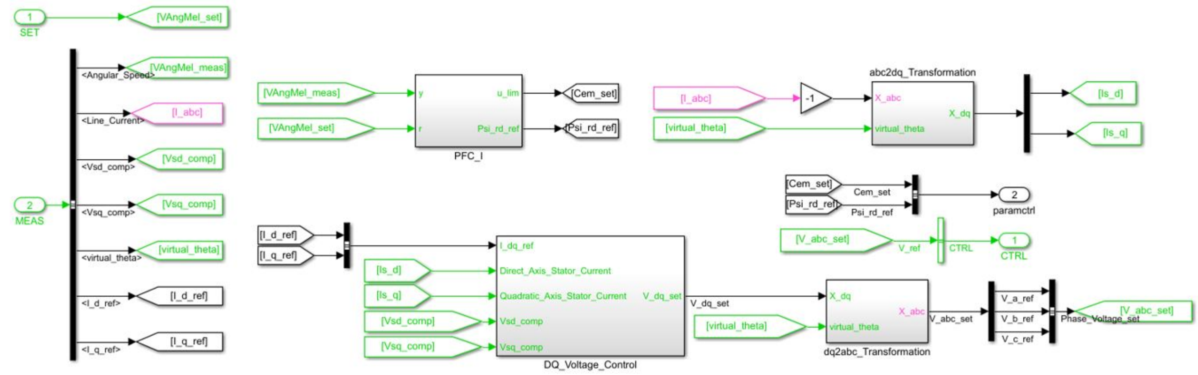

Figure 42: Control subsystem for Induction motor PhiSim implementation

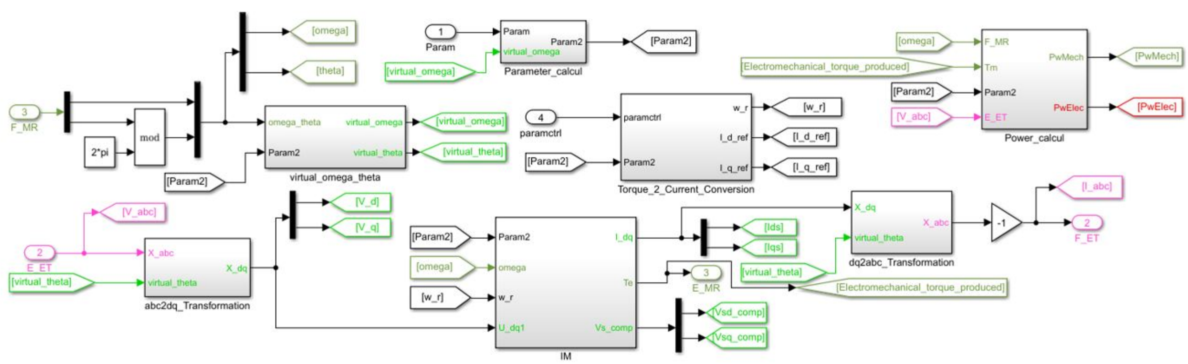

Figure 43: Mathematical model subsystem for Induction motor PhiSim implementation

Figure 42 represents the control block of the model-based design. This subsystem contains the current controller, speed controller, and field weakening parts, which are explained in the mathematical modeling section. The set value was determined as 1000 rpm, 1500 rpm, and 2000 rpm at each three-step time. The angular speed and torque results must match to the specified this set value. Figure 43 contains the machine equations defined in the mathematical modeling section. In addition, angular speed, electromechanical torque, angular position, mechanical power, and electrical power are calculated in this subsystem.

An interface is designed for the model-based design of the asynchronous machine. This interface is shown in Figure 44. Thanks to this designed interface, the user can change all parameter values on this interface without changing the internal structure of the model. You can get the desired result values through this interface.

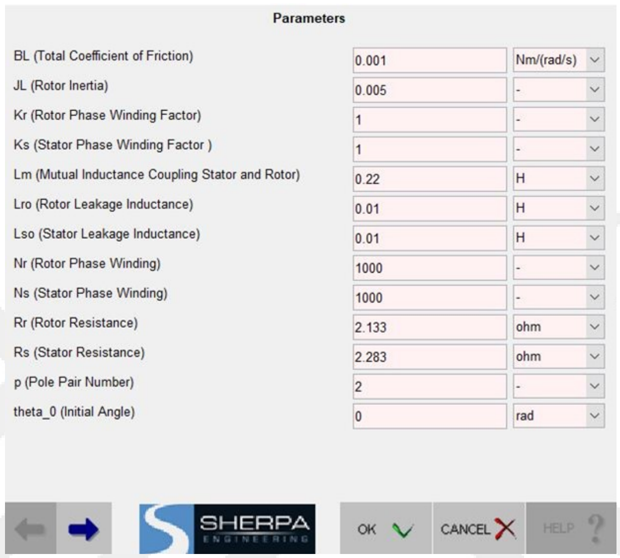

Figure 44: Interface designed for asynchronous motor parameters

Figure 45: Interface designed for asynchronous motor results

CHAPTER VII

SIMULATION RESULTS

By means of DC current and flux components obtained as a result of transforming the motor voltage, current, and flux components into space vectors rotating with the rotor, linear control methods have been applied to the machine by simulating the machine to a direct-current machine. The system was linearized by adding the terms that disrupt linearity in the equations to the model by being calculated from the measured quantities with the help of machine parameters.

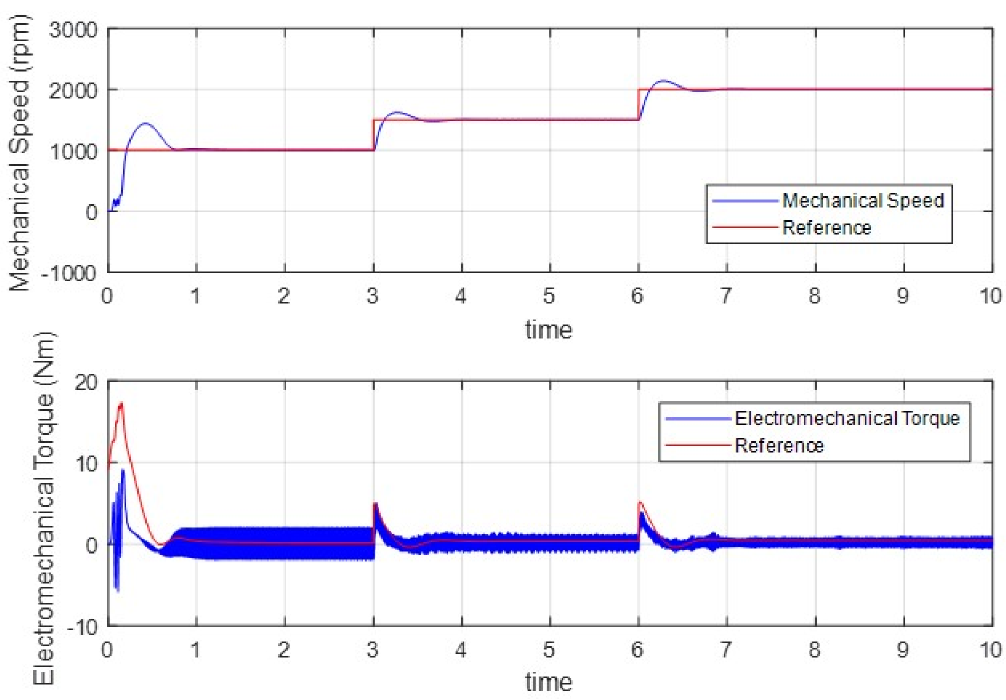

Figure 46: Graph of mechanical speed and electromechanical torque

The set value was determined as 1000 rpm, 1500 rpm, and 2000 rpm at each three-step time. The angular speed and torque results must match to the specified this set value. The machine is restricted to exceed its nominal power at the desired speed value, it follows the reference values with a small excess. It is shown in Figure 46.

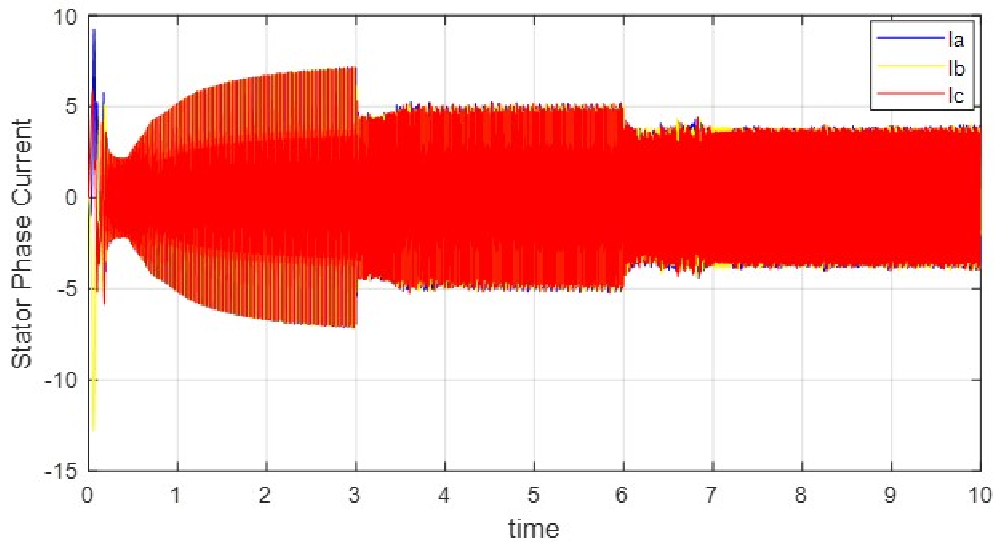

Figure 47: Graph of stator phase current

It is seen that the d-axis current component of the machine decreases when the rated speed value is exceeded, that is, when the field weakening region is entered. Because the d-axis current component controls the rotor flux, that is the excitation field. When this field strength is reduced, a lower torque will be produced for the same q-axis current component flowing from the rotor, and the desired speed will be achieved by keeping the power constant at the nominal value.

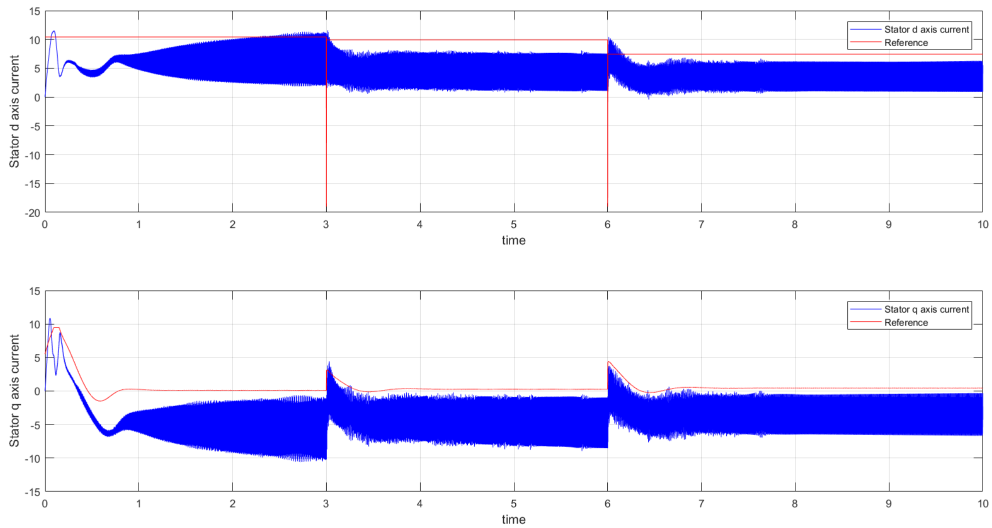

Figure 48: Stator D-Q axis current components graph

Sudden changes in speed reference create a jumping effect on stator currents. These effects are seen in Figure 48. Because speed change means sudden torque change. Since the voltage is indirectly a derivative operator between the torque and the current, a spike effect occurs in the stator currents. The lower the load on the machine, the more current jumping will occur in sudden speed changes, because the flux component of the rotor axis is given as an external reference, not by measuring and controlling it, and a jump time has to pass until the rotor flux reaches this reference value.

In addition to these results, two different scenarios were applied to the model.

First scenario:

The application of the first scenario to the model is shown in Figure 49.

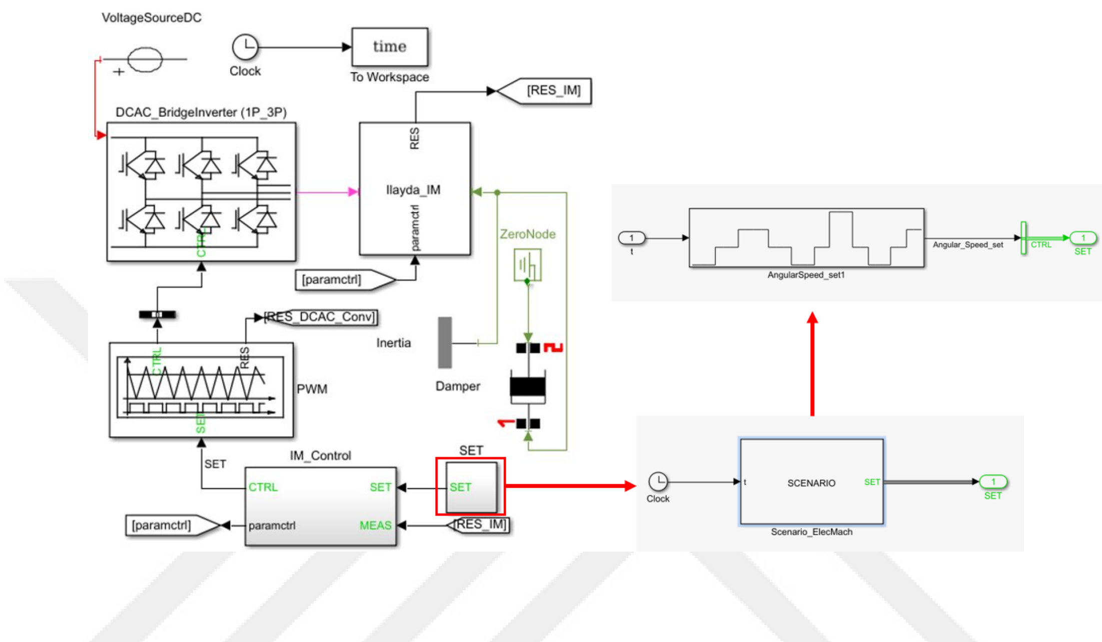

Figure 49: Applying the first scenario to the induction machine model

It is assumed that this induction machine model is used in a vehicle. Different situations of the vehicle in traffic were examined. A vehicle in traffic has different speed states. These are constant speed , acceleration and deceleration , sudden acceleration and sudden deceleration or braking . A scenario block was added to the model to observe these situations.

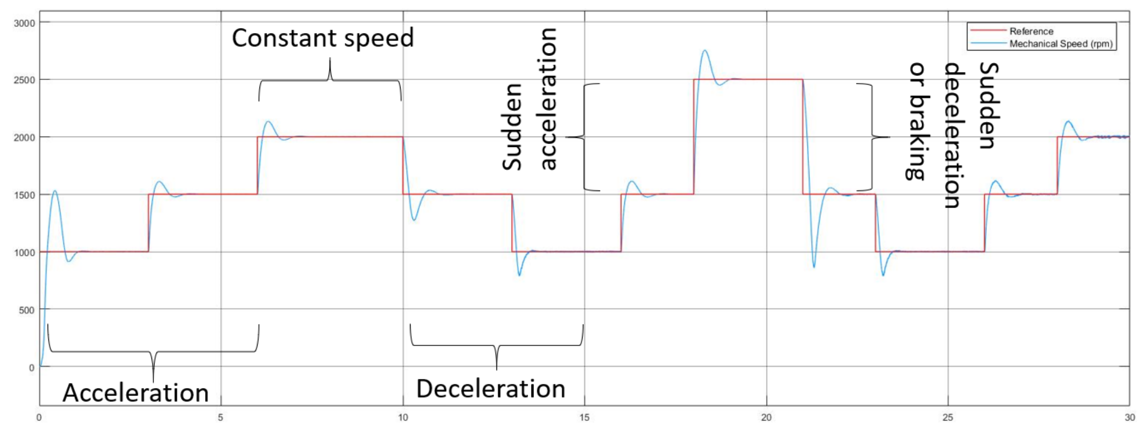

Figure 50: Display of different speed states

Figure 50 shows the parts where the vehicle's speed changes. As observed in Figure 51, the angular speed result must match to the specified this set value. The machine is restricted to exceed its nominal power at the desired speed value, it follows the reference values with a small excess.

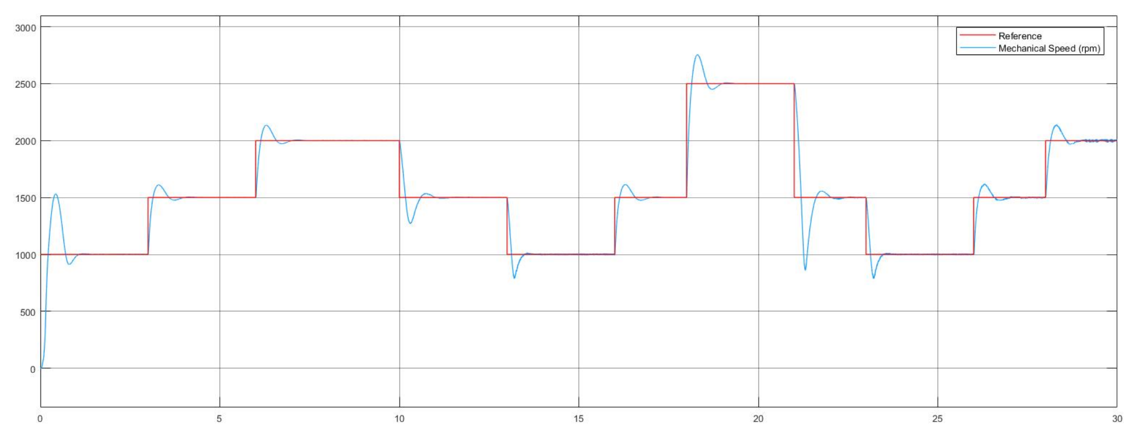

Figure 51: Graph of mechanical speed for the first scenario

As observed in Figures 51 and 52 , it has been observed that the results follow the reference values with a small difference. The torque decreased as the speed increased, and the torque increased as the speed decreased. Also, in the case of sudden acceleration, sudden deceleration or braking, jumps in torque and speed values were observed. However, These values followed the reference value after a while. The jump time has to pass until the variable reaches this reference value.

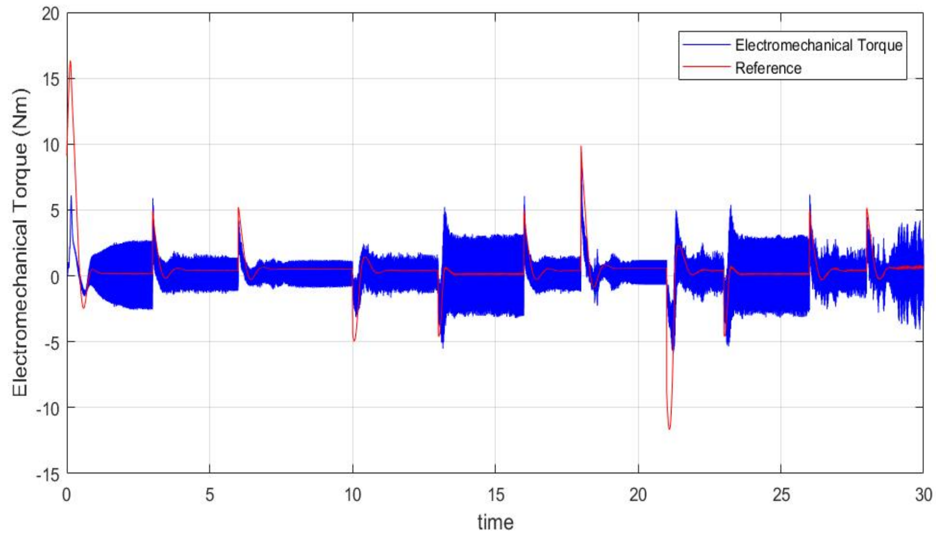

Figure 52: Graph of electromechanical torque for the first scenario

As observed in Figure 53 , sudden changes in speed create a jumping effect on stator currents. Because speed change means sudden torque change. Since the voltage is indirectly a derivative operator between the torque and the current, a spike effect occurs in the stator currents.

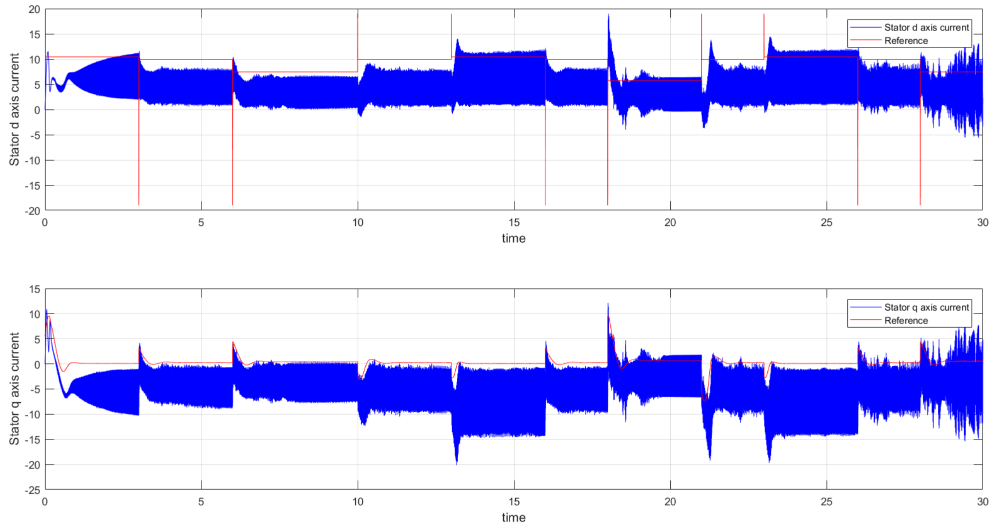

Figure 53: Graph of stator D-Q axis current components for the first scenario

The lower the load on the machine, the more current jumping will occur in sudden speed changes, because the flux component of the rotor axis is given as an external reference, not by measuring and controlling it, and a jump time has to pass until the rotor flux reaches this reference value.

Second scenario:

For the second scenario, it is observed that the T_L value is greater than the T_{en} value. The results are examined when the motor is greater than the rated torque.

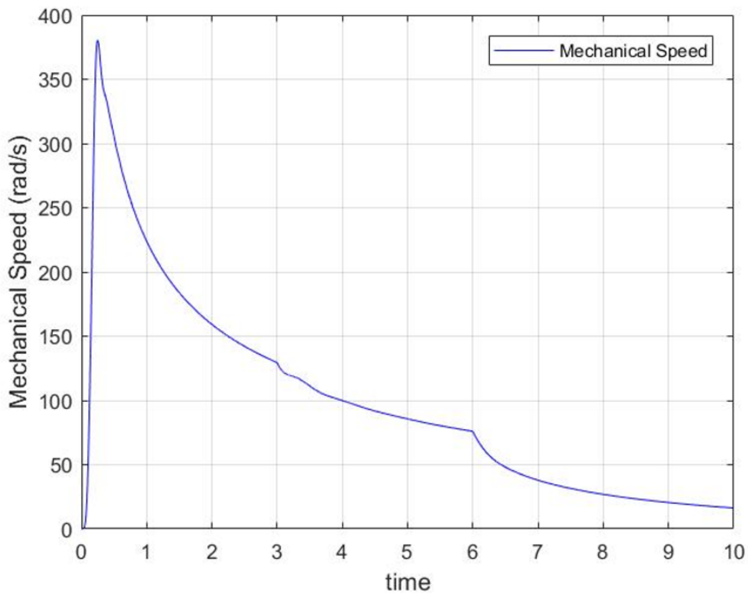

Figure 54: Graph of mechanical speed for the second scenario

As observed in Figures 54 and 55 , the motor overturns when the previously calculated nominal torque is exceeded. As can be seen from the results, when the machine exceeds the nominal speed value, it fell over because it could not provide the required torque and power due to the current restrictions placed on the d and q axis

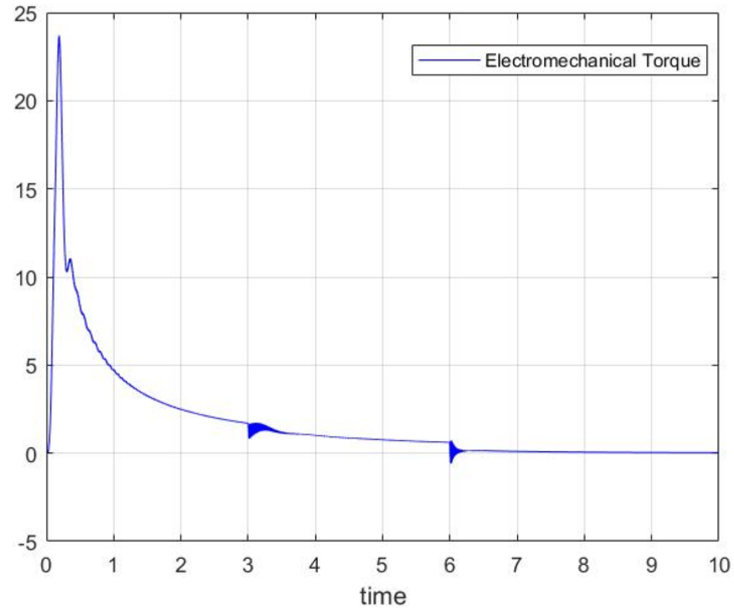

Figure 55: Graph of electromechanical torque for the second scenario

It is seen that when the load value is reduced and the machine is restricted to exceed its nominal power at the desired speed value, it follows the reference values with a small excess. It is seen that the d-axis current component of the machine decreases when the rated speed value is exceeded, that is when the field weakening region is entered. Because the d-axis current component controls the rotor flux, that is, the excitation field. When this field force is reduced, a lower torque will be produced for the same q-axis current component flowing from the rotor, and the desired speed will be achieved by keeping the power constant at the nominal value

CHAPTER VIII

FUTURE WORKS

In software development, the V-cycle represents a development process. The V-cycle shows each stage in the development life-cycle and how they relate to each other. Due to the complexity of the system's software, it is an important cycle for improving quality, increasing development efficiency, and planning a development process that will eliminate systematic software errors. V-cycle is given in Figure 7. V-cycle is applied in automotive engineering. The left side of the V-cycle consists of vehicle requirements , sub-systems design and test , components design and test in standard automotive systems engineering. The right side of the V concentrates the main verification and validation activities.

Vehicle requirements provide the service architecture and tool requirements, write use cases, and traceability of allocations. Subsystem design and testing enables building multi-physical sub-systems, choosing physical architecture, and sizing components to meet vehicle requirements. Components design and testing enables to design components and establish requirements for suppliers.

However, in the new automotive systems engineering, the functional design step is included on the left side of the V-cycle. The functional design step, especially the new tasks expected from hybrid and electric vehicles, concerns many subsystems. It allows managing the connections and complexity between vehicle requirements and physical sub-systems. Global energy management is mainly studied here. PhiSystem is used for vehicle requirements step and systemic models step . PhiSystem and PhiEMI are used for key functional architecture step and entire vehicle models. PhiSim and PhiControl are used for multi physic models. With this study, the requirements, functional design, design of subsystems and components on the left side of the V-cycle have been completed. In the future project, the right side of the V-cycle will be completed and the V-cycle will be completed in accordance with the ISO standard of automotive systems engineering.

Three levels of modeling are introduced as in Figure 56 :

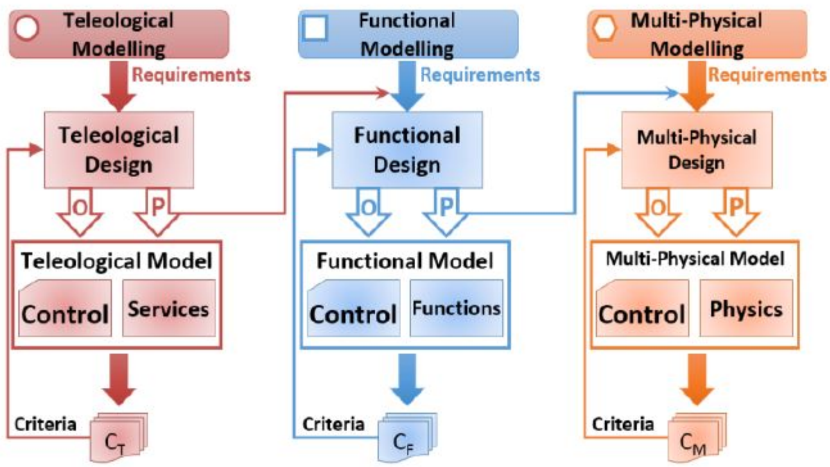

Figure 56: Multi-level integrated design and simulation [27]

The diagram first begins by identifying the requirements. These requirements are then formulated, then parameters (P) and objectives (O) must be defined to obtain a model-based design model and its associated controller.The resulting control mechanism is evaluated at the model-based level using validation steps. If the conditions are met, the parameters of the higher modeling levels will have defined the requirements of the lower modeling levels. This ensures that the high modeling level is the control of the lower modeling level [27].

In the multi-physical methodology, this link is represented by energy transfer. In multi-physical modeling, model design, simulation, and functional validation are long processes.

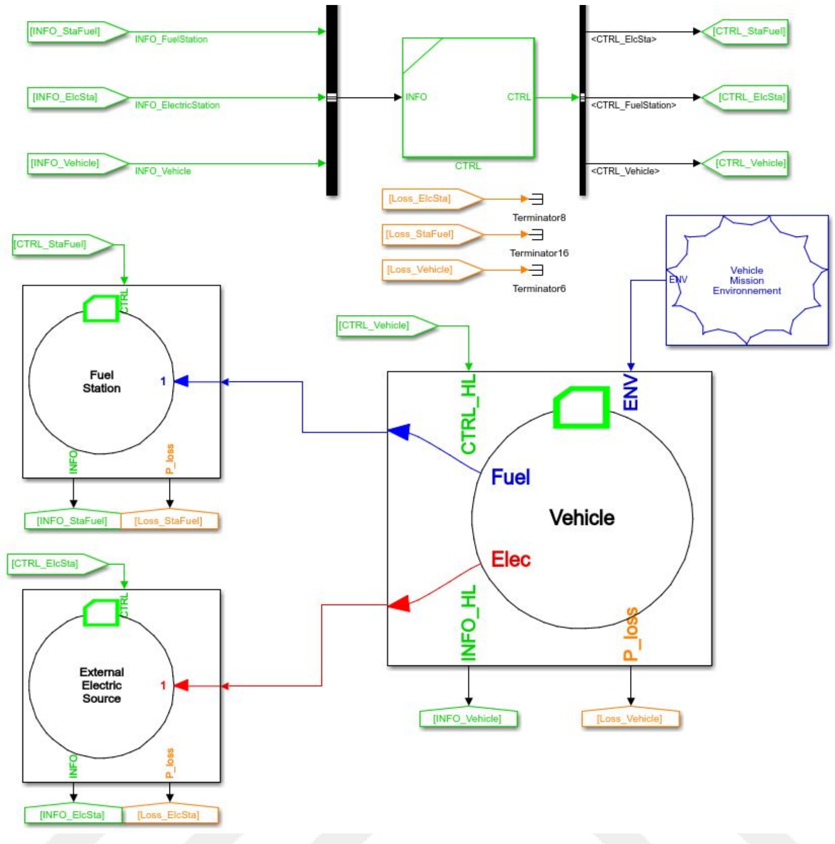

Figure 57: Multi-physical model for electric vehicle [28]

The Multi-physical model for electric vehicle is shown in Figure 57. The need computation starts from the effector. The energy requirement for this model is calculated from the electrical auxiliary element or the vehicle dynamic element blocks. This information is then transferred to the repositories and resources. Thus, the warehouse and resources decide whether they can provide this demanded energy.

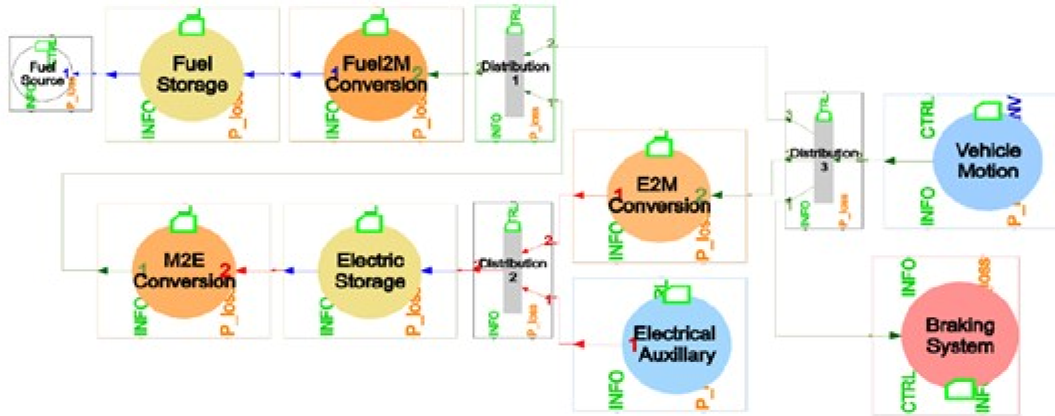

Figure 58: Functional model [28]

The functional model is shown in Figure 58. There are three main elements in the system. Transformations between systems are made with these.

- *F2M (fuel to mechanical) energy trans-formation*
- *M2E (mechanical to electrical) energy transformation*
- *E2M (electrical to mechanical) energy transformation*

It allows to evaluate the fuel consumption, maximum speed, maximum acceleration and regenerative braking power [29].

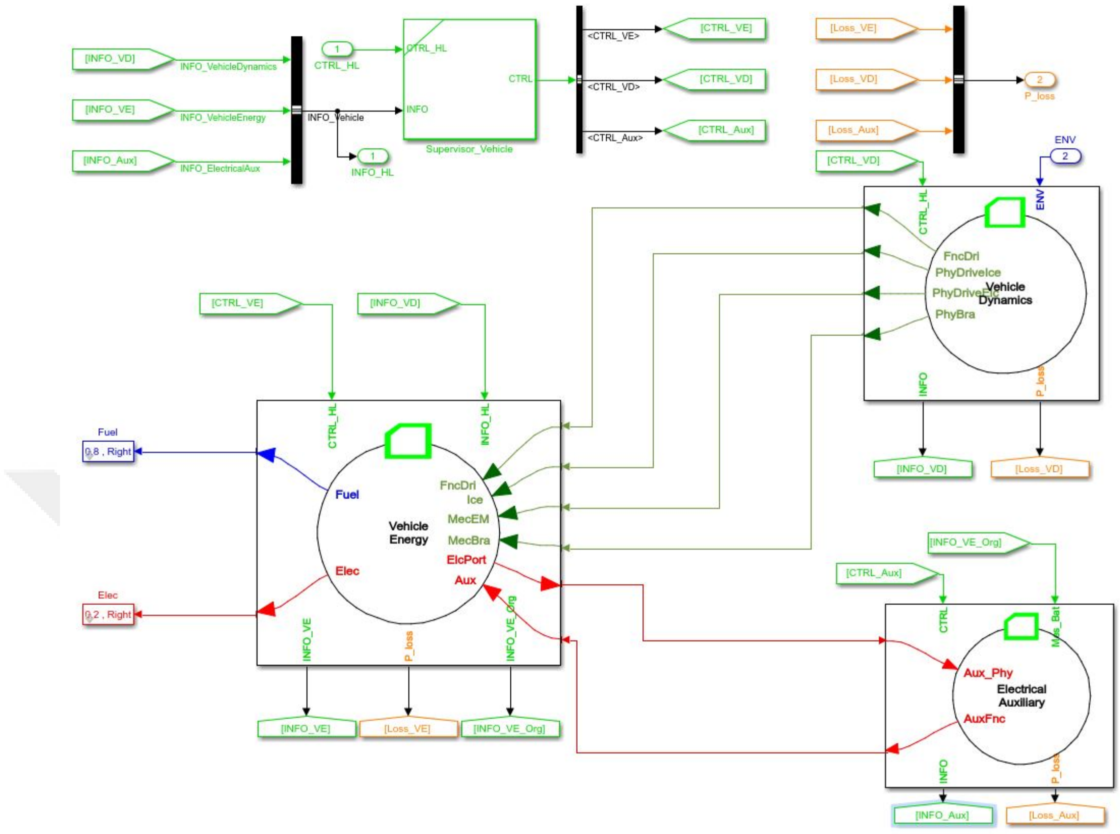

Figure 59: Multi-physical model for vehicle [28]

When designing the functional model, each system must have an energy source and an effector element.The multi- physical model of the system is expressed as follows.

In this thesis, the mathematical model and control of the asynchronous motor will be integrated into this multi-physical model.

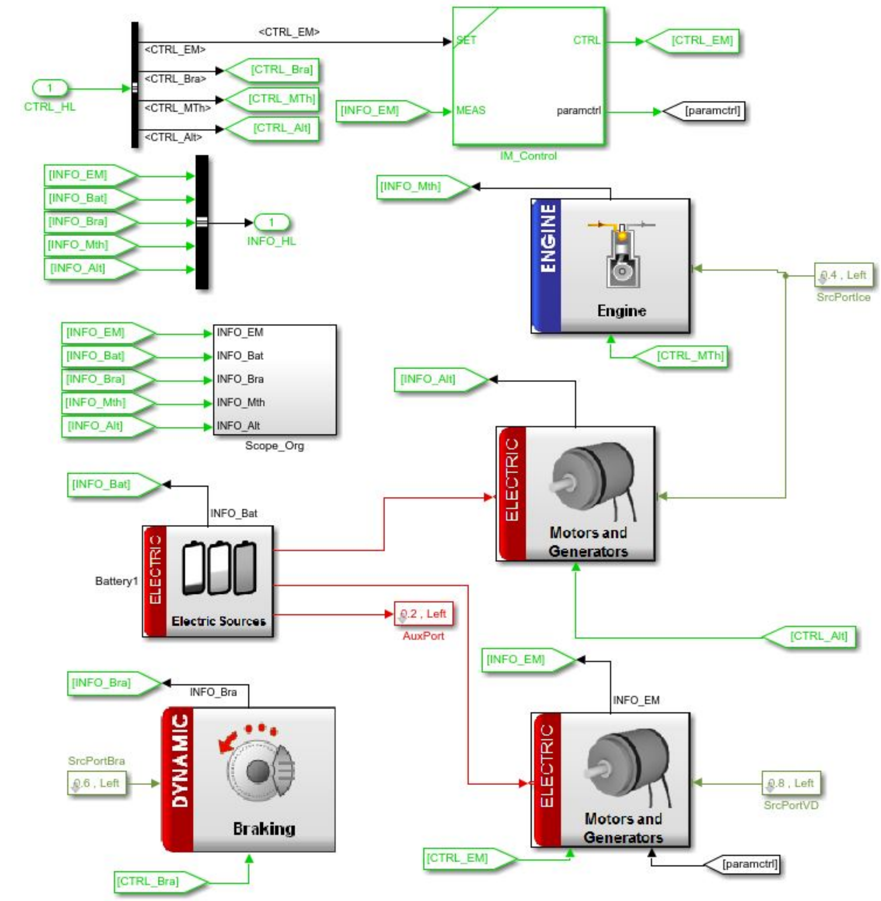

Figure 60: Multi-physical model for electric vehicle energy [28]

FTG function is to transform fuel energy into mechanical energy, input and output energies are different. F2M takes the fuel energy and provides a mechanical energy. Connected to the fuel storage area, the transferred mechanical energy is used for vehicle movement and partially recovered to recharge the battery [28].

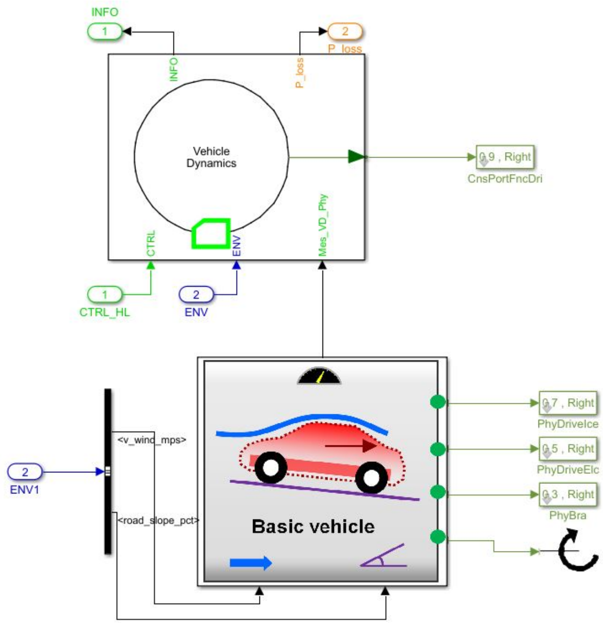

Figure 61: Vehicle dynamics system [28]

The challenge is to find the appropriate expression to connect the functional and multiple physical models of the electric vehicle. This relationship will be made in the part in Figure 62.

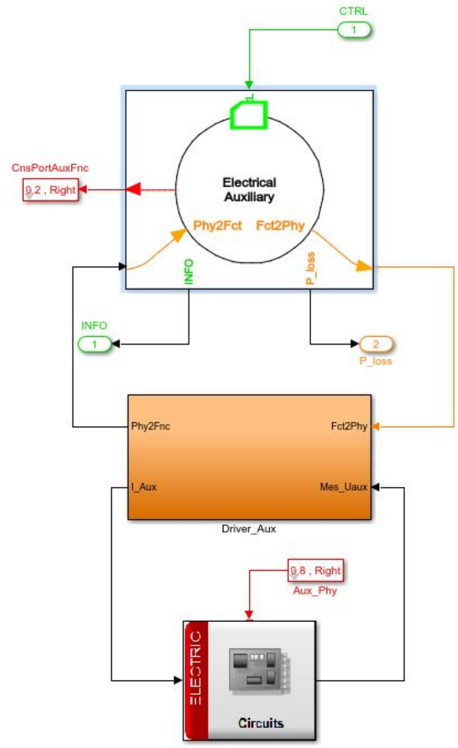

Figure 62: Electrical auxiliary system [28]

Due to environmental pollution, energy-saving, and the decrease in resources, there has been a tendency for vehicles based on renewable energy. For this reason, a lot of work has been done for electric vehicles in recent years. As studies evolve, so does component technology. Thus, the control of the system becomes more complex. For this reason, energy management and control strategies for electric vehicles are among the most important studies of today and the field of study is quite

With this method, detailed analysis of the systems can be made and results based on better sensitivity can be obtained.Therefore, the simulations are more securely validated, completing the right-hand side of the V-cycle. This allows the physical components to be analyzed on this platform using simulation data. Another important advantage of this method is the possibility to reconfigure the system structure while ignoring the analytical modeling in multi-physical modeling. This method allows us to simulate fast, reconfigure the system quickly and safely. In addition, an energy optimization strategy can be assigned to this system and the proposed solution can be transferred to a multi-physical model for a more secure verification in line with the obtained data. So that complex systems can be controlled more easily. This method is of interest to many automotive companies as it simplifies complex systems and simplifies design processes. In addition to all these, the energy management algorithm will be redone with an algorithm based on optimization. Thus, the power distribution within the system will be best managed. Also, a new perspective will be obtained by adding the supervisor strategy.

In this study, it was aimed to gain a new perspective in the automotive industry as well as having a good vision in systems engineering such as multi-domain modeling, testing, and validation of models. This simulation tool has been useful in investment decision-making processes and research.

CHAPTER IX

CONCLUSION

By means of DC current and flux components obtained as a result of transforming the motor voltage, current, and flux components into space vectors rotating with the rotor, linear control methods have been applied to the machine by simulating the machine to a direct-current machine. The system was linearized by adding the terms that disrupt linearity in the equations to the model by being calculated from the measured quantities with the help of machine parameters.

The machine is restricted to exceed its nominal power at the desired speed value, it follows the reference values with a small excess. It is seen that the d-axis current component of the machine decreases when the rated speed value is exceeded, that is, when the field weakening region is entered. Because the d-axis current component controls the rotor flux, that is the excitation field. When this field force is reduced, a lower torque will be produced for the same q-axis current component flowing from the rotor, and the desired speed will be achieved by keeping the power constant at the nominal value.

Sudden changes in speed reference create a jumping effect on stator currents. Because speed change means sudden torque change. Since the voltage is indirectly a derivative operator between the torque and the current, a spike effect occurs in the stator currents. The lower the load on the machine, the more current jumping will occur in sudden speed changes, because the flux component of the rotor axis is given as an external reference, not by measuring and controlling it, and a jump time has to pass until the rotor flux reaches this reference value.

Induction motor Simulink application of vector control for rotor flux was done using PhiSim. The bond-graph technique used simplifies the construction of multi-disciplinary models, clearly shows power transfers, ensures energy balance, clearly shows cause and effect relationships. Only a couple of tools in the world are using this approach to design multi-physics models [8]. This study was used in Sherpa Engineering [8] company's PhiSim library [9] and gave a new perspective for the use of asynchronous motors in electric vehicles for the automotive industry. Asynchronous motor is a good choice for the industry due to its low cost, high efficiency, robustness, high reliability, ability to work in bad environmental conditions, easy recycling, good dynamic performance, high maximum speed, and high range of field weakening [1, 3]. The efficiency of the induction motor is varying from 85 to 95 % [2]. It is a highly efficient motor for automotive applications [3]. Moreover, its speed regulation (SR) is very high [3] so it can be used in applications where load variation is higher. In this study, it was aimed to gain a new perspective in the automotive industry as well as having a good vision in systems engineering such as multi-domain modeling, testing, and validation of models. This simulation tool has been useful in investment decision-making processes and research.

APPENDIX A

MATLAB CODE FOR THE INTERFACE

The code used for the interface designed for the parameters and results of the asynchronous motor is as follows;

```
%
%        Ilayda_IM_dlg.m
%

function struct_dlg = Ilayda_IM_dlg(version)

switch version
    case 1.000
        % Version 1.000
        struct_dlg.source = 'PhiSimModel2/Ilayda_IM';

        struct_dlg.helpfile = '';

        struct_dlg.icons = [];

        struct_dlg.ctrls = [...
                add_expr('BL',  'BL (Total Coefficient of
                   Friction)',   1,      1,       '1',
                   [],      '0.001',         'RotaryDamping'
                   ),...
```

```
add_expr('JL', 'JL (Rotor Inertia)', 2,
        1, '1', [], '0.005',
        'Unitless'),...
add_expr('Kr', 'Kr (Rotor Phase Winding
   Factor)', 3, 1, '1',
   [], '1', 'Unitless'),...
add_expr('Ks', 'Ks (Stator Phase Winding
   Factor )', 4, 1, '1',
   [], '1', 'Unitless'),...
add_expr('Lm', 'Lm (Mutual Inductance
   Coupling Stator and Rotor)', 5,
        1, '1', [], '0.22', '
   Inductance'),...
add_expr('Lro', 'Lro (Rotor Leakage
   Inductance)', 6, 1, '1'
   , [], '0.01', 'Inductance'),...
add_expr('Lso', 'Lso (Stator Leakage
   Inductance)', 7, 1, '1',
       [], '0.01', 'Inductance'),...
add_expr('Nr', 'Nr (Rotor Phase Winding)'
   , 8, 1, '1', [], '
   1000', 'Unitless'),...
add_expr('Ns', 'Ns (Stator Phase Winding)
   ', 9, 1, '1', [], '
   1000', 'Unitless'),...
```

```
add_expr('Rr', 'Rr (Rotor Resistance)',
           10,     1,      '1',    [],
     '2.133',          '
  ElectricResistance'),...
add_expr('Rs', 'Rs (Stator Resistance)',
          11,     1,      '1',    [],
  '2.283',        'ElectricResistance'),
  ...
add_expr('p',   'p (Pole Pair Number)',
  12,      1,      '1',    [],     '2',
      'Unitless'),...
add_expr('theta_0',     'theta_0 (Initial
  Angle)',      13,      1,      '1',
  [],      '0',     'Angle'),...
add_result('V_sd',      'V_sd (Direct Axis
   Stator Voltage)',    1,      2,       '
  1',    [],      '',      'Voltage'),...
add_result('V_sq',      'V_sq (Quadratic
  Axis Stator Voltage)', 2,      2,
  '1',    [],      '',      'Voltage'),...
add_result('i_sq',      'i_sq (Quadratic
  Axis Stator Current)', 3,      2,
  '1',    [],      '',      'Unitless'),...
add_result('is_d',      'is_d (Direct Axis
   Stator Current)',    4,      2,       '
  1',    [],      '',      'Unitless'),...
```

```
        add_result('theta',      'theta (Angular
           Position)',      5,       2,       '1',
               [],      '',      'Angle'),...
        add_result('virtual_theta',      '
           virtual_theta (Virtual Angular Position
           )',      6,       2,       '1',     [],
               '',      'Angle'),...
        add_result('RES',        'RES',  7,       2,
               '1',     [],      '',      'Unitless
           '),...
        add_result('I_abc',      'I_abc (Line
           Current)', 8,       2,       '1',     [],
               '',      'Current'),...
        add_result('T', 'T ( Electromechanical
           Torque Produced)',       9,       2,
               '1',     [],      '',      'Torque')
           ,...
        add_result('V_abc',      'V_abc ( Phase
           Voltage)',       10,      2,       '1',
               [],      '',      'Voltage'),...
        add_result('omega',      'omega (Angular
           Speed)',         11,      2,       '1',
               [],      '',      'AngleVelocity')];
    struct_dlg.titles = {'Parameters','Results'};

    otherwise
        % Version 1.000 (Last Version)
```

```
            struct_dlg = Ilayda_IM_dlg(1.000);

end
```

APPENDIX B

MATLAB CODE TO CALCULATE ψ_{RD}^{REF}

The script used to calculate ψ_{rd}^{ref} is as follows ;

```
s_nom=0.0467;
p=2;
w_ref=(1430:0.1:2100)*2*pi/60;
w_ref_max=max(w_ref);
w_s_max=p*w_ref_max/(1-s_nom);
w_s=linspace(100*pi,w_s_max,length(w_ref));
w_s_nom=2*pi*50;
T_e_nom=18.0474;
P_nom=w_ref(1)*T_e_nom;
p=2;
Rr=2.133;
Psi_rd=zeros(1,length(w_ref));
for ii=1:length(w_ref)
    T=P_nom/w_ref(ii);
    w_r=w_s(ii)-p*w_ref(ii);
    Psi_rd(ii)=sqrt(T*Rr/(p*w_r));
end
w_ref=w_ref*30/pi;
```

Bibliography

[1] D. Zechmair and K. Steidl, "Why the induction motor could be the better choice for your electric vehicle program," *World Electric Vehicle Journal*, vol. 5, pp. 546–549, 06 2012.

[2] B. Lu, W. Cao, and T. Habetler, "Error analysis of motor-efficiency estimation and measurement," pp. 612 – 618, 07 2007.

[3] A. Boglietti, A. El-Refaie, O. Drubel, A. Omekanda, N. Bianchi, E. Agamloh, M. Popescu, A. Di Gerlando, and J. Borg Bartolo, "Electrical machine topologies: Hottest topics in the electrical machine research community," *Industrial Electronics Magazine, IEEE*, vol. 8, pp. 18–30, 06 2014.

[4] N. El Ouanjli, A. Derouich, e. g. Abdelaziz, S. Motahhir, C. Ali, Y. Mourabit, and T. Mohammed, "Modern improvement techniques of direct torque control for induction motor drives - a review," vol. 4, 05 2019.

[5] M. Begh and H.-G. Herzog, "Comparison of field oriented control and direct torque control," 03 2018.

[6] I. Takahashi and T. Noguchi, "A new quick response and high efficiency control strategy for the induction motor," *tia*, vol. 22, pp. 820–827, 10 1986.

[7] M. Depenbrock, "Direct self-control (dsc) of inverter-fed induction machine," *Power Electronics, IEEE Transactions on*, vol. 3, pp. 420 – 429, 11 1988.

[8] "Sherpa Engineering." https://www.sherpa-eng.com/en/. Accessed: 2021-04-14.

[9] "Sherpa Engineering,phisim." https://www.sherpa-eng.com/en/. Accessed: 2021-04-14.

[10] A. Abdul and A. Altahir, "Park and clark transformations park and clark transformations: A short review," 04 2020.

[11] K. Nguyen Thac, T. Orlowska-Kowalska, and G. Tarchała, "Influence of the stator winding resistance on the field-weakening operation of the drfoc induction motor drive," *Bulletin of the Polish Academy of Sciences: Technical Sciences*, vol. 60, 12 2012.

[12] G. M. Sarıoglu, M. K. and S. Bogasyan, *Asenkron Makinalar ve Kontrolü*. ABirsel Yayınevi Istanbul, 2003.

[13] D. Hroncová, A. Gmiterko, P. Frankovský, and E. Dzurišová, "Building elements of bond graphs," *Applied Mechanics and Materials*, vol. 816, pp. 339–348, 11 2015.

[14] J. Broenink, “Introduction to physical systems modelling with bond graphs,” 06 2021.

[15] “wikipedia.” https://tr.wikipedia.org/wiki/Asenkron-motor. Accessed: 2021-04-14.

[16] G. Mogenier, R. Dufour, G. Ferraris-Besso, L. Durantay, and N. Barras, “Identification of lamination stack properties: Application to high-speed induction motors,” *Industrial Electronics, IEEE Transactions on*, vol. 57, pp. 281 – 287, 02 2010.

[17] M. Dubois, “Review of electromechanical conversion in wind turbines,” 04 2000.

[18] A. Riyaz, S. Singh, and S. Singh, “Potential benefits of self-excited induction generator (seig) in distribution generation,” 11 2012.

[19] X. Xu and D. Novotny, “Implementation of direct stator flux orientation on a versatile dsp based system,” vol. 27, pp. 404 – 409 vol.1, 11 1990.

[20] L. Harnefors, “Design and analysis of general rotor-flux-oriented vector control systems,” *Industrial Electronics, IEEE Transactions on*, vol. 48, pp. 383 – 390, 05 2001.

[21] M. Filippich, “Digital control of a three phase induction motor,” 06 2021.

[22] K. Kyslan, M. Lacko, Ferková, and P. Zaskalicky, “V/f control of five phase induction machine implemented on dsp using simulink coder,” 09 2020.

[23] A. Moustafa and S. Mahadevan, *Structural Seismic Design Optimization and Earthquake Engineering: Formulations and Applications*, pp. 342–369. 05 2012.

[24] D.-H. Jang, “Problems incurred in a vector-controlled single-phase induction motor, and a proposal for a vector-controlled two-phase induction motor as a replacement,” *Power Electronics, IEEE Transactions on*, vol. 28, pp. 526–536, 01 2013.

[25] E. Kabalcı, *Power electronics and drives used in automotive applications*, pp. 249–273. 01 2014.

[26] KULANDHAIVELU, S. Kulandahivelu, and D. RAY, “Voltage regulation of 3-Ø self excited asynchronous generator,” *International Journal of Engineering Science and Technology*, vol. 2, 12 2010.

[27] P. Fiani, L. Taleb, S. Chavanne, and M. Mokukcu, “Modélisation pour la conception et l’évaluation de systèmes complexes,” *Ingenieurs de l’automobile*, 04 2016.

[28] M. Mokukcu, P. Fiani, S. Chavanne, L. Taleb, C. Vlad, and E. Godoy, “Control architecture modeling using functional energetic method - demonstration on a hybrid electric vehicle,” pp. 45–53, 01 2017.

[29] M. Mokukcu, P. Fiani, S. Chavanne, L. Taleb, C. Vlad, E. Godoy, and C. Fauvel, “A new concept of functional energetic modelling and simulation,” pp. 582–589, 12 2018.

[30] E. Akpınar, *Elektrik Makinalarının Temel İlkeleri.* Dokuz Eylül Üniversitesi Mühendislik Fakültesi Yayınları, İzmir, 2016.

[31] J. A. E. Fitzgerald, C. Kingsley and S. D. Jmans, *Electromechanical-energy-conversion principles.* 6 ed, McGraw-Hill, 2003.

[32] S. Chapman, *Electric Machine Fundamentals.* 01 2012.

VITA

Ilayda Demircioğlu graduated from Dr. Binnaz Ege - Dr. Rıdvan Ege Anatolian High School in June 2011. She graduated from Dokuz Eylul University Electrical and Electronics Engineering in 2018. During her undergraduate period, she worked on electrical and solar vehicles and robotic systems. She has won national and international awards. Many of her interviews and writings have been published in the national and international press.

She has been working on vehicle systems climate control module of vehicles for PSA / Stellantis in Sherpa-Figes engineering since 2018. She continued to work as a team leader as of 2020. She started Özyegin University Master of Science in September 2019. In 2021, her paper named "Induction Motor Simulink Implementation of the Rotor Flux Oriented Direct Vector Control Method for Electric Vehicles" was published as the first author at the "2021 17-th International Conference on Electrical Machines, Drives and Power Systems ELMA2021" conference.